GROWTH AND CHARACTERIZATION OF NOVEL GAN HIGH ELECTRON MOBILITY TRANSISTOR STRUCTURES WITH ENHANCED TWO-DIMENSIONAL ELECTRON GAS

By

Jeffrey R. Simpson, M.S.

A dissertation submitted to the Graduate Council of
Texas State University in partial fulfillment
of the requirements for the degree of
Doctor of Philosophy
with a major in Materials Science, Engineering, and Commercialization
December 2016

Committee Members

Edwin Piner, Chair

Mark Holtz

Casey Smith

Alex Zakhidov

Edward Beam

FAIR USE AND AUTHOR'S PERMISSION STATEMENT

Fair Use

Duplication Permission

DEDICATION

I dedicate this work to my family. Thank you for your support and patience.

ACKNOWLEDGEMENTS

I would like to acknowledge my committee members for their input in the planning, execution, and completion of this work. I would especially like to acknowledge my committee chair and advisor Edwin Piner for his guidance and support. Additionally, I would like to thank my research group, especially Jon Anderson for his microscopy work and general support.

TABLE OF CONTENTS

LIST OF TABLES

Table **Page**

LIST OF FIGURES

Figure **Page**

LIST OF ABBREVIATIONS

Abbreviation **Description**

2DEG – Two Dimensional Electron Gas

AFM – Atomic Force Microscopy

Al_2O_3 – Sapphire

AlGaN – Aluminum Gallium Nitride

AlInGaN – Aluminum Indium Gallium Nitride

AlInN – Aluminum Indium Nitride

AlN – Aluminum Nitride

BAlGaN – Boron Aluminum Gallium Nitride

BAlN – Boron Aluminum Nitride

BGaN – Boron Gallium Nitride

BN – Boron Nitride

c-BN – Cubic Boron Nitride

CDA – Clean Dry Air

CMOS – Complementary Metal Oxide Semiconductor

CTE – Coefficient of Thermal Expansion

CVD – Chemical Vapor Deposition

EDAX – Energy Dispersive Spectroscopy

EELS – Electron Energy Loss Spectroscopy

FET – Field Effect Transistor

FIB – Free Ion Beam

FWHM – Full Width at Half Maximum

GaAs – Gallium Arsenide

GaN – Gallium Nitride

HAADF – High Angle Annular Dark Field Imaging

h-BN – Hexagonal Boron Nitride

HEMT – High Electron Mobility Transistor

HNPS – High Nitrogen Pressure Solutions

HRXRD – High Resolution X-Ray Diffraction

HTVPE – Halogen (or Halide) Transport Vapor Phase Epitaxy

HVPE – Hydride Vapor Phase Epitaxy

III-N – Group III Nitride Material

InGaN – Indium Gallium Nitride

InN – Indium Nitride

LED – Light Emitting Diode

MBE – Molecular Beam Epitaxy

MFC – Mass Flow Controller

MOCVD – Metal Organic Chemical Vapor Deposition

MQW – Molecular Quantum Well

OM - Organometallic

OMVPE – Organometallic Vapor Phase Epitaxy

RMS – Root Mean Square

RSC – Research Service Center

SEM – Scanning Electron Microscope

Si – Silicon

SiC – Silicon Carbide

SIMS – Secondary Ion Mass Spectroscopy

SiNx – Silicon Nitride

SiO_2 – Silicon Dioxide or Silicon Oxide

STEM – Scanning Tunneling Electron Microscopy

TEB – Triethylboron

TMA – Trimethylaluminum

TMB – Trimethylboron

TMG – Trimethylgallium

TMI – Trimethylindium

TSU – Texas State University

VCR – Vacuum Coupling Radiation

w-BN – Wurtzite Boron Nitride

XRD – X-Ray Diffraction

ABSTRACT

Novel gallium nitride based high electron mobility transistor structures were grown using metalorganic chemical vapor deposition. Traditional GaN based HEMT structures incorporate a version of an aluminum gallium nitride / gallium nitride single crystalline heterointerface for generation of a conductive two-dimensional electron gas. The grown structures aim to enhance the properties of their two-dimensional electron gases beyond commercially available designs. Novel material alterations to the traditional HEMT structures have established a new materials platform for this technology. Growth and characterization of these novel materials are presented.

I. INTRODUCTION

Gallium Nitride (GaN) and other Group III-Nitrides (III-N) are superior materials for application in the high power and high frequency performance arenas due to their wide bandgaps, high saturation electron velocities, and large breakdown voltages [1]. Table 1 gives comparative metrics for the high power and high frequency capabilities of silicon (Si), gallium arsenide (GaAs), silicon carbide (SiC), and GaN. The cornerstone of their superiority is the potential for the formation of a two-dimensional electron gas (2DEG) at the interface of two compositionally different III-N materials. It is this 2DEG, combined with inherently beneficial GaN material properties, that make the III-N material platform superior for high electron mobility transistor (HEMT) development and commercialization.

The foundation of HEMT technology is the field effect transistor (FET) which first emerged in 1930 [2]. The development of FET technology would be dominated by the Si-SiO_2 interface [3] leading to the silicon complimentary metal-oxide-semiconductor (Si-CMOS) platform in the 1960s [4]. While the Si-CMOS platform is still commercially vibrant today, the need for higher power and higher frequency devices provides opportunity for wider band gap compound semiconductors to supplant silicon as the dominant materials platform [5].

Table 1. Comparative material metrics for high power and high frequency application [1].

	Si	GaAs	4H-SiC	GaN
Bandgap (eV)	1.1	1.42	3.26	3.39
Mobility (cm^2/Vs)	1350	8500	700	1200 (Bulk) 2000 (2DEG)
Saturation Velocity (10^7 cm/s)	1	1	2	2.5
Breakdown Field (MV/cm)	0.3	0.4	3	3.3

The III-Ns are ideally suited for these applications [5]. GaAs devices are capable of competing with similar silicon devices in terms of chip size and power. Measured in watt per millimeter gate length, GaAs achieved 1.4 W/mm at 8 GHz operating frequency in 1981 [6], 2.1 W/mm and 3.6 W/mm at 2-3 GHz in 2004 and 2007 respectively [7], [8]. These figures, while comparable given the differences in operating frequencies, were competitive with incumbent silicon technology. Even more appealing for high frequency power devices is GaN. While GaAs is a reasonable competitor with Si technology, their bandgaps are comparable at 1.42 eV for GaAs and 1.12 eV for Si, GaN boasts a bandgap of 3.4 eV and as a consequence is capable of significantly higher breakdown voltages; on the order of 3 MV/cm [9], or approximately an order of magnitude higher than Si breakdown voltage. Through inherent material benefits, mature processing techniques and advanced device structures, GaN devices have exceeded 40 W/mm at 4 GHz [10], almost a full order of magnitude improvement relative to the GaAs analog [11], [12].

Production of the III-Nitrides starts with epitaxial growth by such methods as metalorganic chemical vapor deposition (MOCVD) and molecular beam epitaxy (MBE).

The level of III-N materials development necessary to optimize and properly utilize interfacial properties depends entirely on the ability to grow single-/mono- crystalline materials. Chemical vapor deposition (CVD) growth of GaN-based materials was first published in 1969 with GaN growth from ammonia and chloride transported gallium [13]. This single crystalline GaN had a reported band gap of 3.39 eV and suffered from nitrogen dissociation from the surface producing significant nitrogen vacancies. The halide transport vapor phase epitaxy (HTVPE) process utilized collects gallium containing vapor from gallium metal through the use of halide vapor, such as chlorine. Non-GaN products of HTVPE include hydrogen halides, such as hydrogen chloride, which can react with the growth substrate and introduce new gaseous elements resulting in as-grown crystal impurities [14]. The first utilization of organometallics as precursors for III-N growth came in 1971 with the growth of AlN and GaN from ammonia and trimethylaluminum (TMA) and trimethylgallium (TMG), respectively [14]. The efforts produced single crystalline AlN on Si, and GaN on SiC and sapphire. The grown GaN structure shapes were crystallographically decorated steps and similar free standing needles. GaN growth process development would continue until the discovery of the intimate relationship between GaN crystal quality and the properties of underlying III-N buffer layers in 1986 [15]. The GaN crystal quality was found to heavily depend on AlN buffer thickness and growth temperature. This dependence would ultimately lead to modern III-N structures including buffer / transition layers with varying composition to optimize the GaN crystal quality.

Modern III-N MOCVD material growth for power devices aims to produce high quality wurtzite crystals. The wurtzite structure is shown in Figure 1 and exhibits a

significantly asymmetric ordering of alternating atomic planes of like-atoms [16]. This asymmetry is responsible for the strong polarization found within the crystal; specifically, the spontaneous polarization that is responsible, in large part, for the 2DEG formation. The alternating planes of group III and group V atoms allow for discrete material interfaces to be formed in addition to discouraging diffusion in the c-direction which could reduce the abruptness of such an interface. Through the beneficial arrangement of every atom of either group III or V being bonded to an atom of the other group, there is little direct diffusion through such ordinary means as vacancy driven diffusion, as an atom would need to occupy an interstitial position or an oppositely polar position to diffuse successfully.

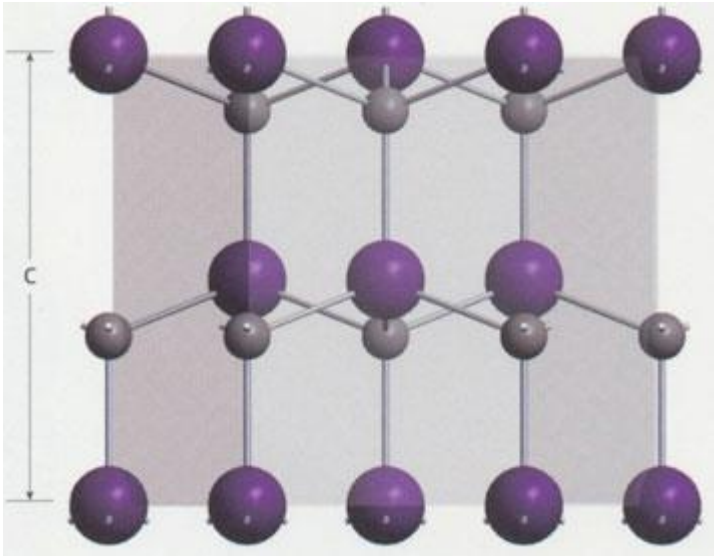

Figure 1. Alternating planes of like-atoms arranged in widely spaced pairings of group III (purple atoms) and group V (grey atoms) layers define the pronounced asymmetry which is fundamental to the III-N wurtzite crystal structure [16].

MOCVD grown III-N materials commonly orient along the [0001] direction (i.e., the + c-direction) which corresponds to the G a-polar face of GaN. Within the wurtzite crystal, polarity is defined as the direction in which a single bond is pointing away from its host atom, towards the growth direction and normal to the substrate surface, the opposite

side of which are three bonds which angle away from their host towards the close plane of bound heteroatoms all of which have a single bond pointed away from the growth direction towards the substrate. Whichever of the two types of atoms satisfies this condition determines the face of the polarity. Figure 1 shows the orientation for Ga-polar GaN, taking the upward vertical direction as the growth direction. Figure 2 shows the same crystal structure in an orthogonal view. This is the top-down view along the [0001] direction which represents the face of a growing surface. The drawing illustrates the hexagonal symmetry within the crystal structure and the stacked nature of adjoining layers. The Ga-polar face is evident due to the three bonds going into the image from the most superficial gallium atoms to the bound nitrogen atoms of the next atomic layer.

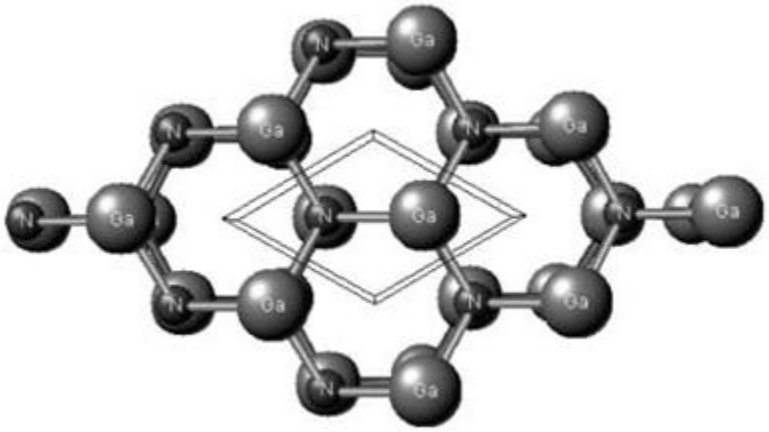

Figure 2. Ga-polar wurtzite GaN viewed down the [0001] direction of the first few atomic layers. The hexagonally symmetric structure is emphasized by the drawing [17].

MOCVD growth usually produces Ga-polar GaN, although the process (and MBE) can be tailored to produce N-polar material, as well as GaN crystals with mixed polarity domains. Intentional polarity inversion has been achieved from N-polar to Ga-polar [18], [19] and Ga-polar to N-polar [20], [21]. Both inversions have been successfully accomplished through exposure to magnesium. Magnesium has also been

responsible for a phase change from typically grown wurtzite GaN to a zinc-blende structure [22]. Inherent to the staggered planes of III-V atoms within the GaN crystal is the need for specific heterostructure designs to best utilize the material properties. This asymmetry in III-N wurtzite crystals, which is exploited at III-N interfaces for 2DEG generation, is direction dependent. As such, a N-polar III-N material structure must utilize a different device stack to induce a functional 2DEG than a Ga-polar structure. Figure 3 illustrates the impact of polarity for the same material stack and the relative position of the 2DEG resulting from polarization contributions of the stack design.

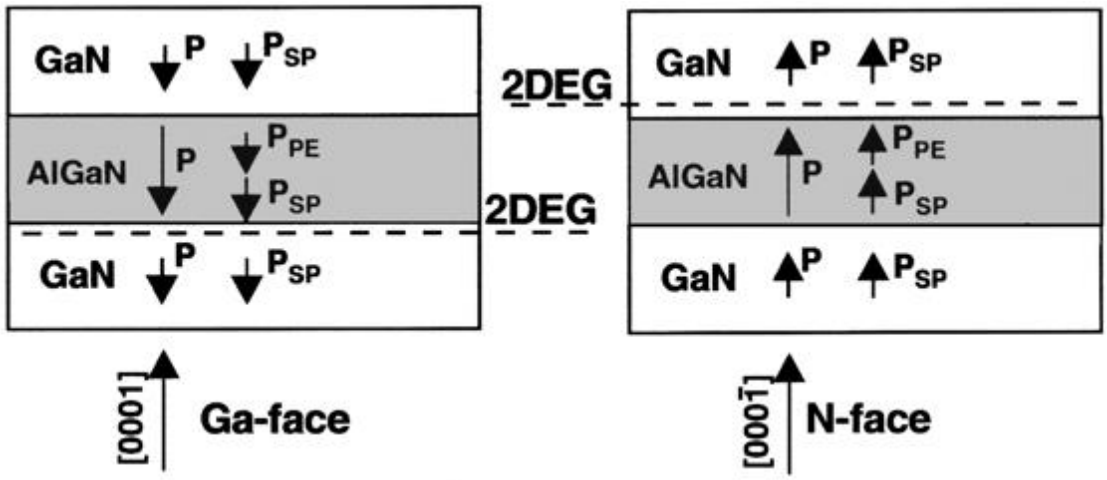

Figure 3. Impact of polarity on device design and 2DEG generation [23].

N-polar GaN is well suited for high speed devices. The defining property responsible for this preference is the difference in superficial layer thickness between Ga- and N-polar materials required for 2DEG formation. The superficial AlGaN layer of Ga-polar AlGaN/GaN heterostructures determines the 2DEG properties, as such, device performance and 2DEG quality are highly dependent on this layer thickness. N-polar superficial layers are not under such restraints. Given that the AlGaN/GaN

heterostructure is fundamentally flipped upside down for the N-polar device, the superficial layer is GaN. This layer can be as thin as a few nm and still retain a functional 2DEG. This is a benefit in high speed devices as it puts the biased gate material that much closer to the conductive channel which offers significantly more gate control.

Ohmic contacts of N-polar device structures can be much more efficient than similar Ga-polar contacts. GaN has lower inherent resistance than AlGaN, and a thinner material provides less resistance than a thicker one. Given these benefits, research into N-polar GaN devices is quite popular. Currently the technology is limited by vertical confinement of the 2DEG at high fields [24].

While the presence and position of a 2DEG for a given III-N stack can be evidence for polarity determination, represented by Figure 3, certain assumptions about the relationship between the crystallographic and piezoelectric axes must be made [25], [26]. The establishment of a reliable method rests on the work done in the 1980's to determine polarity so as to define the Ga-polar and N-polar directions of III-N materials and their corresponding properties [27]–[33]. Through the various characterization methods and experiments, a "standard framework" was created to describe trends and material properties of typical growth techniques of the time and to define the crystallographic directions for III-N polarity [27].

Heteroepitaxy

The lack of naturally occurring GaN on this planet combined with the difficulty and expense of creating GaN substrates forces growth on foreign substrates. In general,

epitaxial growth on non-native substrates is known as heteroepitaxy. The consequences of growing material on non-native substrates are centered on the material differences between the substrate and the growing film. Lattice spacing and coefficients of thermal expansion (CTE) mismatches are the primary concerns for heteroepitaxially grown films, assuming the materials are chemically compatible to allow growth by the given technique. For MOCVD films, the epitaxial growth direction is normal to a planar substrate. While this is beneficial for creating planar surfaces and interfaces, a consequence of the planar growth regime is that it allows for little termination or paired annihilation of those dislocations that are generally oriented in the growth direction. The growth mechanism responsible for this inability to terminate vertically oriented dislocations is known as Volmer-Weber thin film growth [34] which is headlined by the preferred surface association between adatoms resulting in island growth and eventual coalescence. These persistent dislocations are common due to the need to grow III-N epilayers on substrates with mismatched lattice parameters. Interfacial bonds will line up as energetically favorably as possible with the inevitable creation of substrate dangling bonds and epilayer dislocations. Figure 4 depicts the interface bonding configuration between wurtzite AlN (0001) and Si (111) [35], [36]. The figure depicts an idealized interface. In reality, as with any strained interface, ideality will partially give way to compromise, preferentially altering material structure locally to satisfy dangling bonds.

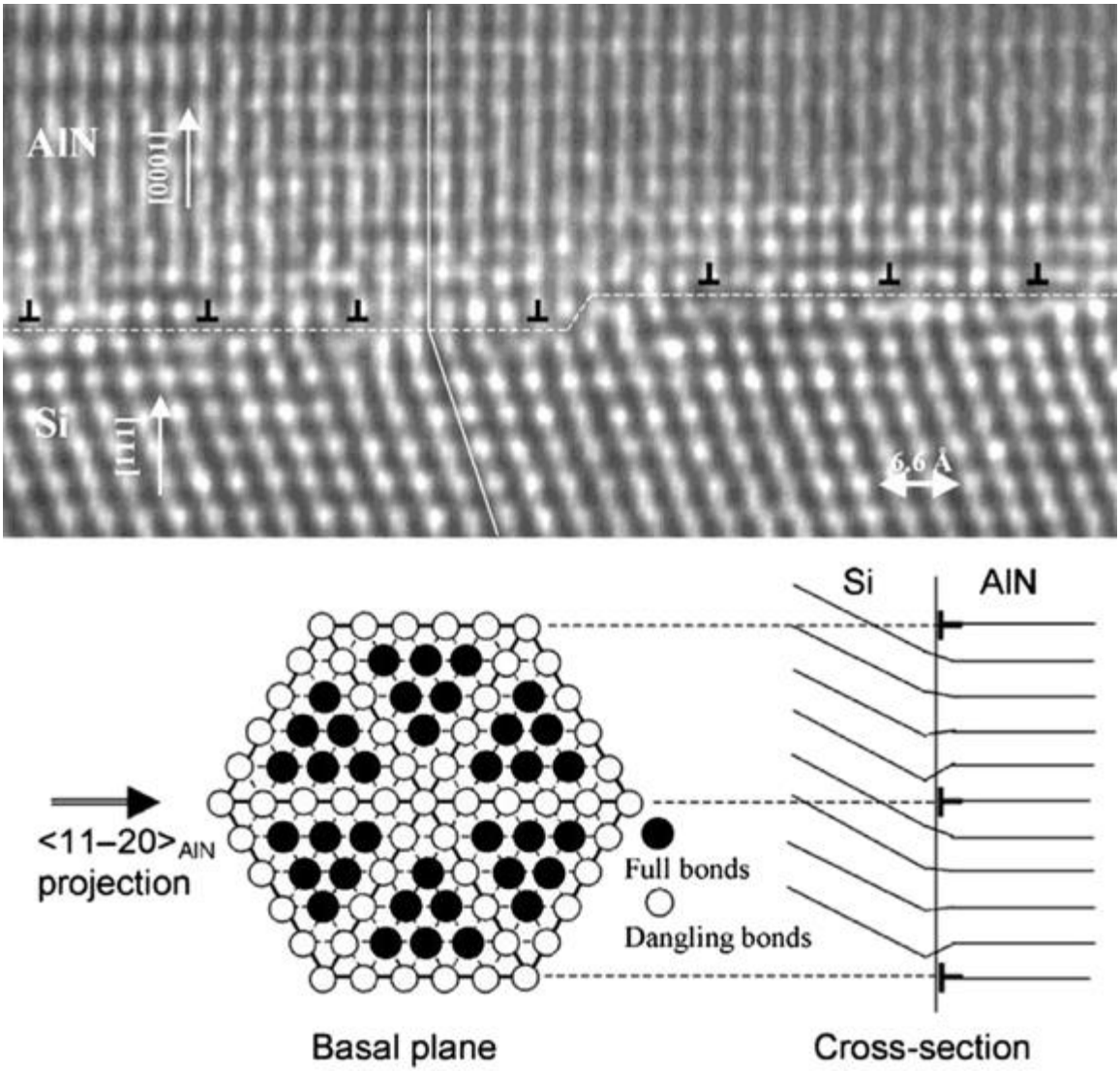

Figure 4. Atomic arrangement of AlN/Si (111) interface. Mismatch at the interface causes misalignment leading to dislocations [35], [36].

These threading dislocations can continue from the substrate/film interface through the transition layers to the superficial device layers. Despite these dislocations, III-N devices are quite reliable, even though edge defects can cause localized shifts in threshold energetics on the order of 10^{11} e/cm^2 over a 30-50 nm radius about the defect core [37]. Efforts to mitigate the threading dislocations caused by interfacial lattice mismatch have been fruitful and are headlined by the concept of lateral overgrowth [38]. To summarize

the technique: a perforated hard mask is used to limit the growth surface area of a III-N crystal reducing the propagated threading dislocations significantly. The roughly vertical dislocations must persist through the hard mask openings to remain present in the growing crystal. Once epitaxial layers protrude through the hard mask, selective epitaxial growth conditions can favor a lateral growth over the hard mask, joining the protruding structures. The newly grown III-N material has significantly reduced defect density [39]. Figure 5 illustrates the impact of the lateral overgrowth technique on GaN crystal quality.

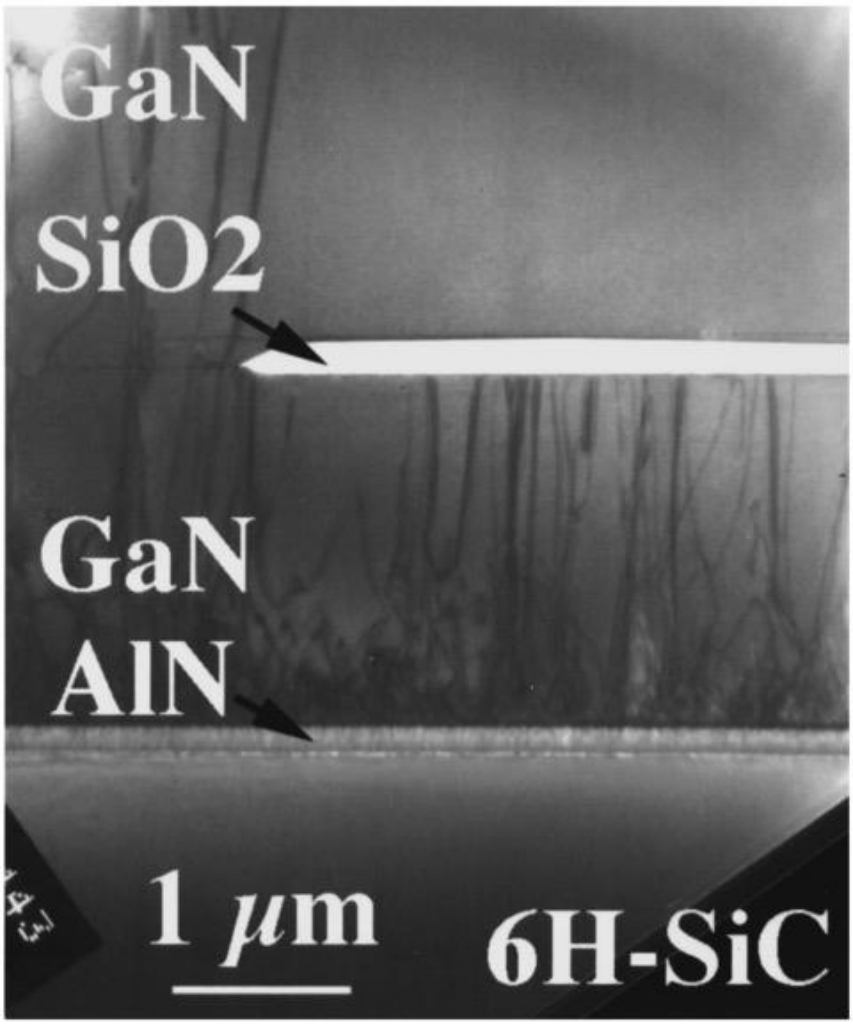

Figure 5. The concentration of threading dislocations is significantly reduced by lateral overgrowth [38].

The fundamental concept on which this technique is predicated is that GaN growth does not initiate the dislocations found in epitaxial GaN but instead these dislocations are a direct result of relaxation of the growth interface with its mismatched substrate. The development of GaN technology has historically been hindered by the lack of native substrates and as such, III-N materials must be grown heteroepitaxially on non-native substrates such as sapphire, silicon carbide, and silicon (111) [17].

Substrates for Heteroepitaxy

Sapphire (Al_2O_3) is the dominant substrate, historically, for GaN and was used in the first CVD grown single-crystalline GaN in 1969 [13]. Sapphire's popularity for GaN growth remains today. Yet as a growth surface with approximately a fifteen percent lattice mismatch, dislocation densities are high in the grown GaN; on the order of 10^{10} cm^{-2} [40]. This mismatch is optimized from a potential ~30% mismatch through a 30° rotation of GaN axes relative to c-plane sapphire [17]. Sapphire is not well-suited for high power applications due to its relatively poor thermal conductivity [41], however it is still a preferred substrate for GaN-based optical devices such as light emitting diodes (LEDs) [42]. Further hindering it for high power applications, sapphire can serve as a source for diffused oxygen into epitaxial films which contribute to the background electron concentration as unintentional dopants [43].

Silicon carbide (SiC) is a very appealing substrate for GaN, particularly in high power arenas, due to its high thermal conductivity [44]. 6H-SiC has roughly a fifteen to twenty fold advantage in thermal conductivity as compared to sapphire [17], [45], [46]. SiC also holds a significant advantage in lattice mismatch with an approximately 3%

mismatch with GaN, relative to sapphire's ~15% [47]. This relatively small mismatch must still be accommodated with transition layers, and is responsible for threading dislocations as can be seen in Figure 5. Despite the benefits of SiC for heteroepitaxial growth of GaN, it is not the generally preferred substrate choice due to one very compelling disadvantage: cost. Historically, SiC substrates sell at a 20 × multiple (or greater) of high resistivity silicon substrates.

Silicon benefits from substantial industry development as it is the most perfect mass-produced material, in the form of single crystal ingots, today. Silicon wafer production has matured to keep up with the ever growing demands of silicon-based technology. The result is large, inexpensive, widely available, and highly mature wafers for use in many technologies. While these benefits of silicon substrate use are appealing, silicon has a poor lattice mismatch to GaN of about 17% [47]. In addition to the lattice mismatch, the thermal expansion of silicon substrates is roughly 55% less per temperature increase than GaN which creates a tensile strain on the contracting GaN during cooldown [48]–[50]. Efforts to address this issue have been fruitful and are headlined by the growth of superlattices which accommodate the resulting strain from the thermal expansion mismatch [50]–[52]. The thermal expansion differences between GaN and its substrate usually limit the total III-N epitaxial thickness to a few microns. But through research efforts to address this issue, layers as thick as 9 µm have been grown [52]. The growth of GaN, or its alloys, directly on a silicon substrate is not favorable without an interlayer separating the gallium species from the silicon surface as a gallium silicide is likely to form which dramatically disrupts growth surface planarity and uniformity, preventing III-N nucleation. Through the growth of transition layers to

accommodate the lattice mismatch and the stress associated with the thermal expansion mismatch, GaN growth has been successfully achieved and substantially developed using silicon (111).

Naturally, the search for viable substrates for III-N growth would include other III-V materials. Many have been successfully utilized, including GaAs, AlN and even GaN itself. The primary property limiting GaAs as a growth surface is the poor thermal stability of GaAs in traditional GaN MOCVD growth conditions, specifically an ammonia rich environment above 700 °C [17]. GaAs substrates have found use for GaN growth in two general regimes: through non-MOCVD growth techniques which, in addition to growing wurtzite crystals, can be used to produce alternate phases of GaN such as cubic [53]–[56] and, through the use of alternative nitrogen precursors [55], [57], can eliminate the detrimental combination of GaAs and ammonia. AlN as a growth surface for GaN may be the most ideal for high power applications, even more so than a GaN substrate as the thermal conductivity of AlN is nearly double GaN and the two III-N materials have similar lattice constants with ~2.5% mismatch [17], [46], [47]. Given that AlN is a preferred transition layer employed with heteroepitaxial growth on other substrates, it is not surprising it would be an appealing substrate for GaN growth. The primary issue hindering GaN on AlN technology is the relative dearth of AlN substrates available; combined with their small size and high price tag, AlN wafer costs outweigh their potential benefits.

Substrates for Homoepitaxy

Bulk GaN crystal growth is a popular research topic which aims to maximize GaN technology efficacy by providing GaN substrates which are free of the consequences of heteroepitaxy. Threading dislocation density is a direct result of the heteroepitaxial growth process due to a mismatch of lattices at the substrate to epitaxy interface. GaN HEMT growth on GaN substrates has been effective to reduce the prevalence of these dislocations [58]. This is desirable for device performance by the reduction of the potential failure mechanism of contact metal diffusion along a dislocation. A negative consequence of this dislocation concentration reduction is the necessity for advanced ohmic contact formation which does not utilize the dislocations for diffusion pathways [58]. Despite this consequence, growth of GaN substrates is highly desirable. Arguably the most effective method practiced today for the production of bulk GaN crystals is the Ammonothermal Method [59], [60]. Initially patented in 2003 [61], it is an approach to growing bulk GaN crystals which derived from a comparable high pressure quartz growing technique [62], [63]. It boasts good scalability and cost-effectiveness and has proven success in reliably producing bulk GaN. Iterations of the original method all have a similar structure: GaN crystals recrystallized in a high pressure, supercritical ammonia solution from GaN material stock. GaN seeds are often used as epitaxial surfaces for the recrystallization, though spontaneous self-nucleated crystals have been produced [59]. A fundamental aspect of this method is the utilization of a mineralizer which functions to improve the GaN solubility in ammonia. The mechanism of increased solubility is the intermediate polarity of the mineralizer relative to ammonia and GaN. Mineralizers used to achieve this soluble interaction include: basic

approaches with alkali metal amides such as $NaNH_2$ [60] or acidic approaches with ammonium halides such as NH_4^+F [59]. The ionic nature of the mineralizer allows association of the polar GaN species with the less polar supercritical ammonia in solution. An interesting scientific result of this technique is that the coordination of basic mineralizers to GaN exhibits counterintuitive solubility with temperature. The GaN-mineralizer complex has a higher prevalence in the supercritical ammonia at lower temperatures than at higher ones [63]. Intuitively, and as with most solutions, solubility increases with temperature. While this may also be the case for the GaN complex in the ammonia solution, the reverse-temperature dependence of concentration observed in this system is due to the dissociation of the complex with rising temperature thereby decreasing the concentration despite any solubility preference at higher temperatures. While the fundamental science of solutions is not likely violated, the effective solubility does decrease with temperature which is a scientific oddity. This relationship does not apply to acidic mineralizers which follow normal solubility expectations. Unbound GaN molecules can offer a diverse array of dimers and trimers [64]–[69] which, under the conditions of this ammonothermal method, could be coordinated with multiple stabilizing mineralizer ions which would complicate solution-stable intermediates beyond the scope of this brief introduction.

Hydride Vapor Phase Epitaxy (HVPE) also known as Halogen Transport Vapor Phase Epitaxy (HTVPE), noted previously in this chapter, was an early precursor to MOCVD. The HVPE growth technique and its derivatives are quite effective in producing bulk GaN crystals [56], [70]–[72] and are some of the most practiced methods for the task. The process generally exploits the reaction of gallium chloride, produced

from reacting hydrogen chloride with a gallium species such as liquid gallium [72] or TMG [56], with ammonia to grow GaN epitaxially on a GaN surface. The HVPE technique is headlined by high (0001) direction growth rates, well over 100 μm/h [72], but total thickness is limited by parasitic GaN growth away from the intended substrate. This extra material in the growth chamber alters growth conditions by consuming reactants [71]. The selection of a HVPE substrate heavily influences the resulting GaN crystal. If heteroepitaxially grown GaN is used, threading dislocations remain from the original foreign substrate, though they can be significantly reduced by the process [71], [73], [74]. If GaN substrates from bulk GaN techniques are used, then a relatively low dislocation density can be achieved in the HVPE grown homoepitaxial layers [71], [74]. The benefit of a heteroepitaxially grown GaN substrate is the variety of available sizes of the foreign substrates; the drawbacks of high dislocation density and interface strain causing wafer bowing make homoepitaxial GaN substrates appealing despite their smaller available surface areas. As a result, wafers larger than 2 inches in diameter are not commonly produced due to the significant curvature from the inherent strain.

The preferred method for bulk silicon growth is the Czochralski process involving solid monocrystalline boules of material being drawn from a melt using specialized seed crystals which determine boule crystallinity [75]. Similarly, liquid phase growth methods for bulk GaN are possible, though not through identical means. The limiting criteria for a Czochralski method of producing GaN boules are the high melting point of GaN coupled with its low decomposition temperature which favors decomposition into liquid gallium and gaseous nitrogen. In a vacuum, GaN decomposition rates increase rapidly at 970-980 °C [76], [77]. The ionic-like nature of the wurtzite structure of GaN crystals contributes

to this relatively high thermal stability. A mechanism for decomposition is the evolution of nitrogen in the form of both atomic and molecular nitrogen [78]. The wurtzite structure discourages the formation of molecular nitrogen with the segregation of nitrogen atoms. Each nitrogen atom is bonded to four gallium atoms, preventing direct association to form the molecular nitrogen dimer. Spatially, the nitrogen atoms within the wurtzite crystal are ~3.2 Å apart while the molecular product bond length is ~1.07 Å [78]. Through exploitation of this decomposition-limiting mechanism, GaN decomposition rates significantly increase in the presence of H_2 gas. A weight loss from GaN samples in H_2 environments occurs around 600 °C [79] and significantly increases at 800 °C [80]. The effective mechanism responsible for decreasing the decomposition equilibrium temperature is the formation of ammonia from surface nitrogen. Given the limitation of the nitrogen escape mechanism for decomposition, the addition of hydrogen allows nitrogen to escape as ammonia without the need for autocatalysis in the formation of molecular nitrogen. A significant variable in the decomposition of GaN under hydrogen is the effect of pressure. At lower temperatures, increases in H_2 pressure have a larger effect on decomposition rates than increases in temperature [81]. Given the strong preference of decomposition over melting of the wurtzite GaN crystal, substantial measures must be taken to preferentially melt GaN. To make a melt-based recrystallization process viable, a large pressure of nitrogen is needed to push the decomposition equilibrium of nitrogen escape in favor of a more stable solid phase allowing it to reach a melt transition temperature and eventual recrystallization. At the N_2 pressure of 2 GPa (~15 million Torr), decomposition of GaN occurs around 1650 °C [82], [83]. A true melt of GaN was achieved at 2215 °C under 6 GPa N_2 pressure [83].

The phase diagram resulting from these data is shown in Figure 6. Upon cooling, this melting process produced multiple ~100 µm sized monocrystalline pieces of yellow-tinted transparent GaN crystals. Further optimization of this high pressure melt process could result in a method of forming single crystalline GaN in a manner similar to the Czochralski method for producing silicon. The requisite pressure of 6 GPa (~45 million Torr) makes this a difficult technology to pursue.

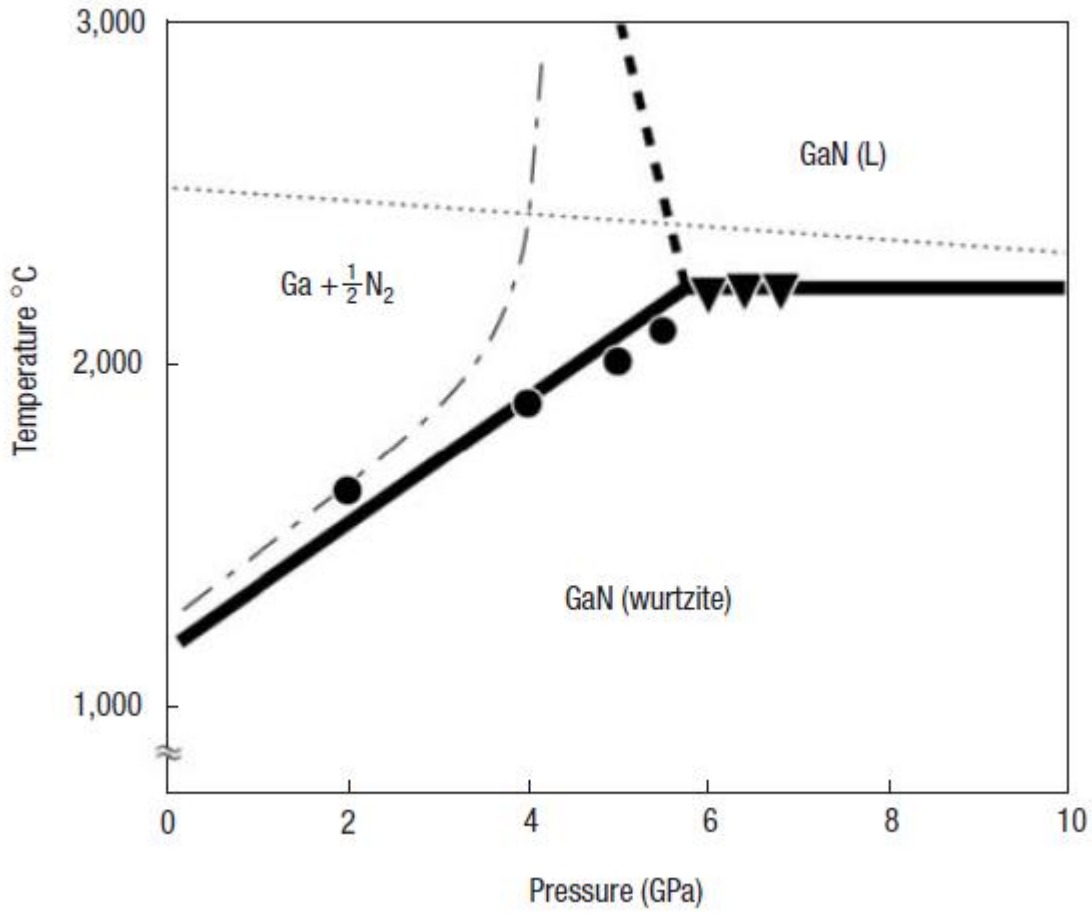

Figure 6. Phase diagram of GaN – decomposition is favored over the liquid phase at lower pressure [83].

Alternative liquid phase epitaxy methods have been successful in growing GaN crystals. The High Nitrogen Pressure Solutions (HNPS) method is an intuitive approach to GaN growth involving the direct reaction of nitrogen gas with gallium. Given the inert status usually ascribed to nitrogen gas, high pressure and temperature conditions must be employed to induce the reaction for GaN growth. Originally attempted in 1972 [84], the process has evolved to reach temperatures as high as 2000 °C and a pressure of 1 GPa (over 7 million Torr) [85]. This technique utilizes the three phase equilibrium of gaseous N_2, liquid Ga, and solid GaN over a temperature range at a set pressure. This equilibrium was originally established in 1984 [82] and the nitrogen solubility further resolved for this process in 1991 [86]. The basic principle defining this approach is the solubility and diffusivity of nitrogen in liquid gallium made possible by the extreme conditions defining the technique. Once solvated by the gallium liquid, the dissolved nitrogen moves through the liquid bulk towards the GaN surface submerged in the liquid facilitated by convection currents. The solid GaN surface is held at a lower temperature than the overlying gallium liquid so to create a local supersaturation of dissolved nitrogen which encourages precipitation of GaN on the growth surface [85]. The process benefits from a seed surface for planar growth. Without an appropriate surface, precipitation occurs in the form of small platelets or needles [74], [85], [87]. Another Liquid Phase Epitaxy commonly called the sodium flux method was developed in Japan in the late 1990s [88]. Growth of GaN occurs within a Ga-Na melt in a gaseous nitrogen environment. Initially grown from NaN_3 and metallic Ga [88], the more common approach today is production of the melt from metallic Na, metallic Ga, and N_2 [89]. As is popular with other methods, seed crystals can be used to impress a large planar surface area for epitaxial

growth. Despite high threading dislocations in seed crystals, the Na flux method has been shown to produce added GaN material with decreased dislocation densities relative to other methods [90]. Discoloration to the point of producing black GaN crystals has been prevalent with the process when growing spontaneous GaN material or using smaller crystal seeds [72]. Given that the ideal GaN crystal would be transparent to all visible wavelengths, the heavily darkened GaN is evident of crystal impurities, in this case it is primarily due to nitrogen vacancies [91]. Various elements have been added to the melt which alter the grown crystal's appearance and material properties including producing transparent GaN [89]. Increasing the nitrogen solubility in the Ga-Na melt would reduce the vacancies incorporated into the crystal. This can be achieved through the addition of calcium and lithium into the melt at molar concentrations on the order of 0.1% [89]. Additionally, an issue where solid GaN grows away from the desired growth surface, including spontaneous nucleation, has been solved by the addition of carbon into the growth solution [92]. Neither sodium nor additive elements are found within the GaN crystal at detectible levels, though dopants can be added in a similar fashion to alter the resistivity of the grown crystal [89].

While efforts to produce GaN substrates for III-N-based devices have been successful overall, further development is needed to supplant the less expensive and more mature mismatched substrates. GaN thin film based technology has been commercialized wholly on heteroepitaxially grown GaN. A large part of the development efforts focuses on transitioning from the foreign substrate to a GaN single crystal surface with controlled properties and morphologies. This transition occurs through various layers of single

crystalline material whose purpose is to provide a gradation of properties so to accommodate the mismatch between substrate and the eventual GaN thin film.

II. III-Nitride Materials

Transition Layers

Fundamental to the discussion of III-N on silicon HEMT structures and device properties is the interface science that dictates device performance as it pertains to (1) accommodating the mismatch for non-native substrates and (2) functionalizing the conductive properties of the 2DEG. Buffer / transition layers do not play an active role in device performance, aside from engineering and exploiting their electrically insulating properties. (They can even be removed during processing, for certain device structures.) Functionally, they provide a means for GaN crystal growth by transitioning from a lattice constant appropriate for nucleation on the silicon (111) surface to the larger lattice constant of GaN.

Multiple layers are necessary for relaxed GaN growth on silicon, and to accommodate the coefficient of thermal expansion mismatch. Typically, buffer / transition layers include an AlN nucleation layer and aluminum gallium nitride alloys with ever increasing gallium content to serve as a template for GaN epitaxy [93], [94]. The layers must be of sufficient thickness to allow for and overcome relaxation events caused by mismatch at the various interfaces resulting in dislocations, as previously described. While such relaxation events are detrimental in the device layers, they are necessary for heteroepitaxial crystal growth and, thus, are implemented a micron or more away from the 2DEG forming heterointerface. Ideality for the 2DEG heterointerface is a completely relaxed and planar GaN surface on which the lattice-strained barrier layer(s) can be grown. This condition, when using a silicon substrate, is the purpose for the

transition layers which allow the relatively gradual compensation of lattice and CTE mismatch between the substrate and the ideally relaxed, unstrained GaN layer. Generally, mobility is benefitted by the planar surface, allowing a more concise and direct conduction path within the 2DEG. Carrier concentration would be reduced if the piezoelectric contribution to the 2DEG were lessened by strain within the GaN crystal.

Once a relaxed GaN surface has been grown to sufficient thickness, barrier layers are grown which, combined with the immediately superficial GaN, are the functional layers of a III-N Ga-polar device, despite only representing a small fraction of the growth process time and crystal thickness. Establishing a relaxed planar GaN surface is the foundation on which Ga-polar devices are produced. Each substrate will require its own accommodating transition layers. 6H-SiC, for example, requires that AlN be the nucleating species due to the non-planar nucleation growth preferred by GaN on a SiC surface [17]. Once established, GaN may be grown with no other transition layers. Similarly, GaN cannot be grown directly on silicon due to the preferential formation of gallium silicide which locally deforms the planar growth surface and discourages further nucleation. Through the various requirements along the path for GaN growth as a basis for HEMT production, the ultimate goal of the efforts is to create a functional 2DEG.

Barrier Layer & The Two-Dimensional Electron Gas

The 2DEG is formed to compensate for a positive sheet charge produced by polarization differences of interfacing III-N materials [23]. Spontaneous polarization is inherent to the asymmetry of wurtzite crystals as they contain alternating sheets of Ga + N atoms which are spaced as close pairs with significant space between the paired sheets.

The combination of a close plane and a far plane of atoms on top of or below a given plane is the cause of this polarization as the electronic environment is different for either side of that given plane. The difference in this spontaneous polarization of the two materials at the interface can result in a net positive sheet charge which is compensated by the formation of a high concentration of electron states known as the 2DEG [23], [95]–[99]. Band bending occurs in response to the positive sheet charge to force the lower portions of the conduction band below the Fermi level, thereby allowing conduction band states to be filled [100], depicted in Figure 7. Additionally, piezoelectric polarization contributions to the overall charge density originate from strain due to differing preferred bond lengths within the crystal lattices at the interface [26], [96]. Both polarization contributors arise from the difference of material properties on either side of the interface. Intuitively, the greater the difference in material properties which contribute to these polarizations, the larger these contributions will be. It is well established that the defining 2DEG interface in traditional AlGaN/GaN HEMT structures develops a higher density electron concentration as the aluminum concentration of the barrier layer increases [23], [44], [96], [101], [102]. This relationship is shown in Figure 8Figure *8*.

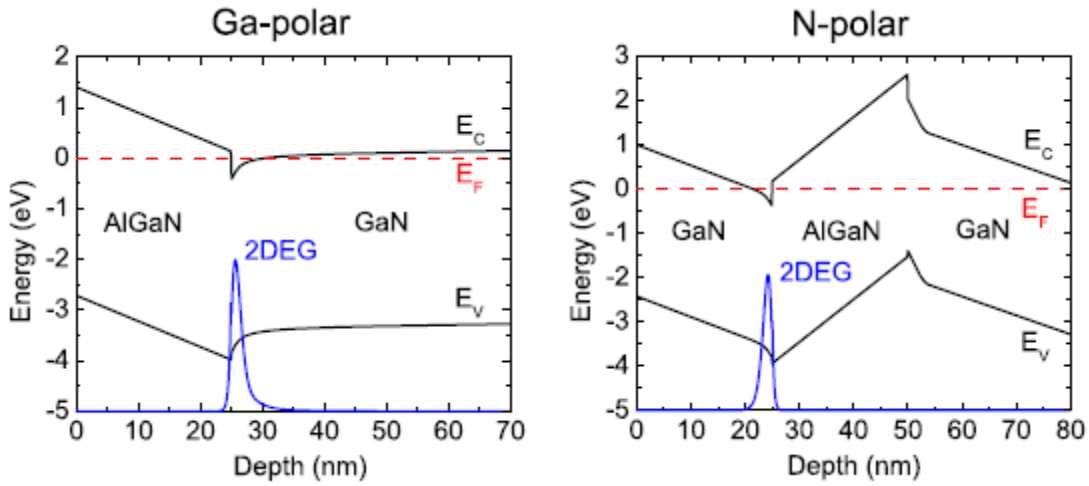

Figure 7. Band diagrams depicting band bending below the Fermi level [24].

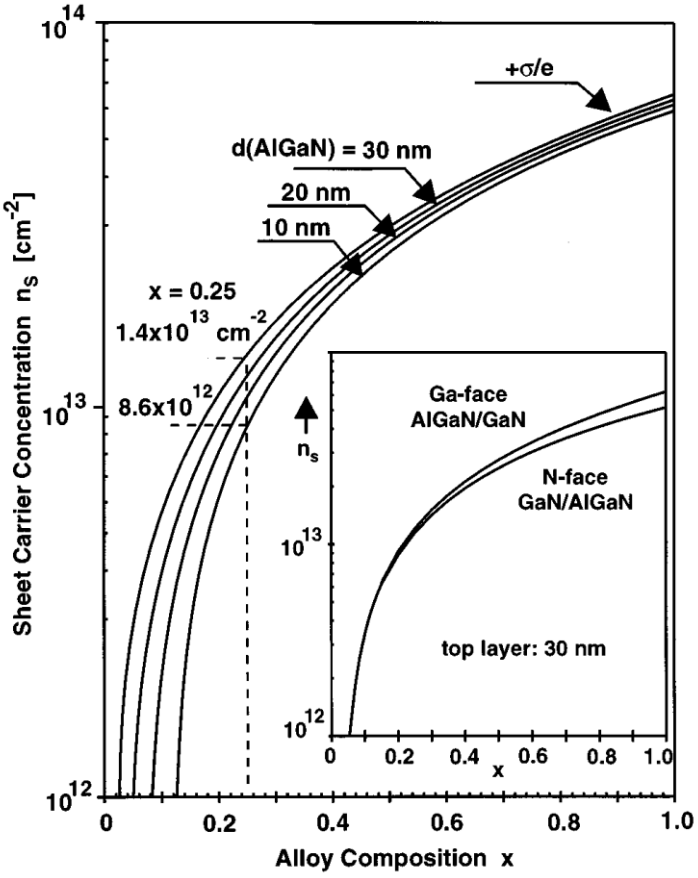

Figure 8. 2DEG carrier concentration increases with aluminum composition in the barrier layer [23].

In Ga-polar III-N based HEMTs, the 2DEG is formed just below the heterointerface and within the GaN interfacing with the more superficial III-N barrier layer. Utilizing this, GaN HEMTs have been incorporated in FET designs since the early 1990s [103]. An early MOCVD grown GaN-based structure comprising a 6000 Å single crystal GaN layer on sapphire with a thin AlN nucleation layer, provided an electron mobility of 350 cm^2/Vs [104]. The researchers grew the same structure with a 250 Å $Al_{0.13}Ga_{0.87}N$ film on the surface of the GaN producing an enhanced mobility of about 600 cm^2/Vs [103]. This preliminary work produced what must have been a 2DEG despite the device being particularly defective and fabricated with elementary techniques [105]. Following this initial effort, the 2DEG has historically been formed by the interface of an AlGaN barrier layer grown directly on a GaN surface. Originally patented in 1993 by M. Asif Khan and coworkers [106], the AlGaN/GaN heterostructure has served as the technological foundation for GaN based HEMT research and device optimization. Generally, MOCVD ternary growth can be challenging: AlGaN/GaN interfaces suffer from alloy scattering and issues surrounding a beneficial high aluminum content such as high growth temperatures, low V/III ratios and morphological issues due to non-planar growth regimes preferred by AlN and its alloys. Alloy scattering results from local non-uniformity of the ternary crystal composition at the GaN interface. While the AlGaN/GaN interface is well defined in the growth scheme, locally within the crystal the interface perceived by the GaN surface may be poorly defined. A typical prescribed AlGaN barrier may have an overall composition of 30 % aluminum [107]. That 30 %, while representative on the macroscopic scale, actually involves the inherent formation of local segregations of aluminum and gallium. Conceivably, pockets of gallium would

grow on the GaN surface extending its relaxed crystal structure away from the intended interface monolayer by monolayer. This scenario is visualized in Figure 9Figure *9*.

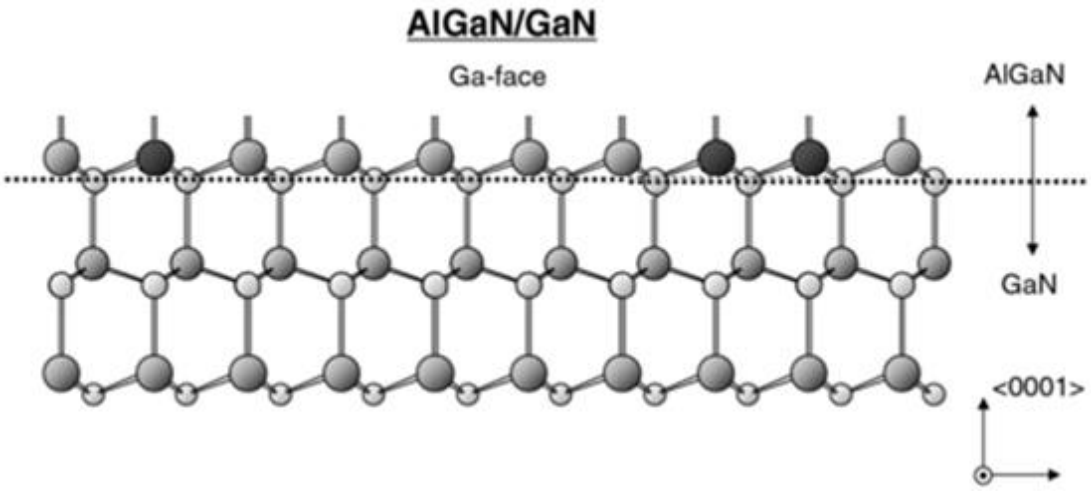

Figure 9. $Al_{0.3}Ga_{0.7}N$/GaN interface depicting the potential compositional non-uniformity of the AlGaN layer. The drawing of this wurtzite crystal structure contains three colors of atoms which correspond to nitrogen, gallium and aluminum in order of increasing darkness. The dotted line represents the intended AlGaN/GaN interface. The actual interface is poorly defined as illustrated by the non-uniformity of the AlGaN.

When such a region encounters aluminum, the expected polarization contributions to mobile electron states occur. The non-uniformity of such an interface will reduce the mobility of the resulting 2DEG as it deviates from its ideal planar configuration over the many monolayers necessary to transition to the AlGaN barrier [97]. Intuitively, increasing the aluminum content of the barrier layer will reduce the impact of alloy scattering, but the increased strain of such a layer of highly concentrated AlN in AlGaN on a GaN surface will suffer from strain induced band gap shrinkage, morphology / interface roughness issues, and relaxation events limiting the efficacy of the increased aluminum content [97], [108].

One solution to the problem of alloy scattering is the growth of a thin barrier interface layer of binary AlN directly on the GaN surface with an AlGaN layer superficial to the AlN of reduced aluminum composition so as to avoid approaching the critical thickness [102]. In addition to the reduction of alloy scattering and the consequential increase in planarization of the interface and therefore mobility, the spontaneous and piezoelectric polarizations of the higher aluminum interface increases the positive sheet charge and confines a larger concentration of electron states closer to the interface than in the AlGaN analog. Comparative data of the two HEMT structures are shown in Table 2. The improvement in mobility from the insertion of an AlN binary layer at the AlGaN/GaN interface is on the order of 30% [109]. The corresponding carrier concentration can be increased by roughly 20%, depending on the thickness of the AlN layer [108], [109].

Table 2. Comparative 2DEG metrics for the introduction of an AlN binary at the AlGaN/GaN interface. The data presented is temperature dependent. The plain text data is from room temperature Hall measurements and the bold text data is from measurements at 10 K [109].

300 K / **10 K**	Carrier Concentration (10^{12} cm^{-2})	Mobility ($cm^2/V*s$)
AlGaN/GaN	8.57 / **8.96**	1523 / **6032**
AlGaN/AlN/GaN	10.03 / **10.44**	1937 / **10700**

Despite the advantages of such a barrier interface layer, critical thickness limitations due to strain, and more fundamentally the difference in preferred bond length of the two binaries, can diminish the desirable qualities of the 2DEG through changes in the lattice at the interface such as deviations in periodicity caused by morphology changes, misfit dislocations, and cracking [110]–[116].

A strained heteroepitaxial layer will eventually reach its critical thickness which is dependent on the degree of strain, and in the case of an AlGaN/GaN interface – barrier layer ternary composition [110], [117], [118]. One solution to this design limitation in GaN HEMT structures is a latticed matched barrier layer which maintains beneficial compositional differences from GaN allowing the spontaneous polarization contribution to the 2DEG to remain while ideally mitigating thickness limiting strain. Such a layer incorporates the ternary Aluminum Indium Nitride (AlInN) [119]–[121] or the quaternary Aluminum Indium Gallium Nitride (AlInGaN) [99], [122]–[127]. Lattice matching is the practice of composing a barrier layer such that the average bond length parallel with the growth surface is equal to the relaxed GaN bond length. The functional attribute of these compositions is the indium nitride (InN) content which naturally has a longer average bond length than GaN. In an alloy with AlN, the larger lattice constant of InN can balance the average bond length of the alloy to match GaN. These lattice matched layers still utilize an AlN barrier interface to planarize the 2DEG and benefit from the piezoelectric polarization contribution to the carrier concentration. 2DEG improvements from such a ternary layer are seen in Figure 10. Improvements to both carrier concentration and sheet resistance of the 2DEG result from the lattice matched barrier layer. Barrier alloy properties can match to the interfacing GaN in three ways: lattice spacing, band gap, and polarization. The common three binary III-N alloy engineering options and their relative compositions are shown in Figure 11. The trends in III-N binary properties of band gap, lattice spacing, and polarizability should ideally include the remainder of the group III elements, particularly boron, enabling a new branch of III-N device design.

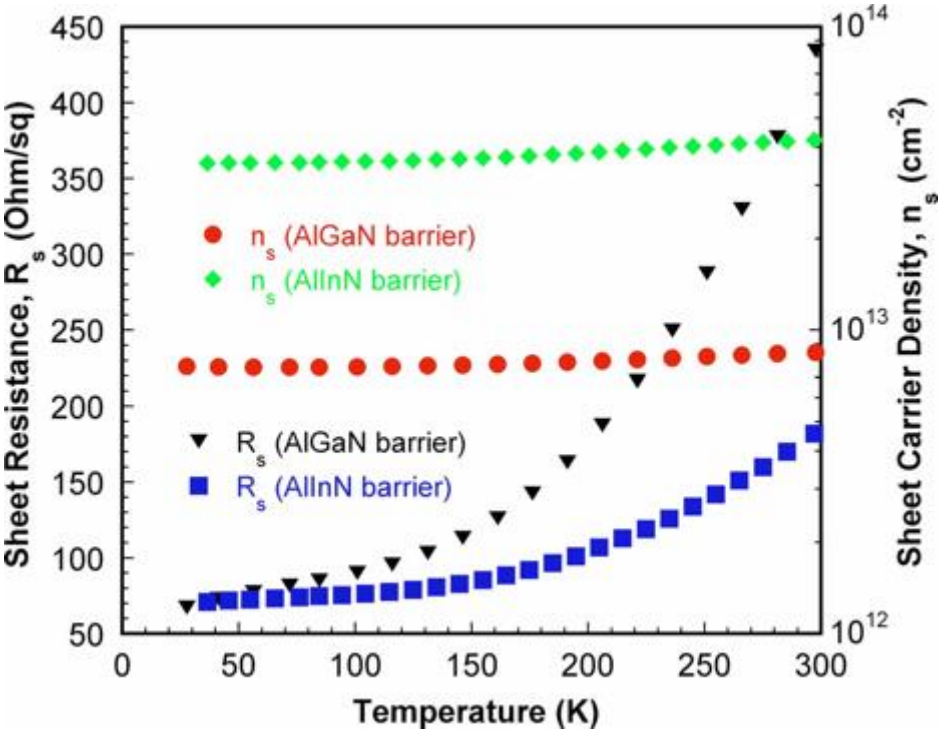

Figure 10. Carrier concentration and sheet resistance of AlInN/AlN/GaN vs AlGaN/AlN/GaN material stacks [121].

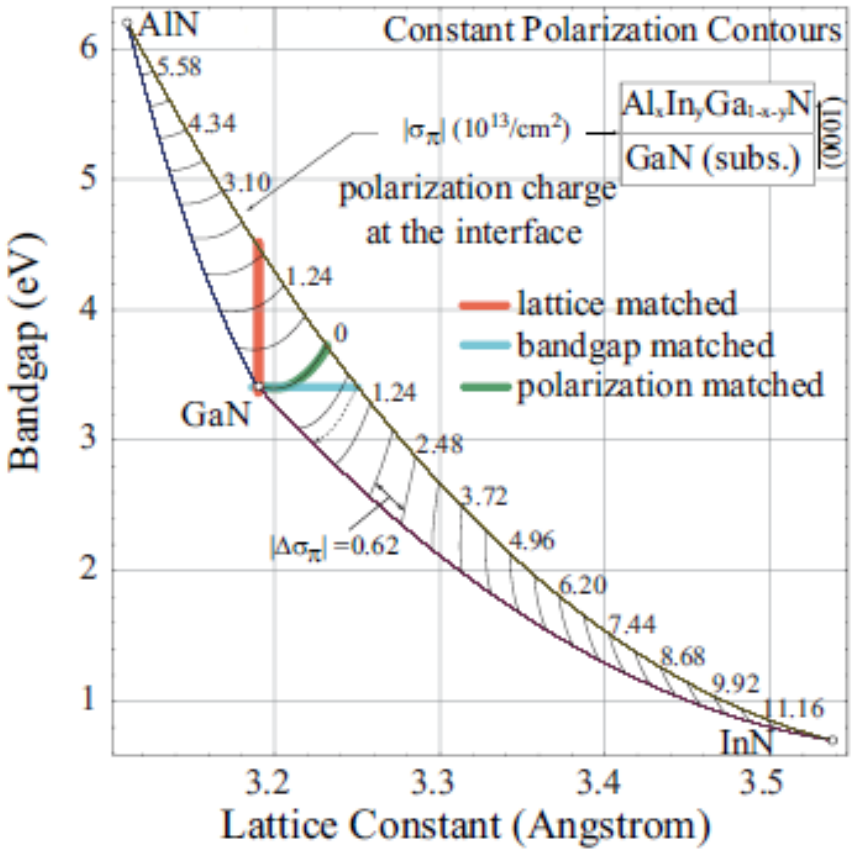

Figure 11. Polarization engineering of III-N alloys with matched interfacial parameters with GaN [99].

Boron Nitride

Boron Nitride (BN) is a versatile material with numerous phases which are used in a variety of applications. One of the more commercially viable epitaxial growth processes of BN is as a template for graphene [128], though the primary commercial use of crystalline BN is as a super hard abrasive material comparable to diamond for wear resistance, usually in the form of cubic BN (c-BN) [129]. Hexagonal-BN (h-BN) is very similar to graphene in that it can occupy a single monolayer and has lattice spacing similarities with graphene, serving as a functional template. Due to its planar, two-dimensional nature, h-BN has also found use as a mechanical transfer layer for III-V

materials [130], [131]. The individual planes of the crystal are weakly adhered and can be separated mechanically while leaving the superficial device layers intact. BN has also received attention as an ultraviolet photonic material due to its exceptionally wide band gap [132].

III. MOCVD

Metal Organic Chemical Vapor Deposition (MOCVD), for the purposes of this work is synonymous with Organometallic Vapor Phase Epitaxy (OMVPE). The general conditions to satisfy this growth technique are simple, though their manipulation to grow single crystalline compound semiconductors for use in electronic devices is quite complex. Generally, reactant species are brought together into the reaction chamber which contains a heated, rotating single-crystalline substrate. These species are meant to preferentially react on the surface of the substrate wafer such that only the condensed product of their reaction is added to the mass of the wafer. This preference is accomplished by significantly cooling all chamber surfaces, other than the reaction surface, which is heated so to sufficiently increase the reactivity of reactant gases near the surface. The reactant gases are injected via fine control of various input regions of the roof, or injector, of the chamber (in Texas State's MOCVD reactor design). The injector plate has periodic perforations, or nozzles, which resemble the multiple openings of a showerhead; as such it is referred to as the showerhead. Gas lines feed various regions of the showerhead to diffuse reactants uniformly across the chamber injector so to achieve a relatively homogenous distribution prior to entering the reactor's reaction zone.

The gas flows are controlled by software via digitally regulating mass flow controllers (MFCs) which operate via precise calibration to their prescribed gas species' heat capacity: metering flow through the minute heating of a small volume and monitoring that volume's temperature rise per the heat it received. This precise control is essential to optimize growth conditions necessary for III-N semiconductor growth by MOCVD. The gas streams contain the gas phase reactants at prescribed concentrations

so to achieve the desired compositions and growth rates of their solid product. Multiple MFCs, along with pressure controllers and valves, are located within a MOCVD system which control and direct gas flow to the reaction chamber in appropriate amounts at appropriate times and with spatial, radially symmetric, uniformity.

For the III-Ns, ammonia is the preferred source of reactant nitrogen. The control of ammonia flow is relatively simple. In the source tank, or cylinder, ammonia is a liquid whose vapor pressure is sufficiently high as to contribute a significant pressure of gaseous ammonia into the gas lines. This flow of ammonia is essentially pure and will be diluted with hydrogen during its delivery to the showerhead and reaction surface.

The pickup of organometallic vapor is more complicated. Each organometallic source is housed within a stainless steel container with a single input and single output. This design is inherently precautionary as most organometallic compounds are liquid at room temperature and pyrophoric: they will react rapidly and energetically with molecular oxygen or water. The inputs to these containers deliver a carrier gas, usually hydrogen, to the bottom of the container. This carrier gas will bubble up to the surface of the organometallic liquid forming an overpressure of mixed H_2 saturated with OM vapor at the top of the container. Hence, these containers are commonly known as ‘bubblers’. This overpressure serves to evacuate part of the saturated vapor through the outlet of the bubbler. The concentration of the output vapor is precisely controlled through the temperature of the organometallic liquid. The natural vapor pressure must be exploited to extract and exactly maintain the necessary reactant concentration and consequent molecular flow.

Precursor selection for use in the MOCVD growth of the III-Ns must adhere to specific requirements to be effective. Typically, the vapor pressure of a given precursor source is on the order of a few Torr to a few tens of Torr. The precursor must not react with or condense on any surface that would impede its progress towards the reaction chamber. The bubblers are kept in large baths of ethylene glycol and water which are constantly circulated while being heated or cooled appropriately to tightly maintain their desired temperature and precise OM vapor pressure. Once collected, the concentration of OM vapor goes through a MFC or pressure controller to stabilize the flow prior to introduction into the reaction chamber. A steady state flow is achieved by maintaining carrier gas input into the bubbler and dumping the vapor to the exhaust line until such a time as the reactant is needed in the chamber. Some OMs must be diluted further to best utilize them as MOCVD reactants. Altering the concentration and flow of OMs to the chamber is the most direct route to control the growth rate of a given layer, as the overall III-N growth rate is typically limited by the column III element concentration. The OM molecules will remain at approximately room temperature in the lines until, ideally, just above the reaction surface so to prevent premature OM decomposition and/or reaction.

The gas lines feeding the chamber are segregated into two main sections: the alkyl and hydride lines. Alkyl refers to the organo- part of the OMs as a generic alkane group and the hydride refers to the group V precursor's groups which are simply hydrogens. Reactant gases are segregated in this way until they reach the reaction chamber. Reaction ahead of the desired wafer surface would lead to unwanted deposition in the gas lines, thus it is beneficial to prevent mixture. This segregation allows for a wide range of different relative concentrations of group III and group V precursors in the chamber.

This key growth parameter is called the V/III ratio and is normally on the order of a few hundreds to a few thousands upwards of hundreds of thousands, for III-N processes. The need for such an excess of group V species is the difference in reactivity and volatility between ammonia, which is generally very stable, and the organometallics which decompose readily at the reaction temperature and are less volatile due to their size. A consequence of the difference in reactivity of the two reactant families is the amount of time a given molecule is active on the surface. This time is referred to as the molecule's dwell, or residence, time. This is a general concept for activated transition state stability and molecule movement. The reaction surface is intimately involved in incorporating material into the single crystalline lattice. The surface dwell time of the hydride species is markedly less than the alkyl. While transition state theory is a significant component in the III-N reaction chain, dwell time is more a consequence of molecular behavior than a factor which contributes to required V/III ratios.

A necessary factor for a generally high V/III ratio is the large overpressure of nitrogen species needed to tip the solid/vapor growth/decomposition equilibrium in favor of maintaining a solid with reasonable stoichiometry. For example, GaN will readily decompose to molecular nitrogen and metallic gallium at the reaction temperature. This decomposition is enhanced in the presence of molecular and atomic hydrogen, both of which are present at the reaction surface and will contribute to the formation of ammonia. An insufficient V/III ratio during the growth of GaN will result in nitrogen vacancies in the layer, or in the extreme, solid decomposition.

Reaction temperature is inherently the largest knob a researcher may turn. Every reaction intermediate is directly affected by temperature. Given the complexity of an

MOCVD reaction pathway, many possible iterations of the reaction intermediates between an OM and ammonia could become the preferentially stable product of the reaction. A sufficiently high temperature ensures that those intermediates will not only have enough energy to form, but will effectively incorporate into a solid. III-N binary or alloy growth is dependent on the temperature range to not only produce the desired solid composition but to maintain good crystallinity which is usually achieved at higher temperatures [133].

Pressure is also a more significant MOCVD parameter. Its impact on gas flow dynamics and precursor availability can alter reaction behavior and the resulting material properties. Increased pressure can generally increase growth rate through increased precursor availability [134], but a potential consequence is the increased probability of parasitic gas phase reactions leading to particles as is common for higher aluminum content alloys [135]. Pressure can also change the solid growth composition for alloys [134], [136].

Other MOCVD reactor conditions can play a pivotal role in the effective growth of the III-Ns. The majority of these conditions are reactor specific and include reactor geometry [137], gas flow direction [138], substrate rotation speed [139], and many more experimental design options.

MOCVD Growth of III-N Binaries and Their Alloys

The primary knobs, or control inputs, which one can manipulate to effect MOCVD growth are temperature, pressure, and V/III ratio. Each will affect the binary III-Ns; BN, AlN, GaN, and InN, differently due to the different electron affinities, and

the resulting thermal and chemical stability, of their group III constituents [140]. Trends exist along the group III column which correspond to a binary solid's thermal stability. The larger the group III atom, the less stable it is under high temperature, low pressure conditions. This is a consequence of bond strength which is determined by valence shell distance from the atomic nucleus which increases with the size and weight of the members of the group III column. Accordingly, decomposition rates in a vacuum for AlN, GaN, and InN increase exponentially at temperatures of 1040 °C, 850 °C, and 630 °C, respectively, as evidenced by a sharp increase in outgassed nitrogen at those temperatures [141]. This relationship is most appreciable in MOCVD growth as an ever decreasing preferred growth temperature going down the group III column as well as the corresponding need for higher ammonia concentrations to combat the position of the growth / decomposition equilibrium. Table 3 lists experimental ranges for the successful growth of BN, AlN, GaN and InN by MOCVD.

Table 3. MOCVD chamber conditions which successfully grew the prescribed wurtzite III-N. Both binary and alloy growth conditions are included with BN and InN data coming primarily from alloys due to a dearth of binary information for BN and a general incompatibility for InN binary growth due to ammonia's high thermal stability coupled with InN's low thermal stability. BN data include additional sp3 bonded phases which are non-wurtzite. Some alternative precursors are also included which are in line with the general MOCVD growth process.

	Temperature (°C)	Pressure (Torr)	V/III Ratio
BN	**750 – 1600** [142]–[152]	**52 – 100, 300** [142]–[148], [150], [151]	**20 – 70** [153] **300 – 1000** [145], [147], [148], [154] **1350** [151]
AlN	**850 – 1500** [48]–[50], [141], [155]–[163]	**41 – 50, 100** [48], [156], [158], [160], [162], [163]	**116 – 584** [162], [163] 1100 – 4000 [50], [158]
GaN	**525 – 1170** [48], [50], [135], [141], [156], [158]–[161], [164]–[166]	**41 – 200** [48], [49], [135], [141], [158], [160]	**1000 – 4000** [50], [135], [158], [161]
InN	**460 – 800** [141], [165], [167]–[173]	**37 – 300, 600** [166], [168], [170], [171], [173]	**5000 – 360000** [166], [168]–[173]

The table includes successful growth attempts resulting from a variety of research objectives. Some data points, most notably the higher pressure AlN and lower temperature GaN examples, are out of the general norm for those materials. Appropriate growth conditions for a given material need to be found empirically for a given MOCVD reactor.

Boron Nitride

BN has large ranges for temperature and V/III ratio. The most typical MOCVD-grown BN examples in the literature generally favor a relatively high growth temperature (1200-1500 °C) and a low V/III ratio (300-1000, more popularly 600-700) [131], [132], [147], [148], [154], [174]. It is important to note that the majority of that data comes from hot-walled MOCVD and other comparable deposition methods. There have been few reports of successful BN synthesis without high energetic assistance, such as plasma [175], [176] or ion bombardment [177], and those reports are generally of sp^2 bonded BN [148], not sp^3 hybridized as is necessary for wurtzite growth. One example of BN being grown on a wurtzite AlN surface produced sp^2 phase BN, but when very thin layers were grown, the resulting BN was not a particular phase, but consisted of mixed phases [148]. This verifies that the growing surface effects the BN growth phase and for extremely thin layer growth, the BN is likely to maintain a wurtzite arrangement when grown on a wurtzite surface. A group at Texas Tech University has grown BN directly on AlN and $Al_{0.62}Ga_{0.38}N$ [174]. This group was attempting to grow h-BN for its ultraviolet photonic properties. They reported having to grow a "BN buffer layer" in order to get adhesion of the h-BN to its wurtzite growth surface. This buffer layer, grown at 800 °C with a very similar deposition method as the presently researched MOCVD process, was grown in thicknesses that ranged from 20 to 140 nm in their experiments. Given that this buffer or transition layer was not the focus of the research; little attention was given to it for materials characterization. To accomplish their goal of h-BN growth on a III-N surface, they tested BN buffer layer thickness as it affects the material quality evaluated by the full width at half maximum (FWHM) of a h-BN's XRD peak. The results from their study are presented graphically in Figure 12.

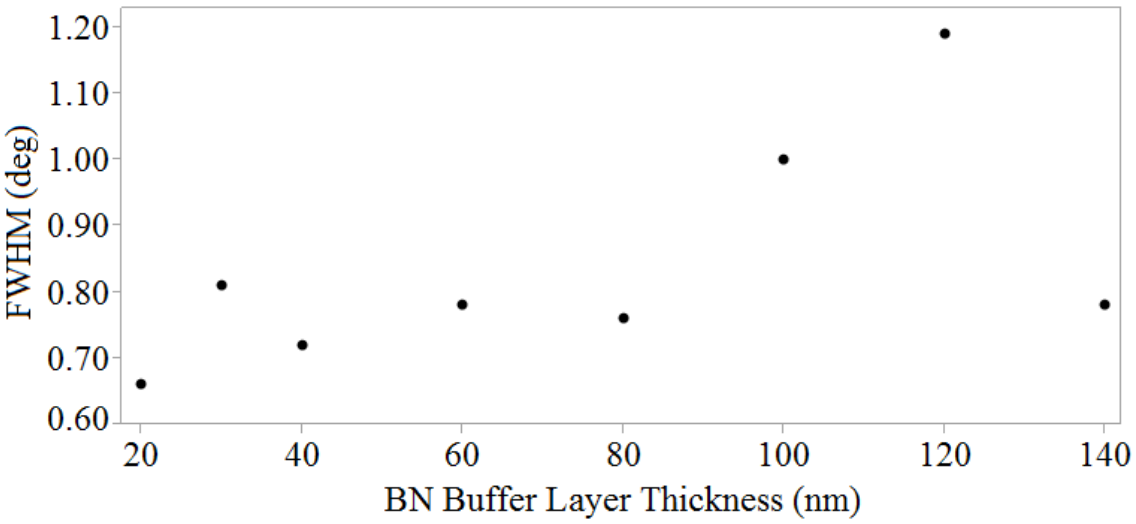

Figure 12. Study of BN buffer layer thickness grown on wurtzite surfaces and the resulting XRD FWHM of h-BN layers grown atop the BN buffer layers [174].

The FWHM of the grown h-BN is not entirely related to the BN buffer layer thickness, as the graph would indicate. This is likely due to inconsistencies in the BN growth behavior. An interesting observation is that the BN buffer layer is not observed in XRD measurements which resulted in the FWHM study. This is due to the lack of a precise phase over the 20 to 140 nm, which is essentially the goal of the layer, to phase transition from the wurtzite surface to h-BN. This is further evidence that a very thin BN layer grown on a wurtzite surface under MOCVD growth conditions may retain the growth surface's wurtzite crystalline structure.

Aluminum Nitride

The remaining III-Ns have considerably more information available as they have been incorporated in MOCVD growth for some time. Good crystal quality AlN generally favors higher temperatures, and lower V/III ratios [162]. The higher temperature is thought to improve aluminum atom surface mobility which allows for planar growth instead of the brainy island-like texture typical of high Al-content III-Ns. Higher

pressures have been known to produce a higher incidence of parasitic gas phase reactions for AlN and its alloys [135] though that scenario is not applicable in all reactors and growth conditions. Parasitic reactions are responsible for the preference of a lower V/III ratio. It has been reported that a lower V/III ratio results in a higher growth rate [163]. With the increased ammonia concentration comes an increased opportunity for parasitic gas phase reactions [136]. Figure 13 shows the dependence of the AlN growth rate on V/III ratio illustrating the impact of increased ammonia and the resulting Al precursor depletion on the growing film [163].

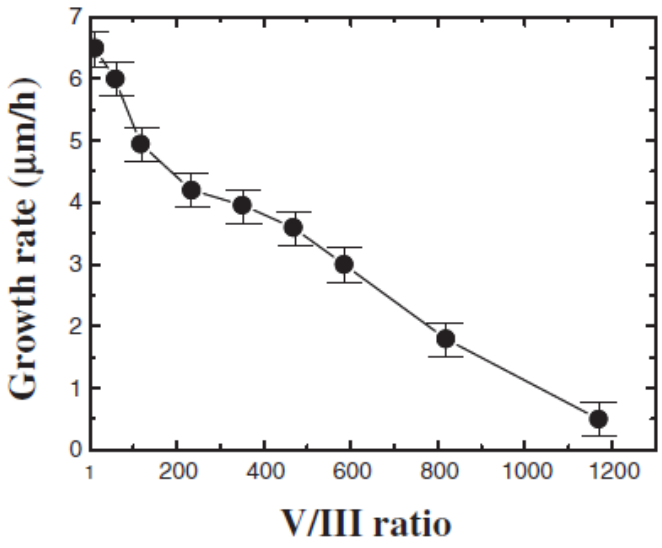

Figure 13. The dependence of growth rate on V/III ratio for AlN layers on c-plane sapphire substrates grown by high-temperature MOVPE. The growth rate reduction with increased ammonia concentration is due to competing gas phase reactions which limit the precursor available to incorporate into the solid film [163].

Gallium Nitride

Unlike AlN, GaN thermal decomposition occurs at a significantly lower temperature than MOCVD techniques require to properly utilize the reactivity of ammonia to grow GaN. This condition, as previously discussed, requires an excess of the nitrogen precursor to push the growth / decomposition equilibrium towards growth.

Generally, the V/III ratio needed to successfully grow GaN is over 1000 at temperatures around 1020 °C. At lower ratios GaN may successfully grow, but there is a high likelihood of a large concentration of nitrogen vacancies resulting from partial decomposition and desorption of nitrogen during growth which will diminish the quality of the grown crystal. Stoichiometric GaN is the ideal solid ratio. Certain reaction variables must be considered in the successful growth of stoichiometric GaN, most notably the equilibrium point for growth / decomposition. This equilibrium point is temperature specific and will favor decomposition at higher temperatures and lower pressures. Factors which contribute to this equilibrium point for MOCVD processes include gaseous precursor concentration, decomposition, diffusion to the growth surface, adsorption on the surface, available surface sites for bonding, surface diffusion for film incorporation, and desorption from the solid by thermal decomposition or catalytic dissociation [65], [78], [140], [141], [161], [178]–[187]. These factors hold true for all MOCVD growth of III-N materials, but as the parent material for the majority of III-N technologies, GaN is especially studied as its material quality holds the largest impact on device performance.

In regards to experimental design, factors such as surface diffusion and adsorption will be temperature specific and others such as precursor concentration and solid film composition will be controlled by the V/III ratio. These two variables play a significant role in the material quality of MOCVD grown GaN. Figure 14 illustrates the relationship between the V/III ratio and growth temperature as it pertains to GaN material quality and resulting material properties [178]. As discussed, an excess of the nitrogen precursor is necessary to grow good quality material. This excess is on the order of 1000x due to the

differing activation rates and dwell times of the two reactant species which both favor the group III species.

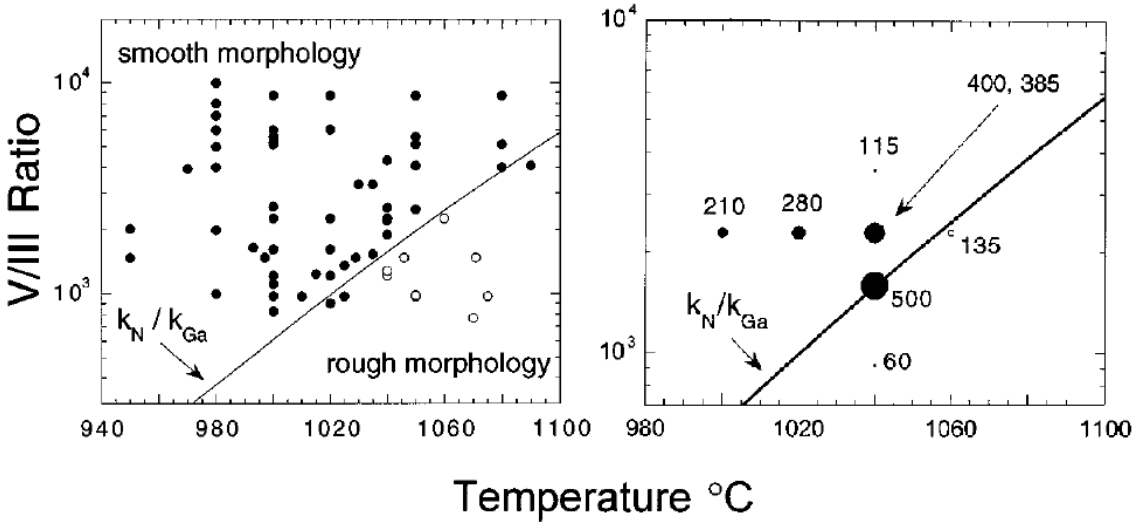

Figure 14. V/III ratio vs growth temperature for MOCVD grown GaN. The solid lines represent the calculated equilibrium for desorption of nitrogen and gallium and is the condition where both species' desorption rates are exactly equal indicating that after a desorption event or many, stoichiometric GaN will persist in the solid. The left graph, compiled by [178], depicts the surface morphology of GaN films grown under various conditions. Open circles indicate a rough appearance and filled circles indicate a smooth appearance. Samples to the left of the solid line have satisfied the decomposition rate of nitrogen, those to the right have a nitrogen deficit resulting in film roughness. The right graph relates the material properties with material performance [178]. Open circles indicate rough surface morphology, filled indicate smooth surface morphology. The size of the circles and the corresponding numerical value represent the measured mobility of the grown films. The best mobility exists on the equilibrium line indicating a stoichiometric GaN is ideal for material quality. The reference gives further data to support the relationship between stoichiometry and optimized material properties.

The left graph in the figure shows the impact on surface morphology. As the V/III ratio is reduced for a given temperature, a condition exists such that the desorption of nitrogen from the solid dominates the desorbed species. Below this condition, nitrogen vacancies will become prevalent and degrade material quality. The solid line in the graphs represents equilibrium for stoichiometric concentrations of Ga and N in the desorbed species. Logically, if the rates of the two species leaving are equal, then the

stoichiometric solid will not change its overall composition after desorption. The right graph Figure 14 illustrates the impact of material quality on material properties. The circle sizes corresponding to the accompanying numbers indicate the mobility of a grown GaN film under different conditions. The best mobility comes from layers grown close to the equilibrium line which implies the stoichiometric composition of GaN produces the best material properties. This is mostly intuitive, but is still a significant point to make when discussing GaN growth by MOCVD.

Indium Nitride

Indium nitride thermally decomposes at an even lower temperature than GaN. Decomposition occurs in a nitrogen ambient between 550 – 600 °C [188] and under MOCVD reaction conditions as low as 510 °C [171]–[173]. The dissociation of ammonia to produce the necessary reactant nitrogen at this temperature is quite poor. Evidence shows that ammonia dissociation is less than 0.1% at 780 °C [189], not reaching even a few percent until ~900 °C [161], [190]. As such, the V/III ratio needed for even modest InN growth is orders of magnitude higher than other III-Ns. As an example, InN growth on GaN on sapphire by MOCVD at 500 °C with a 145,000 V/III ratio resulted in indium droplet formation due to the lack of available nitrogen for incorporation [173]. An increase in growth temperature to 550 °C with the same reaction conditions in the same reactor resulted in an InN film without indium droplets. The availability of dissociated nitrogen from ammonia is a major limiting factor for InN binary growth by MOCVD. The decomposition of any III-N is enhanced by the presence of atomic or molecular hydrogen which facilitates nitrogen desorption in the form of ammonia, as previously discussed. While this effect is generally overcome by normal

MOCVD V/III ratios for other III-Ns, the presence of hydrogen in an InN growth environment inhibits growth dramatically [189]. To overcome this effect, an inert gas, usually nitrogen, is used as a carrier gas for the indium precursor, trimethylindium (TMI), and for the remainder of gas flows into the reactor.

Alloys

Since each III-N binary favors different ideal growth conditions, alloy growth must be achieved through some compromise of intermediate growth conditions of its constituents. Additionally, when creating a material interface or switching from one material growth to another, growth conditions for the first layer may be quite different from the interfacing material's. One must consider the impact changing those conditions may have on overall material quality at the interface and eventual device performance. The consequence of changing growth conditions is time. Time may allow a potential growth surface to rearrange and become less ideal for the interfacing material growth or may allow a change in surface composition due to decomposition of a stagnant film at growth temperatures. Altering growth conditions during the growth of a layer can cause inconsistent growth behavior due to variation in MFC and pressure controller behavior during a ramp. The need for a stable growth environment for repeatability necessarily conflicts with optimizing material growth when creating an interface. A reasonable solution is to grow the new layer atop the old until layer nucleation and coverage is complete to protect a given surface. Over a long enough ramp, slight hardware fluctuations can be negligible in regards to repeatability.

MOCVD grown III-N ternary alloys are traditionally limited to AlGaN, AlInN, and InGaN, given the scarcity of boron and thallium in common MOCVD practices.

Each alloy is very important to III-N technology in its own way. AlGaN is used as a transition layer to address lattice mismatch and CTE mismatch from non-native silicon substrates allowing for the cost-effective production of relaxed GaN and GaN based devices. AlGaN is also the primary barrier layer used to generate a 2DEG for HEMT structures. AlInN is used as an alternative barrier layer which can be lattice matched to GaN thanks to the combination of InN's longer preferred bond length and AlN's shorter preferred bond length, relative to GaN [119], [120], [191]. A lattice matched barrier layer minimizes the potential for strain induced failure mechanisms. InGaN is arguably the most important of the three common ternaries. InGaN can theoretically be used in light emitting devices to cover the entirety of the visible wavelengths and also has the potential to cover a very large range of wavelengths for photovoltaic applications. The combination of GaN's band gap which can produce band edge emissions just outside of the visible spectrum into the ultraviolet, and InN's band gap which is much smaller can produce photons in the infrared, can theoretically produce alloy compositions which could have band edge emissions at any energy level within the visible spectrum.

Growth of ternary III-Ns is subject to compositional limitations and internal strain as a result of the differing properties of the combined binary materials. The general trends associated with the binaries are a road map for preferred compositional growth. As compared to GaN growth conditions, aluminum incorporation into AlGaN benefits from higher growth temperatures for better AlGaN material quality peaking around 1300 °C [162], [163]. This is believed to be due to increased aluminum surface atom mobility allowing for better alloy homogeneity within the crystal [161] and better lateral growth [165]. The consequence of this relationship is at lower growth temperatures increased

aluminum composition will decrease material quality [192]. Since AlN needs a lower concentration of nitrogen precursor for effective growth, it is the GaN V/III ratio which is generally used for AlGaN growth. Internal strain within an alloy and mismatch with its growth surface can limit the composition of the more foreign group III species. For AlGaN the similarities between AlN and GaN preferred bond lengths and thermal stability are such that this type of limitation is not generally seen and instead the solid AlGaN composition is determined by the gaseous composition of the two group III precursors with a moderate preference to solid aluminum incorporation relative to the gas phase at 1000 °C [141], [155], [193]. Figure 15 shows this preference towards aluminum incorporation into the solid AlGaN when compared to the ratio of TMA to total group III species within the reactor [141].

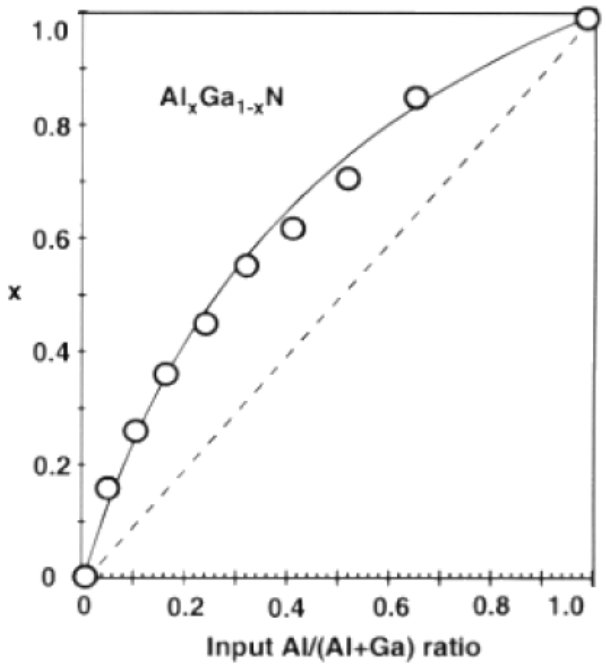

Figure 15. Data for solid AlGaN composition vs relative gas phase ratio of TMA / (TMA + TMG). The dashed line represents the one-to-one incorporation rate. Experimental data indicate a preference for aluminum in the solid relative to the gas phase availability of the group III species [141].

AlInN is an interesting combination of two III-Ns which prefer very different conditions for optimal growth as a consequence of their difference in material properties such as lattice spacing and thermal stability. Its benefits as a barrier layer were discussed previously. Successful growth must be achieved through compromise of AlN and InN growth conditions. Employed growth temperatures are traditionally in the upper regions of tolerance for InN, approximately 700 – 800 °C [121], [136]. A lower temperature will benefit indium incorporation, as expected from the binary growth trends [134]–[136]. V/III ratios can cover a broad range and generally favor aluminum incorporation at low ratios and disfavor it at high ratios due to the previously discussed parasitic gas phase reactions. By the same token, lower pressures give preference to aluminum incorporation while higher pressures increase the likelihood of the parasitic gas phase reaction between TMA and ammonia which favors indium incorporation [135], [136].

InGaN benefits from a lower growth temperature for indium incorporation into the GaN crystal and is generally grown in the 600 – 900 °C range [161]. This window is necessarily narrow as it is limited on the low end by ammonia reactivity / activation and the high end by InN decomposition. InGaN must be grown with increased V/III ratio, relative to GaN, for indium incorporation to accommodate the preference for nitrogen desorption from the film. Like the other III-N ternaries, InGaN compositions can be controlled by altering the growth temperature. Generally, increases in temperature will decrease indium incorporation into the solid InGaN. Figure 16 illustrates the severity of the relationship between InGaN composition and growth temperature at a constant TMI / (TMI + TMG) ratio of 0.4 [135].

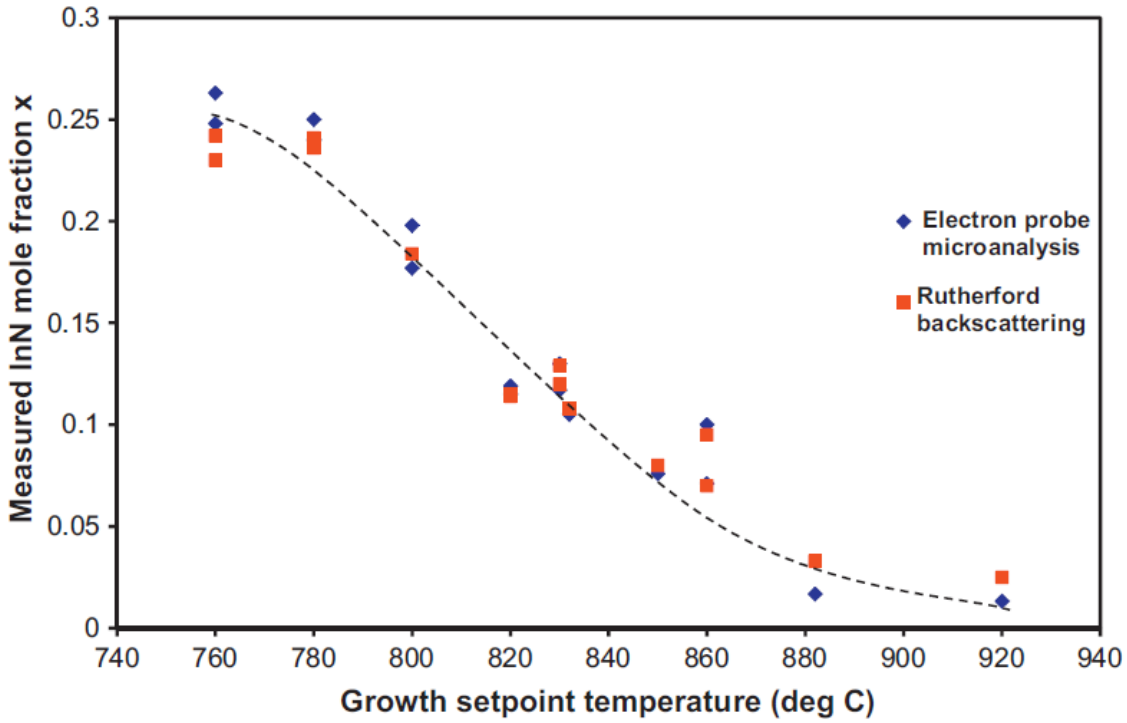

Figure 16. Data for solid InGaN composition vs growth temperature. The TMI / (TMI + TMG) ratio was constant at 0.4 for all growths. Deviating from the lower growth temperatures preferred by InN reduces the InGaN indium composition significantly in this growth temperature range. Poor thermal stability and the resulting thermal decomposition of InN is the fundamental cause for this relationship [135].

At growth temperatures below 600 °C the indium incorporation into an InGaN film is a linear function of the group III precursor gaseous ratio, but above 600 – 700 °C the solid composition efficiency is no longer linear and is limited to low absolute indium compositions when grown on a GaN surface [133], [141], [194].

Quaternary AlInGaN has applications in polarization engineering for lattice matched barrier layers [123]–[125]. Creating a quaternary, as opposed to a lattice matched AlInN, alleviates some compositional limitations of mixing indium and aluminum and improves device performance metrics [124]. A HEMT stack with reduced polarization using a lattice matched barrier can also be used to create a normally off

device, also known as an enhancement mode device [126]. Growth conditions for a quaternary AlInGaN layer will not significantly deviate from the AlInN conditions as the added GaN component is the natural intermediate of both AlN and InN.

Boron containing III-N alloys are not commonplace in industry. Wurtzite BAlN [142]–[144], [150], [195]–[199], BGaN [142], [146], [149], [195], [196], [198]–[201] and various quaternaries [195], [200], [202], [203] can be found in the literature. Alloying boron with the other III-Ns is more challenging than other alloy growth due to the large lattice constant mismatch of wurtzite BN with AlN, GaN and InN. The difference is so large that the other three III-Ns are very similar to one another in comparison with BN. Figure 17 illustrates the magnitude of the material differences between the four binary III-Ns. The lattice constant differences between BN and every other III-N are much larger than any other difference found within the III-Ns.

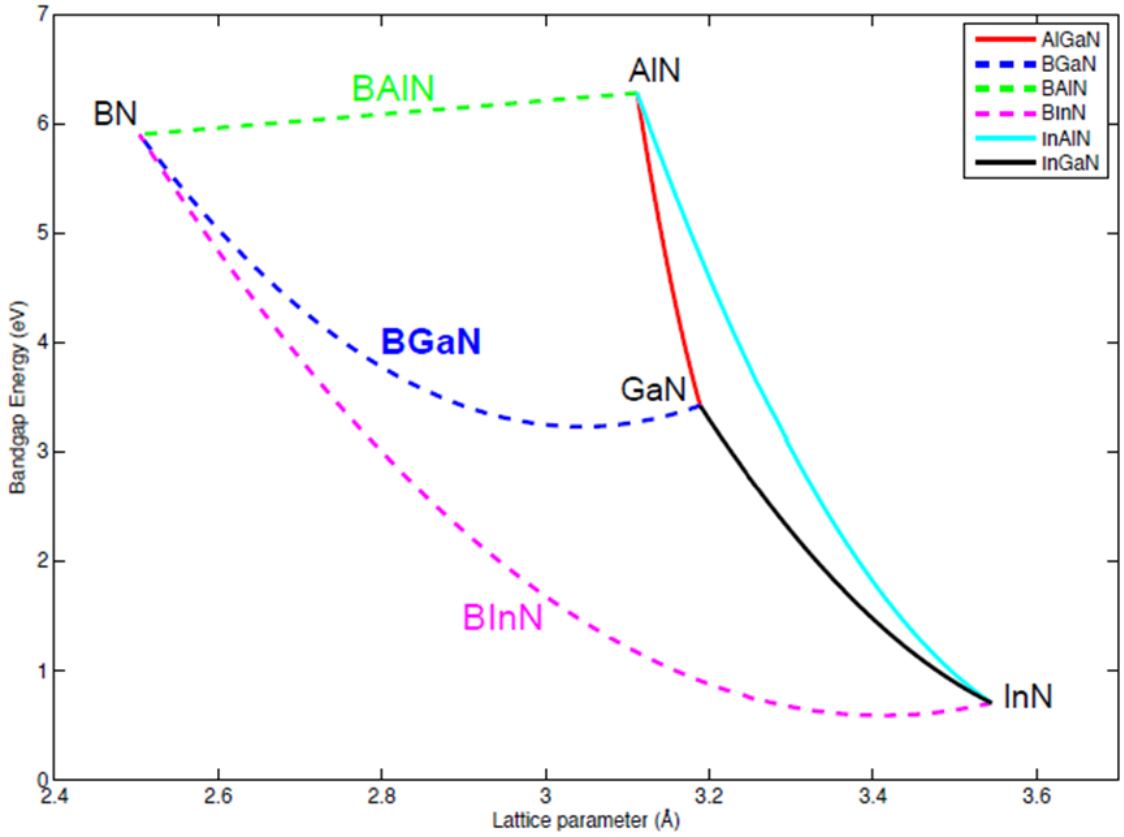

Figure 17. Lattice parameter along *a*-axis vs bandgap energy for wurtzite BN, AlN, GaN, and InN. The curved lines indicate band bap bowing along ternary lines. BN's substantially smaller lattice parameter sets it apart from the other III-Ns [204].

As a result of the large material differences, boron containing III-Ns will incur substantial internal stress such that the group III species are likely to phase separate into high boron and low boron content alloys [142]. Wurtzite BAlN and BGaN alloy composition limitations have been diagnosed directly from grown material and theoretical calculations in the literature. Phase separation into the high and low boron content alloys or away from the wurtzite configuration to a mixed-phase crystal are often the result of exceeding a critical thickness for a given composition. Experimental data for MOCVD grown BGaN has shown a maximum solubility of boron in BGaN of 1.8%, while maintaining a single phase crystal [142]. BAlN composition limitations were

calculated from this data set resulting in a maximum of 2.8% boron incorporation. The BGaN material used as a basis for this calculation was grown for an hour at 1000 °C. With this growth time, any III-N layer should be allowed to adopt its thermodynamically preferable phases. The long growth approach used in these growth efforts and resulting calculations allows for the determination of a thickness-independent minimum stable boron incorporation for the two alloys grown with traditional MOCVD conditions. The higher AlN boron incorporation when compared to GaN is explained by the more similar material properties of AlN with BN. While AlN and GaN are both quite different from BN, AlN is the more similar of the two, hence the higher allowed boron incorporation rate.

Flow-rate modulation epitaxy was used to grow BAlN films on SiC substrates [144]. This method encourages alternating III-N atomic layers to be grown simply because the surface is alternately exposed to each group's precursors in series. The composition of the grown wurtzite BAlN was between 1.5 – 2% boron. The grown films were found to maintain a single phase up to 500 nm of thickness, beyond which the films adopted mixed phases. Of greater interest to the application of boron containing films into GaN based HEMT structures are the compositional limitations of very thin films. Another example of flow rate modulation epitaxy incorporated thin BAlN into superlattices of AlN/BAlN [197]. The boron composition of these BAlN layers was measured at 11%. The grown layers were deemed too thick at this concentration to be monocrystalline. The authors indicate that at this concentration, the STEM images suggest that the critical thickness of BAlN is around 5 nm. They specify: "for different applications, a compromise can be achieved between thickness and boron composition."

They go on to mention: “For ultra-thin layers such as MQWs or strain engineering superlattices, high boron incorporation can be used allowing a large design freedom and it can still be kept as monocrystalline for its thin thickness (below 10 nm).” For thinner boron containing alloys, a metastable boron concentration can be achieved by keeping the thickness of a layer below the critical thickness [197].

Critical Thickness

Critical thickness depends directly on the strain of the layer in question which is often a result of lattice mismatch with its underlying growth surface. The higher the lattice mismatch the more strain is imposed on the layer as a function of overlying layer thickness. Thus, the more strain imposed within a layer the thinner the critical thickness. While this concept seems generally intuitive, the impact it has on 2DEG properties within a GaN HEMT can be significant. In the commercial GaN HEMT incorporating an AlN barrier interface layer, the concept of critical thickness directly applies to the 2DEG inducing AlN layer and the more superficial barrier layers. Figure 18 shows Poisson-Schrödinger simulations for an AlN/GaN interface without additional barrier layers [205]. The figure’s upper half shows the changes to the conduction band at the interface and its response to increases in thickness of the strained AlN layer in the form of an ever deepening dip below the Fermi level. The area of this dip represents the available states filled by the 2DEG and resulting carrier concentration. The lower half of the figure shows the corresponding distribution of 2DEG electron density accompanying the conduction band dip below the Fermi level as a function of depth from the material surface and thickness of the strained AlN layer. The left half of the figure ignores the

bandgap related consequences associated with a strained layer. The right half includes the changes to the band gap as a result of strain. With a tensile strain applied to the AlN, which is effectively lattice-matched to the GaN at the first monolayer, the natural band gap will shrink as the density of the layer is reduced. This phenomenon is known as band gap shrinkage.

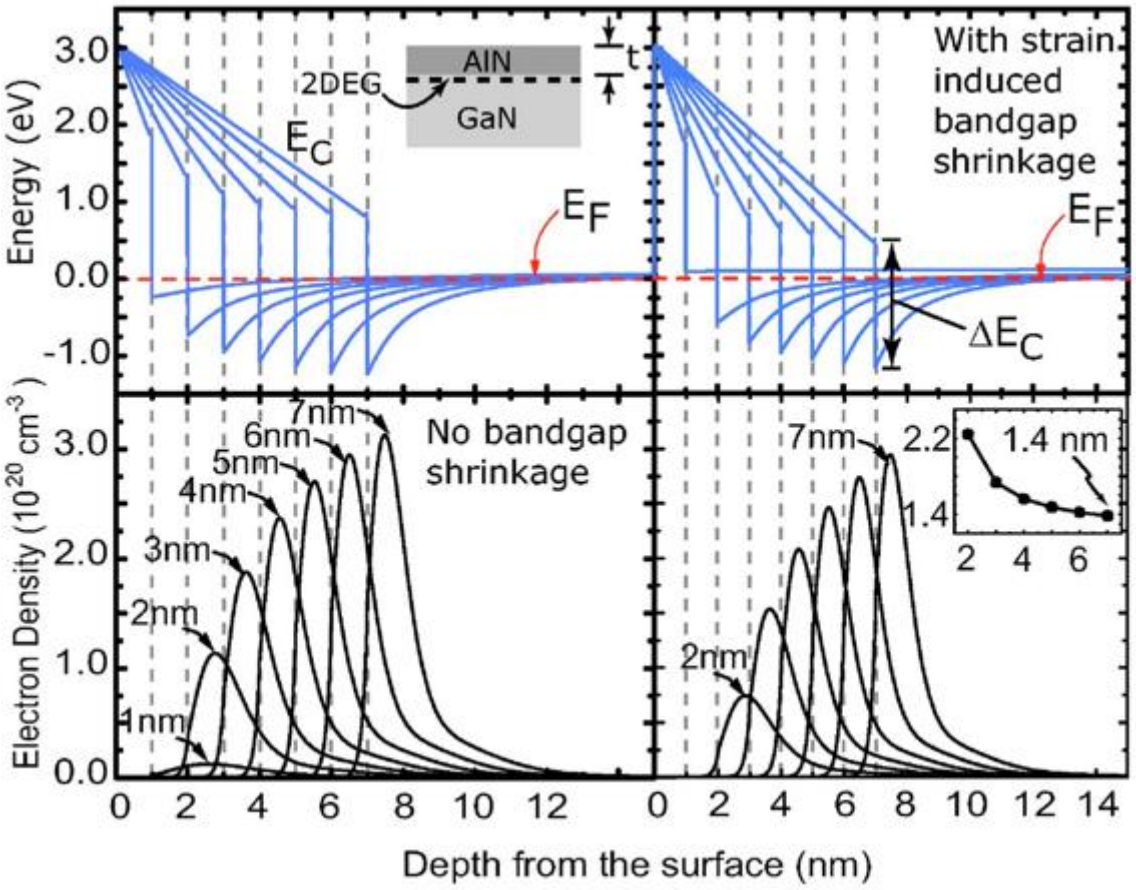

Figure 18. Poisson-Schrödinger simulations for an AlN/GaN interface where no barrier layer is grown atop the AlN barrier interface layer [203]. The x-axis is the depth of the 2DEG electron density from the surface of the AlN. The lower two sections show electron density as a function of depth and AlN thickness; the black thickness indicators at the electron density peaks are the AlN thicknesses responsible for inducing the 2DEG. The upper two sections show the behavior of the conduction band and its relationship to the Fermi level. The left two sections do not take into account the band gap shrinkage due to lattice periodicity changes caused by the tensile stress on the layer; the right half of the figure does take those changes into account, effectively illustrating the consequence of the band gap shrinkage of the strained layer on 2DEG properties.

The consequence of band gap shrinkage is that smaller thicknesses are less effective at inducing a 2DEG due to the reduced dip of the conduction band below the Fermi level, and any given thickness induces a lower density 2DEG relative to unstrained calculations by the same token. The band gap of a tensilely strained thin film will naturally decrease as the periodicity of the film is forced to deviate from its relaxed state. The peaks of electron density in the lower half of the figure initially increase non-linearly in height as the AlN becomes thicker. This is due to the establishment of the piezoelectric contribution coupled with the increase in spontaneous polarization. The peak height increase becomes more linear as the piezoelectric contribution levels off and the spontaneous polarization continues to increase. This leveling off may be due to the AlN/GaN interface reaching an equilibrium as the tolerance of GaN to be compressed is reached and the stress induced by further growth only encourages AlN internal stress to increase leading up to its own tolerance limit which is the essence of its critical thickness. The continued increase in spontaneous polarization is supported by the inset in the lower right portion of Figure 18. This inset represents the depth of the electron density peak relative to the thickness of the AlN layer. As the layer gets thicker, the 2DEG gets closer to the AlN/GaN interface due to an increase in positive sheet charge accumulation which, as discussed, is the effect spontaneous polarization has on III-N interfaces. These simulations predicted an AlN critical thickness, when grown on GaN, of ~6.5 nm. Accompanying experimental structures indicate that AlN surface morphology is smooth (roughness $\leq$ 0.4 nm) up to 6 nm AlN thickness at which point the roughness dramatically increases without visible cracks indicating stress induced morphology change ahead of detrimental cracking which becomes apparent at sample thicknesses of 7

nm and beyond [205]. AFM scans from the experimental structures are shown in Figure 19.

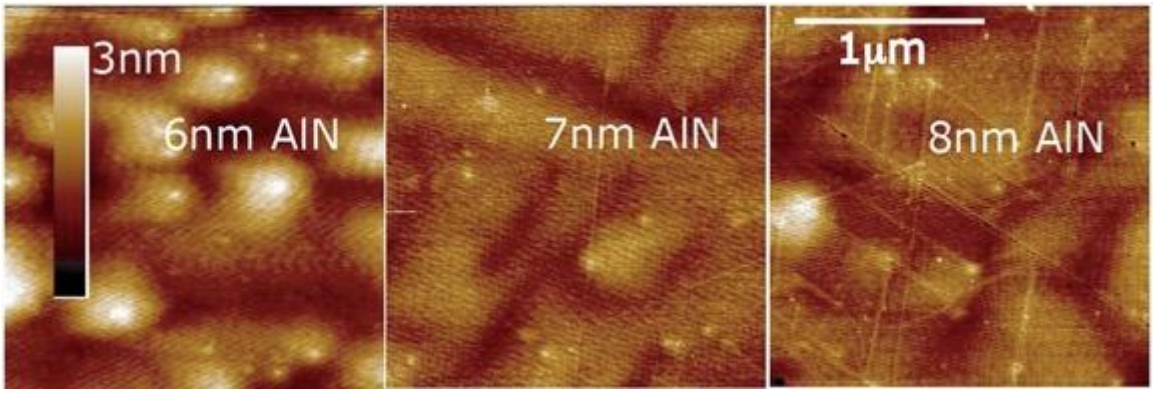

Figure 19. 2 x 2 µm AFM scans of thin MBE-grown AlN/GaN samples. Left: morphology changes precede relaxation events approaching the critical thickness; center: cracking becomes evident as relaxation events occur when reaching the layer critical thickness; right: cracking dominates the layer as critical thickness has been exceeded.

The modeled electron density in Figure 18 for the AlN thickness of 7 nm is greater than the 6 nm layer. This should be counter intuitive since the 7 nm thickness is above the critical thickness used in these calculations. In addition to the increased spontaneous polarization contribution of the 7 nm film, the density increase is due to the relaxation of the AlN in response to misfit dislocations (a consequence of exceeding the critical thickness) at the interface. This relaxation alleviates some tensile force on the film, increasing the band gap of AlN as it relaxes towards its natural unstrained density which increases the conduction band offset intensifying the conduction band dip below the Fermi level. It is reasonable to relate the discussion of the critical thickness of AlN on GaN and the resulting behavior of the 2DEG to a potential BN/GaN interface. The two interface types are both binary/binary and will be heavily strained. The expected difference between the two interface compositions lies primarily on the increased lattice mismatch. This mismatch, responsible for the piezoelectric contribution to the 2DEG

will induce an equilibrium point for GaN compression tolerance more quickly with BN/GaN, as compared to AlN/GaN, as such the former will reach a critical thickness more quickly than the latter.

Other material differences of the two interface compositions to consider are the potential change to 2DEG mobility and the band gap offset. The mobility should not significantly change as the conducting region is still confined within the GaN side of the interface and the presence of a non-gallium containing barrier interface will eliminate mobility issues associated with alloy scattering from a gallium containing barrier interface such as AlGaN. A potential change to 2DEG mobility could be due to the increased BN bond strength relative to AlN. BN dissociation energy is approximately 30% stronger: 389 kJ/mol compared to the dissociation energy of AlN at 297 kJ/mol [206], [207]. This increased bond strength would discourage boron diffusion into the underlying GaN or into the superficial barrier layers which would contribute to interface roughness. The theoretical decrease in interface roughness of BN/GaN, relative to AlN/GaN, would increase mobility by decreasing the resistivity of the conducting 2DEG region by encouraging planarity. The smaller size of boron may counter this benefit. It has been reported that aluminum can and will diffuse into GaN at AlGaN/GaN and AlN/GaN interfaces [208]. Boron should behave similarly. The increased BN bond strength should discourage diffusion frequency, while the decreased atomic radius of boron should allow a diffusing boron an easier diffusion path, potentially increasing its diffusion distance over a given time period.

The differences in band alignment between AlN/GaN and BN/GaN should be minimal aside from the increase of interfacial strain causing a decrease in the lattice

concentration relative to unstrained BN decreasing the band gap more significantly per unit thickness when compared to AlN. Wurtzite BN has a band gap that is reasonably comparable to wurtzite AlN. Literature values span an energy range of roughly 3 eV (5.0, 5.2, 5.23, 5.81, 5.5, 6.39, 6.86, 7.21, and 8.06 eV) [209]–[215]. The nature of the band gap is also fairly well disputed. An indirect band gap, usually in the lower values of the range, is generally favored, but not agreed upon. Figure 20 shows proposed band gap alignments of III-N binaries [216]. The magnitude and relative levels of wurtzite-BN and AlN band gaps reported in this reference are almost identical; as such, other than strain induced shrinkage of the band gap, no other significant material difference is expected in regards to band alignment, though significant assumptions regarding the BN band gap must necessarily be made until empirical evidence contradicts the assumptions.

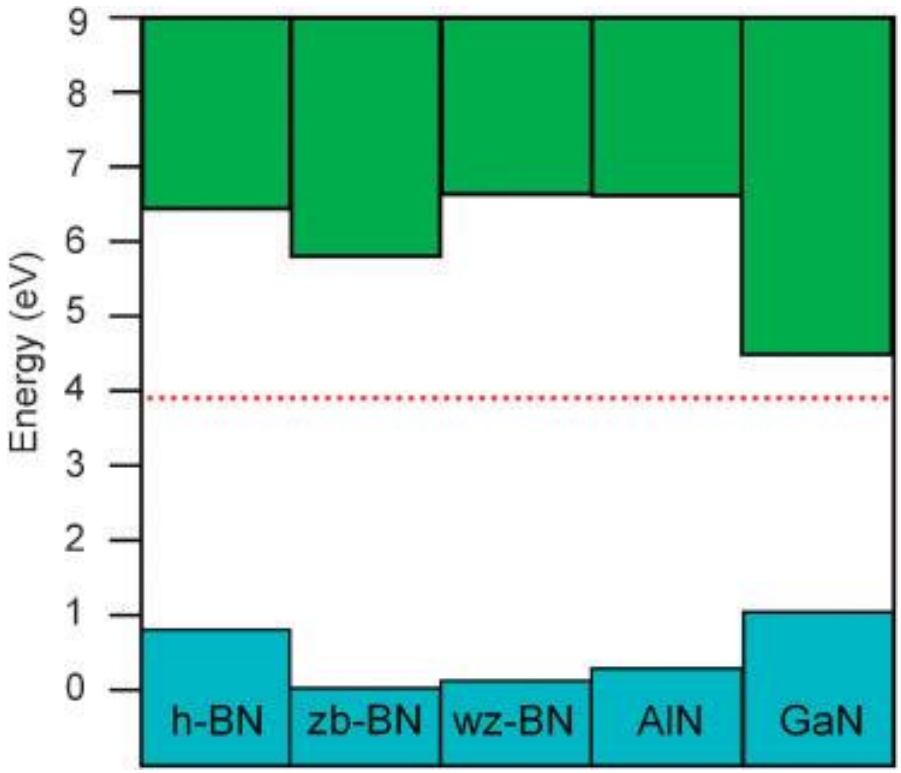

Figure 20. Band alignments of III-Ns [216].

The primary benefit of the proposed BN/GaN interface is the increase in piezoelectric contribution to the 2DEG. The piezoelectric effect results from the difference in average bond length in a direction perpendicular to the growth plane between the two materials of the 2DEG interface. Generally, the relaxed GaN surface imposes a tensile strain on the more superficial barrier layer which is often composed in part of an AlN alloy whose average preferred bond length is shorter than GaN. In turn the barrier layer imposes compression on the GaN surface layers causing their average bond lengths to be shorter than would be required by the relaxed crystal thereby altering electron energies of the shortened bonds [217].

Spontaneous polarization is inherent to the structure of the wurtzite crystal. The alternating planes of group III and group V atoms which are asymmetrically spaced create an electric polarization between the closely spaced and farther planes of heteroatoms on either side of a given atom / plane of atoms. The wurtzite III-Ns have different spontaneous polarization strengths due to the varying electronic structures of their group III constituents. AlN, GaN, and InN generally have well-accepted values for spontaneous polarization, though the method of calculation can change the value, while BN has a less established value. Table 4 lists literature values for the spontaneous polarization of the III-N binaries. Values bolded are noted as the most commonly used for AlN, GaN, and InN. BN has a very large range and does not have a commonly accepted value.

Table 4. Spontaneous polarization values for wurtzite III-Ns. Bolded values are the commonly accepted and used values for the various binaries.

	Spontaneous Polarization (C/m^2)
BN	0, -0.012, -0.032, -2.174 [204], [216], [218]
AlN	**-0.081**, -0.090, -0.094, -0.099, -0.103 [26], [95], [98], [204], [218]
GaN	**-0.029**, -0.032, -0.034, -0.080 [26], [95], [98], [204], [218]
InN	**-0.032**, -0.041, -0.042. -0.043 [26], [95], [98], [204], [218]

TriQuint Semiconductor Donated MOCVD Reactor

Initial experience and understanding of MOCVD fundamentals were forged through process development on an MOCVD reactor donated by TriQuint Semiconductor (now Qorvo Inc., via merger with RFMD Inc.). An Emcore designed system initially created to grow GaAs had been modified by TriQuint to grow GaN on two inch substrates. Initial efforts focused on eliminating oxygen contamination which plagued the process and hindered AlN nucleation layer development. Exhaust upgrades, ubiquitous adoption of VCR connections in place of sterically limited Microflange connections and expansion of leak checking capabilities throughout the compartmentalized system prevented further oxygen contamination. Replacement of the vent/run manifold, injector MFCs, the TMA source, several run lines, nitrogen and ammonia purifiers, as well as repair and replacement of many manual and pneumatic valves removed evidence of

oxygen contamination and alleviated its hindrance on growth efforts and system performance. Initial growth attempts after repairs were successful at growing AlN, though the material quality and surface texture left much to be desired. Prior to further AlN growth optimization, apparent changes were needed due to substrate surface pitting created during heat up. The fundamental cause for this texturing was found to be due to the hydrogen etch rate difference below ~1000 °C of silicon vs silicon oxide. While below ~1000 °C, silicon dioxide etch rates are sufficiently slow as to favor silicon etching, this combined with non-uniformities of the native oxide thickness and the thermal gradient across the wafer surface resulted in pitting at the thinner and hotter spots. A slower ramp during a hydrogen etch intensified the effect. A temperature ramp under nitrogen ambient followed by a hydrogen etch above 1000 °C resulted in a uniform silicon surface. The nitrogen heat up solution allowed AlN development to progress. AFM scans of the surface from three heat up conditions are shown in Figure 21. This experience enforced the importance of surface preparation prior to epitaxy.

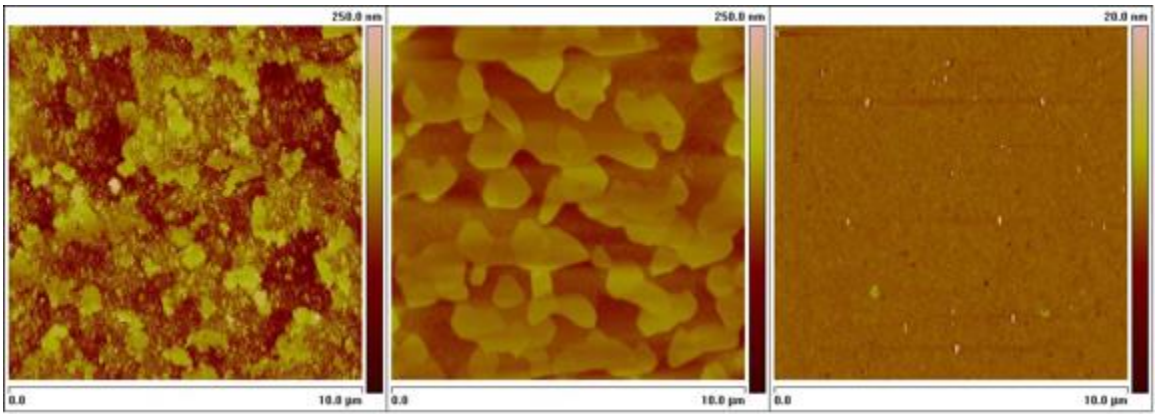

Figure 21. AFM scans of silicon surfaces after different heat up conditions to reach 1000 °C. From left to right: a slow heat up under hydrogen ambient, a faster heat up under hydrogen ambient, and a heat up under nitrogen ambient followed by a hydrogen etch above 1000 °C.

AlN development proceeded using a study of growth temperature and V/III ratio which split from literature reported values of 1000-1200 °C and ~1000, respectively [47], [219]. Grown AlN surfaces are shown in Figure 22.

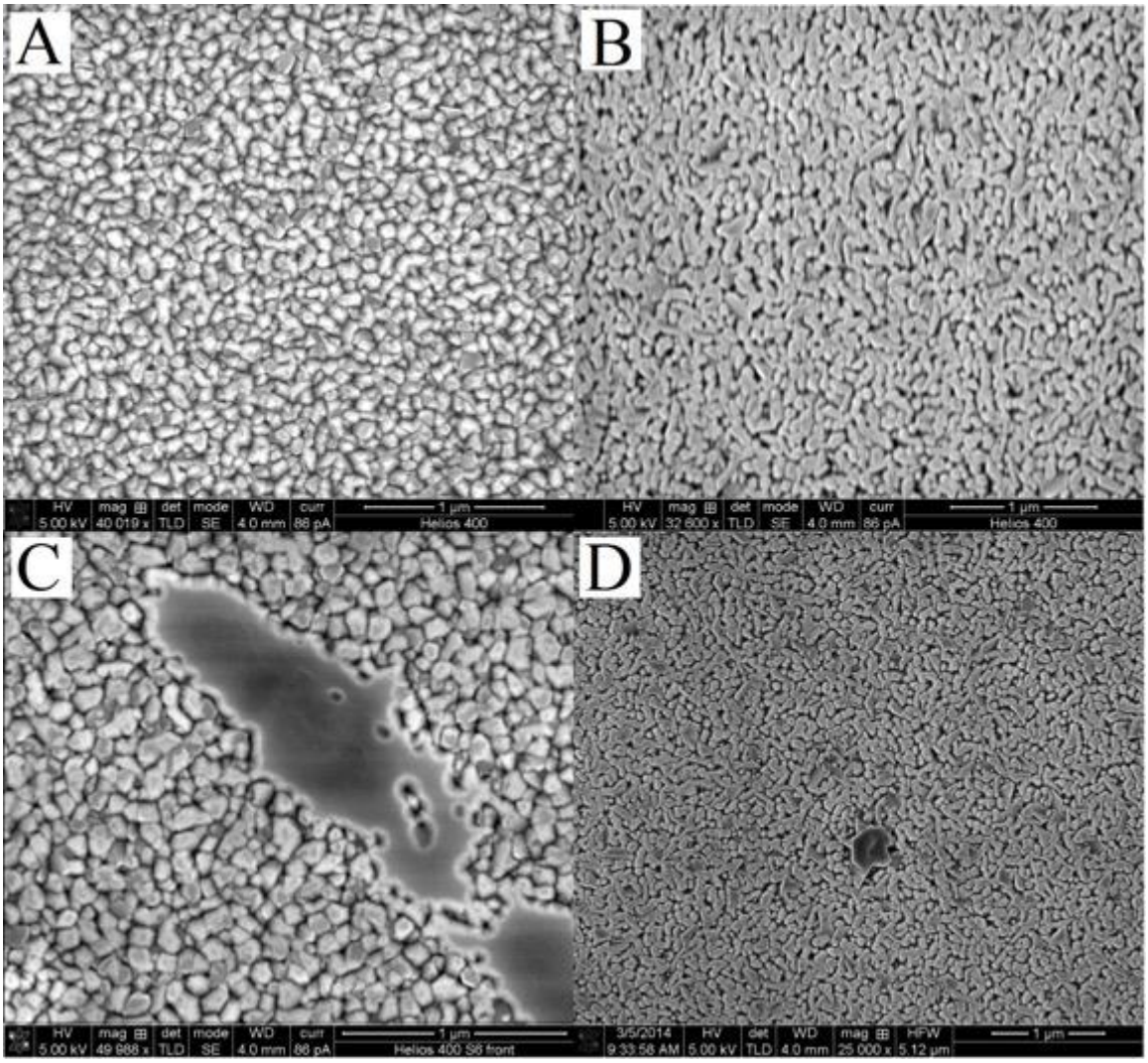

Figure 22. AlN thin films grown on a silicon (111) surface at various temperatures and V/III ratios. The temperature set points do not correspond directly to the surface temperature but to a thermocouple in close proximity to the heating element which was the most reliable temperature monitoring tool available, as such they are markedly higher than the expected temperature of the growth surface. A) 1550 °C, V/III 1200, B) 1425 °C, V/III 1200, C) 1550 °C, V/III 900, D) 1425 °C, V/III 900.

Optimized parameters for AlN growth were ~1650 °C (thermocouple reading, described in the figure caption) and a V/III ratio of 980. Using these settings and growth surface, initial efforts to grow GaN directly produced rough, non-reflective GaN which, upon SEM examination, consisted of non-coalesced islands with poor coverage of the AlN surface which are shown in Figure 23.

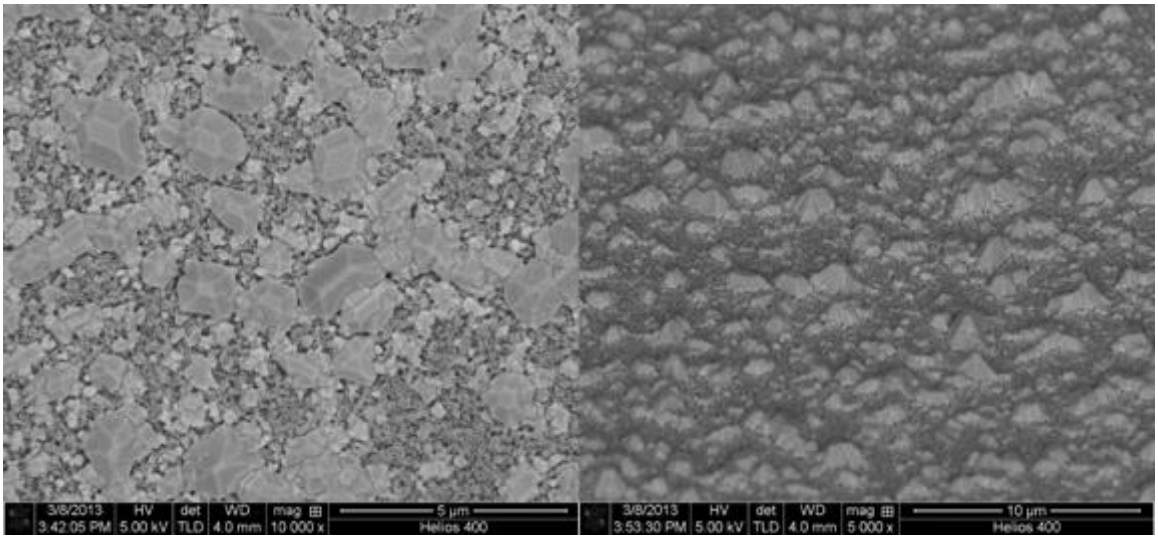

Figure 23. SEM images of a GaN nucleation layer on AlN surface. Direct view on the left, tilted view on the right. Incomplete coverage and poor cohesion are clearly seen.

Increased precursor flow improved coverage but did not produce a concise GaN film on the poorly coalesced AlN surface. Growth of the AlN nucleation layer did not reach the appropriate temperature for sufficient material quality as would be needed for GaN growth and was limited by the maximum output of the power supply. Replacement of the power supply to increase the maximum temperature improved material quality dramatically. After an upgrade to the cooling system to accommodate the increased thermal needs of the system, good GaN on AlN was produced. AFM scans of representative surfaces prior to and following the cooling system upgrade are shown in Figure 24.

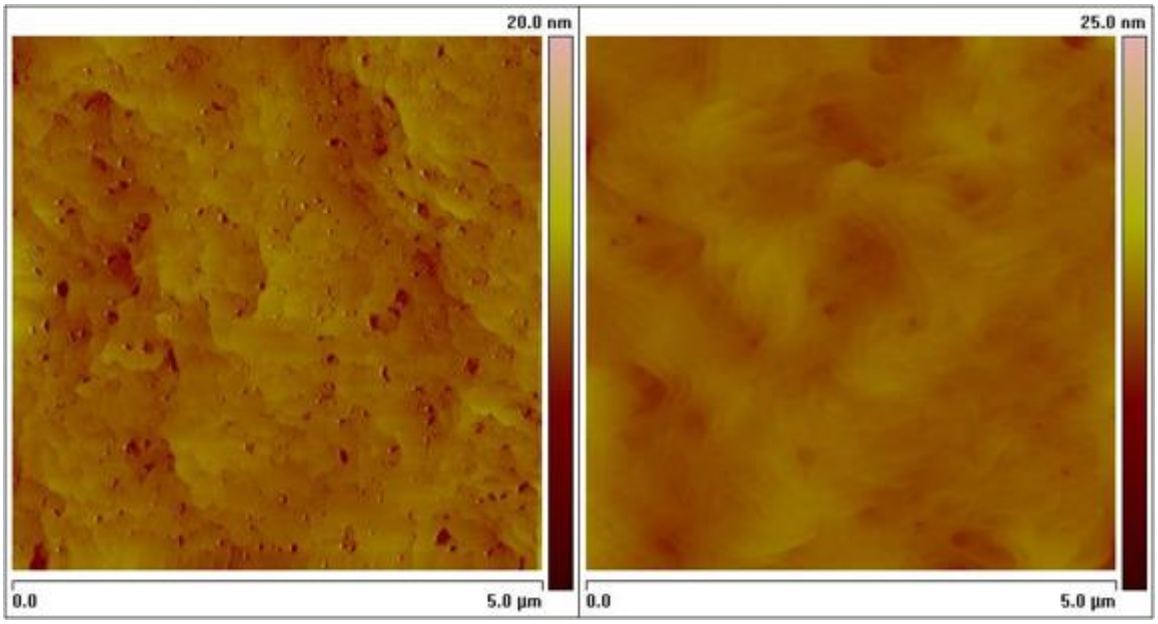

Figure 24. AFM scans of GaN surface of GaN on AlN. Left: sample grown after new power supply installation and prior to cooling system upgrade. Right: sample grown after cooling system upgrade.

Optimization of the growth parameters produced good quality single-crystalline GaN. The importance of effective growth condition ranges, their impact on material quality and more importantly the impact of poor material quality on superficial layers was enforced by this study. A representative cross-section of the grown GaN/AlN samples and XRD scan are shown in Figure 25 and Figure 26, respectively. With the effective growth conditions generally established and a growth process stabilized, the way was set to optimize AlGaN growth settings towards growing relaxed GaN, setting the foundation for a functional HEMT.

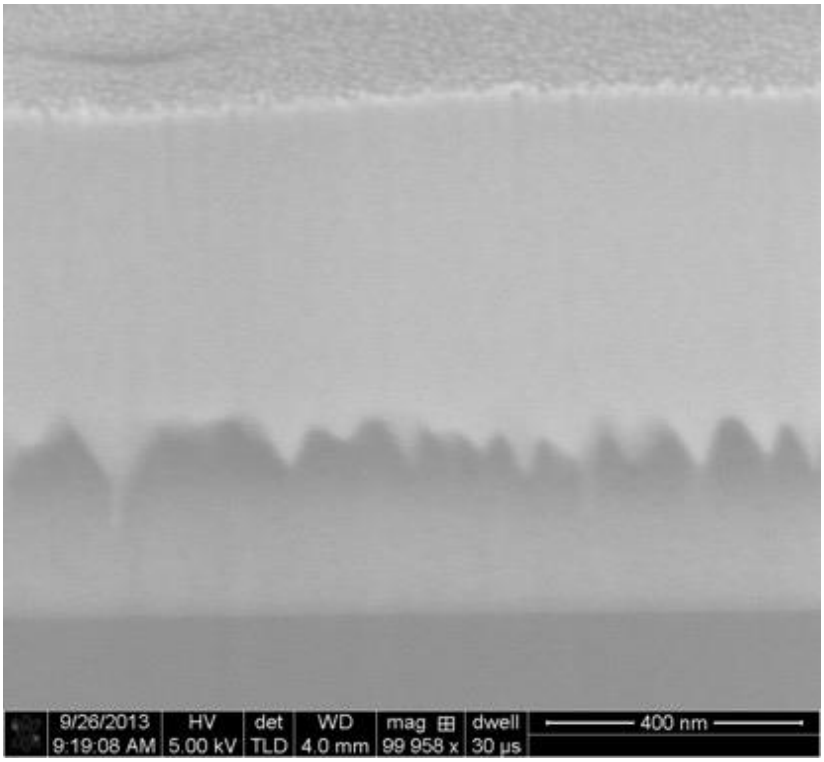

Figure 25. SEM cross section of single crystalline GaN on AlN on Silicon (111) substrate.

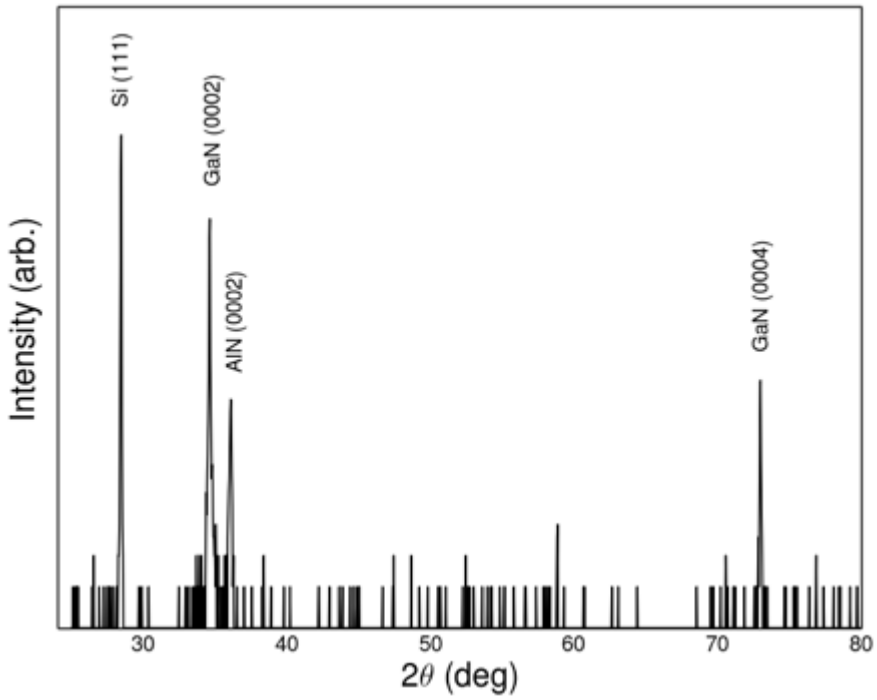

Figure 26. HRXRD scan of GaN on AlN on Silicon (111) substrate. Proof of single-crystalline growth.

AlGaN alloys were targeted to contain 67% and 33% aluminum for a two-step transition into the GaN layer. The system, as designed, severely limited the compositional uniformity across the wafer. In any system, gas flow dynamics must be optimized to deliver a uniform concentration of reactants over the wafer's surface area. Inefficient gas flows can lead to heated reactants recirculating onto the chamber roof and walls creating poorly adhered solid material which can contribute to unwanted particles in the gas flow. A larger contributor to the compositional non-uniformity is the single-zone heater design which creates unsatisfied heat sinks at the substrate holding shaft, at the center of the wafer, and at the wafer's edge due to the flow of gas towards the exhaust. These thermal inconsistencies create a radially symmetric hot ring mid-way across the wafer centered about the shaft position as the material is grown on a rotating substrate. This ring generally has the highest overall growth rate and aluminum composition in alloys as both are favored at higher temperatures. A representative plot of compositional variance of both prescribed AlGaN alloys across a radius of their substrate, from center to edge, is shown in Figure 27Figure *27.* Plots of variance in radial composition of two AlGaN layers with targeted AlxGa1-xN compositions of x = 0.33 and x = 0.67., calculated from relative XRD peak positions using Vegard's law which assumes a linear relationship between peaks for relative binary alloy compositions.

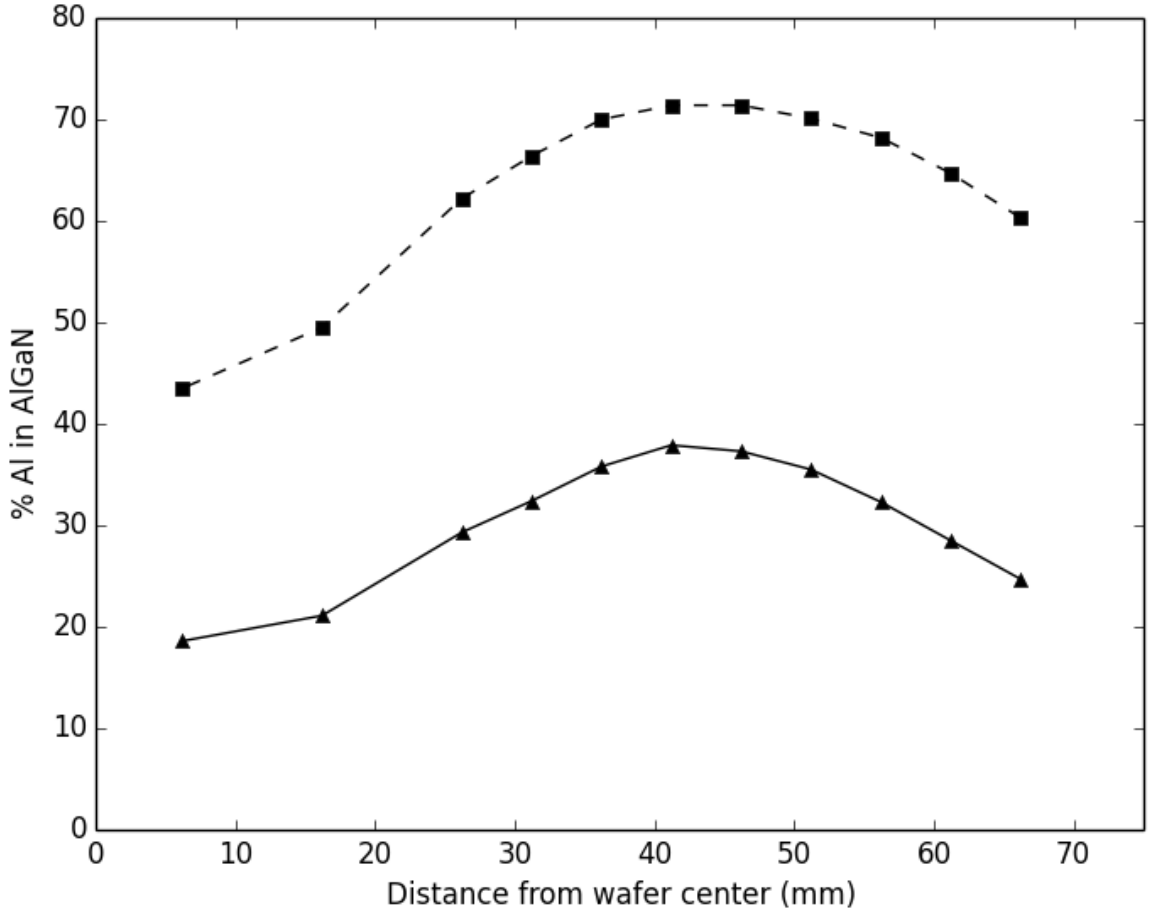

Figure 27. Plots of variance in radial composition of two AlGaN layers with targeted $Al_xGa_{1-x}N$ compositions of x = 0.33 and x = 0.67.

Attempts to optimize gas flow dynamics were not effective to alter this relative distribution across the wafer, as such, it is a safe assumption that the thermal gradient is entirely responsible for the non-uniformity. Though gas flow dynamics were not ideal as particles became prevalent on and within epitaxial layers during the longer growth campaigns. Typically, growth campaigns were limited by the life of their heating elements, which consistently warped due to exposure to process gases and degraded material quality towards the end of their lives, eventually melting at electrical bottlenecks, which severed the electrical patency of the metal.

The TriQuint Semiconductor donated reactor is currently idle, awaiting design improvements to address its primary issues: the limiting thermal control of its single-zone heater by adding two additional zones to directly accommodate the detrimental heat sinks to improve growth uniformity; the limited tungsten heating element lifespans by designing and machining rhenium elements; the inefficient design of its injector showerhead by incorporating a bell collar around the chamber wall to better encourage laminar flow within the chamber during growth and discourage recirculation of hot reactants, thereby preventing particle formation and further encouraging growth uniformity.

An appreciation for MOCVD fundamentals and the consequence of non-ideal growth conditions were established through this material optimization. This foundation would prove invaluable when altering the growth conditions and general structural changes necessary in the efforts accumulated in this body of work.

Nitronex Donated MOCVD Reactor

The reactor donated by Nitronex is a cold-walled vertical flow MOCVD reactor capable of growth on substrates up to four inches in diameter. Necessary components for III-N growth were also included such as OM sources, OM chiller baths, substrate holders (known as susceptors), epi-ready substrates, various grown layers for calibration comparison, replacement reactor hardware, some specific tools required for maintenance, vacuum pumps, water circulator, power supplies, and necessary reactor recipes / procedures. Initial efforts focused on functionalization of the system using the Texas State facility amenities: gas cabinets, gas lines, exhaust lines, house nitrogen and house

clean dry air (CDA) lines were fabricated and installed. Once functional, the reactor was capable of growing high quality AlN, GaN and their alloys. Additional material capabilities, like BN used in this work, would require additional hardware alterations.

Modifying the Nitronex-donated MOCVD reactor to include the capability of growing BN requires specific hardware changes which are determined by the chosen boron precursor. Boron sources for BN growth come in various forms. Boron halides such as BCl_3 have been used [175], [220], but the acidic byproducts (HCl) can be corrosive [221]. Diborane, B_2H_6, is used as a p-type dopant source for silicon technologies and has been incorporated into CVD growth techniques [222]. Diborane is known to be very toxic and explosive; as such, while a potential candidate, it isn't ideal for high temperature growth techniques [148]. A single molecule with stoichiometric amounts of boron and nitrogen within it would be a logical choice to grow stoichiometric BN. One example of a single source molecule is borazine, $B_3N_3H_6$ [223]. Borazine is a useful precursor to develop single BN monolayers and mixed phase thin films after annealing [148], [223], [224]. One obvious drawback for its implementation for epitaxy is the lack of control of reactant ratios, and therefore material quality, when using a single source precursor. A number of organoborane species have been used to grow BN, but since the application for this project is a MOCVD process, literature precursors that contain oxygen were not considered. Most notable among the organoboranes and following suit with typical MOCVD precursors are trimethylboron (TMB) and triethylboron (TEB). Both of these molecules could theoretically find utility in the Nitronex-donated MOCVD reactor. TMB is a gas at all reasonable temperatures (T_b = -20.2 °C), as such it would be the first gaseous organometallic species used in the reactor.

TEB is a liquid at room temperature and its vapor pressure curve lies between trimethylaluminum (TMA) and trimethylgallium (TMG) which are already attached to the reactor. The vapor pressures of the three liquids are plotted against temperature in Figure 28. TEB is a popular boron precursor in the literature [131], [144], [147], [148], [154], [174], [197], [221], [225]–[228]. It has been experimentally determined to be the best boron precursor among the organoboranes [221] for boron inclusion efficiency; its direct comparison to TMB reveals TMB as a highly reactive molecule whose stability is not as well suited for CVD applications [148]. Given the familiar nature of the liquid precursor and the familiar ethylene glycol cooled temperature range over which useful vapor pressures may be achieved, the liquid TEB was the preferred choice for a boron precursor for this work.

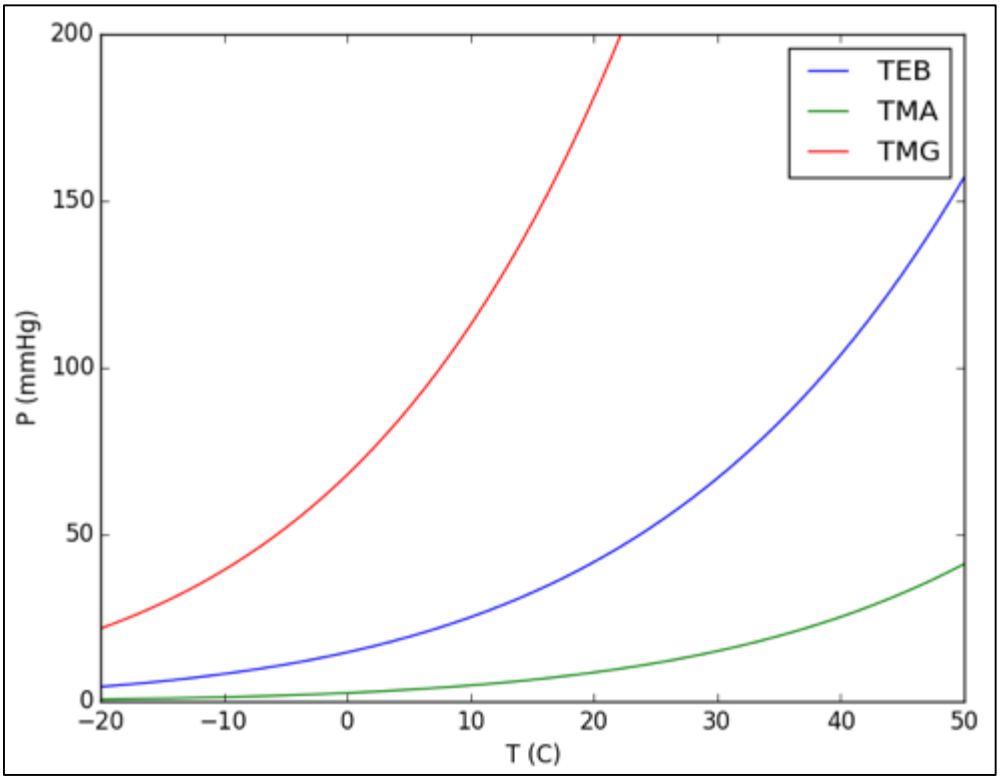

Figure 28. Vapor pressure vs temperature for TEB, TMA, and TMG.

Commercial availability of TEB would prove a significant challenge. Of the six companies which had sold the molecule in years prior to this work, two (Strem Chemicals & DockWeiler Chemicals) had offered it in electronics grade purity and a reasonable quantity. Strem discontinued TEB production in 2012, depleted their inventory in 2013, and was currently not able to offer the product. DockWeiler Chemicals of Germany was able and willing to synthesize and purify the product; it was commissioned in November 2014, shipped February 2015, substantially delayed by the west coast dock worker strike of 2015, and delivered to Texas State in April 2015.

IV. PROSPECTUS

The dissertation proposal described herein pertains to the field of AlGaN/GaN high electron mobility transistors (HEMTs). The material growth was performed at Texas State University (TSU) utilizing the advanced metal organic chemical vapor deposition (MOCVD) capabilities of the Piner research team in the Advanced Functional Materials Laboratory Research Service Center (RSC). Characterization was primarily conducted on site at TSU, utilizing the Nanomaterials Analytical RSC capabilities. The foundation of the project is the traditional AlGaN/GaN HEMT with AlN barrier layer as described in US patent 6,849,882 [102]. A representative HEMT structure incorporating this foundation is shown in Figure 29.

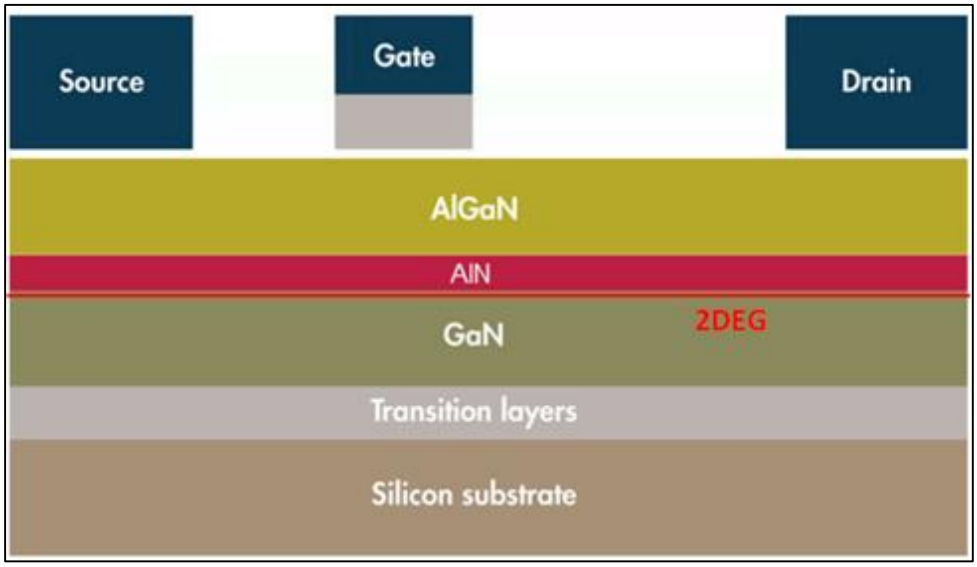

Figure 29. Traditional AlGaN/AlN/GaN HEMT structure grown on silicon utilizing various transition layers to allow low-stress GaN growth. The layer thicknesses are not to scale. The barrier layer thicknesses are greatly exaggerated.

This structure represents the initial, non-inclusive, subject of the body of work for this dissertation which will follow Texas State University Invention Disclosure TSU

2014-011, inventors Jeffrey R. Simpson and Edwin L. Piner, its proof-of-concept and utility optimization. The dissertation's fundamental change to the structure shown in Figure 29 is the incorporation of the smallest group III element, boron, into the barrier interface layer, defined by the red AlN layer, responsible for the formation of the 2DEG. The layers superficial to the GaN layer are generally referred to as the barrier layers, and the layer immediately interfacing with this GaN layer, if compositionally distinct from the barrier layer, as the barrier interface layer.

The researched compositional spectrum of the boron-containing barrier interface layer $B_XAl_{1-X}N$ range is: $0 < X \leq 1$, $X = 1$ being binary BN. This purpose of this compositional change is to increase the interfacial lattice stress between the underlying GaN layer and the proposed barrier interface due to a decrease in relative lattice spacing, increasing the lattice mismatch at the interface compared to the aforementioned AlN barrier layer which is used in today's state-of-the-art high power and high frequency GaN based HEMT technology. Increased interface stress will enhance the piezoelectric contribution to the 2DEG. This contribution increase is anticipated to improve the already high sheet charge density of the 2DEG, potentially enabling a new generation of devices via an alleviation of current device performance limitations.

V. EXPERIMENTAL

Growth Process Stabilization & Preliminary BN Growth

The TEB bubbler was initially installed on a standard OM manifold comprising a single carrier gas MFC, and pressure controller. TEB concentration calculations gave a ball-park range of H_2 carrier gas flows. But without knowing the necessary flows for appropriate BN growth in our reactor, the precise flow range required for the experiments was impossible to determine ahead of empirical evidence. Thus, a 20 sccm OM manifold MFC combined with the variable temperature bubbler bath was determined to be the best center-of-the-range starting point. Using the donated Nitronex growth recipes as a template, a basic recipe was created building off of the production-quality AlGaN/GaN recipe combined with AlN profile layer parameters from an experimental AlN profile recipe. These AlN parameters were used as a control for BN growth conditions. Without adding boron to the epilayers, the template recipe thus produced reference HEMT structures, referred to as the baseline structure. The two layers' parameters such as OM flows, ammonia flows, injector distribution, growth temperature, and chamber pressure provide a direct comparison with the baseline 2DEG platform and more importantly would serve as a starting point for BN profile growth.

Baseline growth processes needed to be reestablished after the initial reactor installation. The setup procedure is common to any shutdown involving opening the chamber or making major alterations or repairs. Growth proceeds in a stepwise fashion starting with AlN layer optimization working towards a full HEMT stack. Calibration wafers were donated with the reactor with known-good layers meant for this exact

comparison. Also inherent to this process is the general coating / conditioning of chamber surfaces exposed to the reactants. This coating can alter the thermal environment and will, by design, reach a steady state after a prescribed set of calibration runs. The AlN nucleation layer, the first AlGaN transition layer, the second AlGaN transition layer, GaN and eventual HEMT structure XRD scans are shown in Figure 30, for the baseline AlGaN/GaN structure. The composition of the iterative calibration layer growths of the AlN / AlGaN 1 / AlGaN 2 / GaN structure are diagnosed from their relative XRD peak positions in Figure 30. The composition of the AlGaN transition layers shown in graph "e" of Figure 30 are $Al_{0.507}Ga_{0.493}N$ for AlGaN 1 and $Al_{0.257}Ga_{0.743}N$ for AlGaN 2. This layer structure contains a sufficient gradient of increasing gallium content for relaxed GaN growth, in practice. Each layer serves to sustain the high quality of the eventual AlGaN/GaN HEMT structure which is dependent on the successful growth of a relaxed GaN with a planar surface, as previously discussed. Following the optimization of the transition layers, the first GaN growth in the reactor produced good quality material. A SEM cross section of this first HEMT layer structure is shown in Figure 31 to accompany Figure 30's XRD scan to validate material quality and Figure 32 shows an AFM scan of the epilayer's surface to validate planarity.

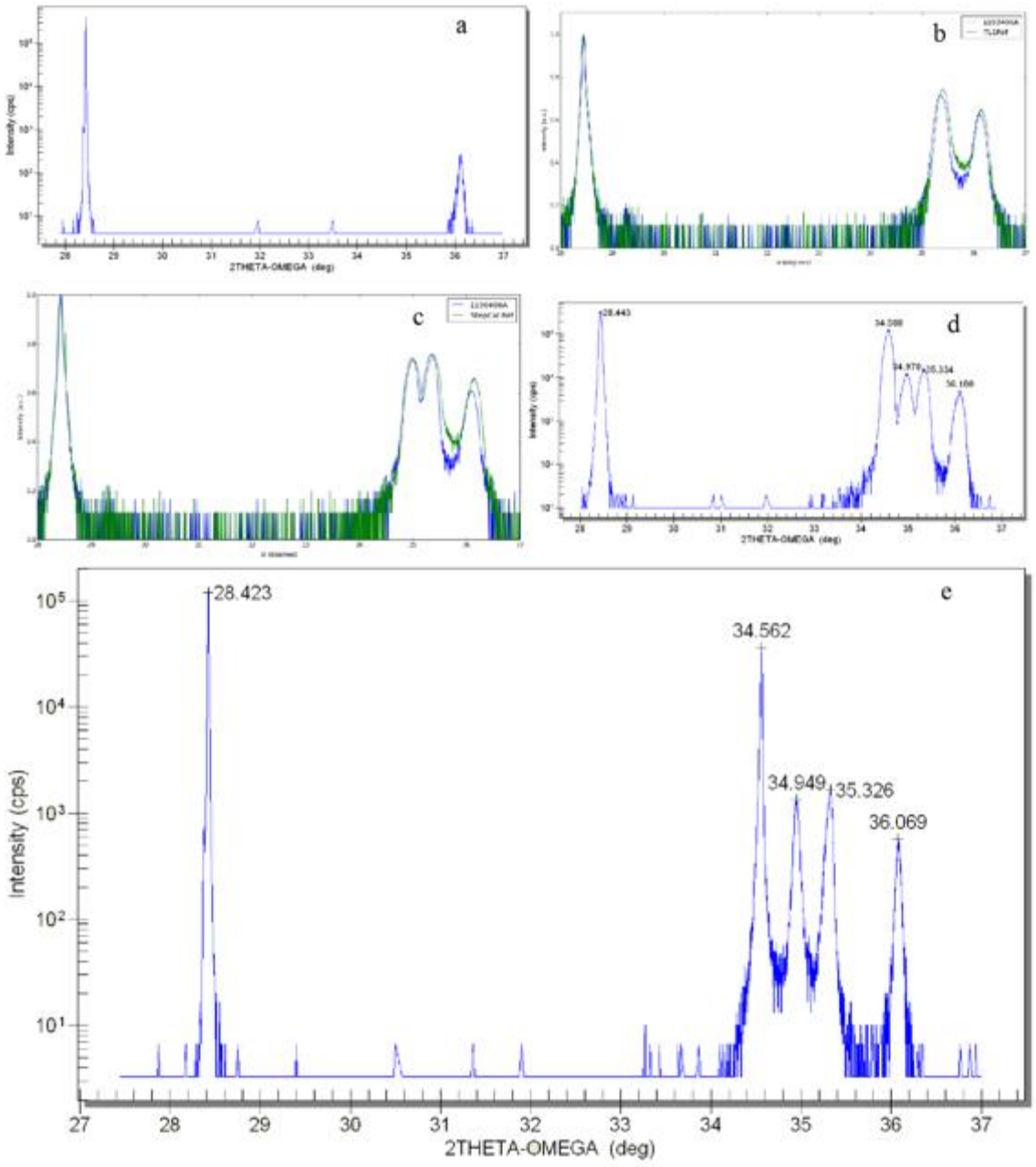

Figure 30. XRD scans of iterative calibration growths: a) AlN; b) AlN & AlGaN 1; c) AlN, AlGaN 1 & AlGaN 2; d) AlN, AlGaN 1, AlGaN 2 & GaN; e) Full HEMT stack.

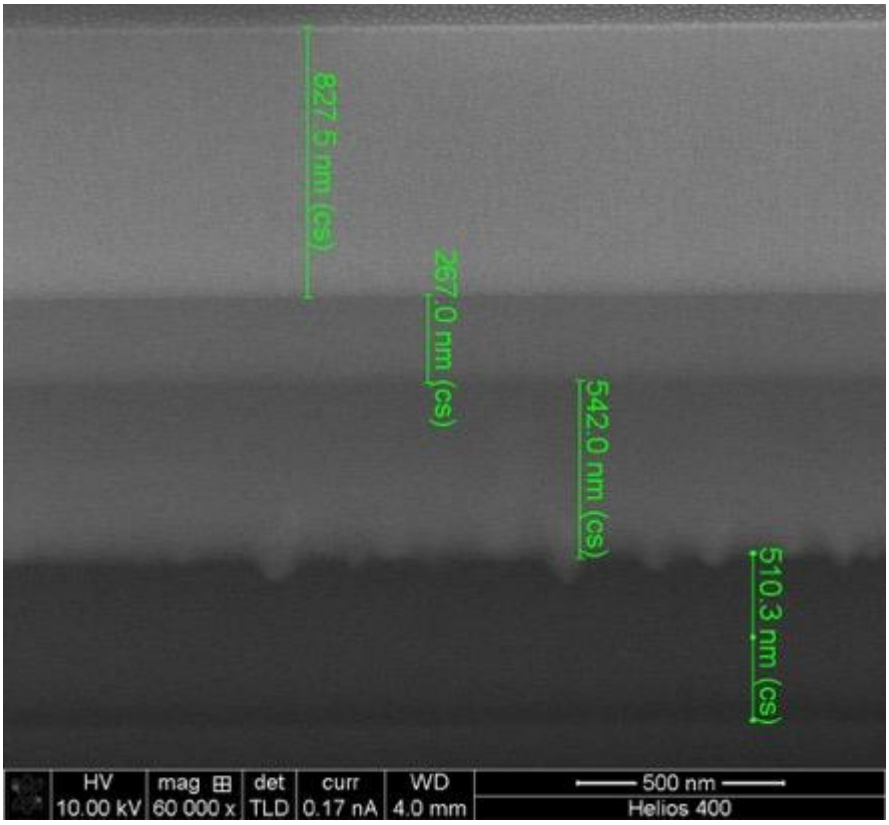

Figure 31. SEM cross section of the first GaN growth. From the bottom to the top, layers are the silicon substrate (unlabeled), AlN, AlGaN 1, AlGaN 2, and GaN, with each layer thickness noted.

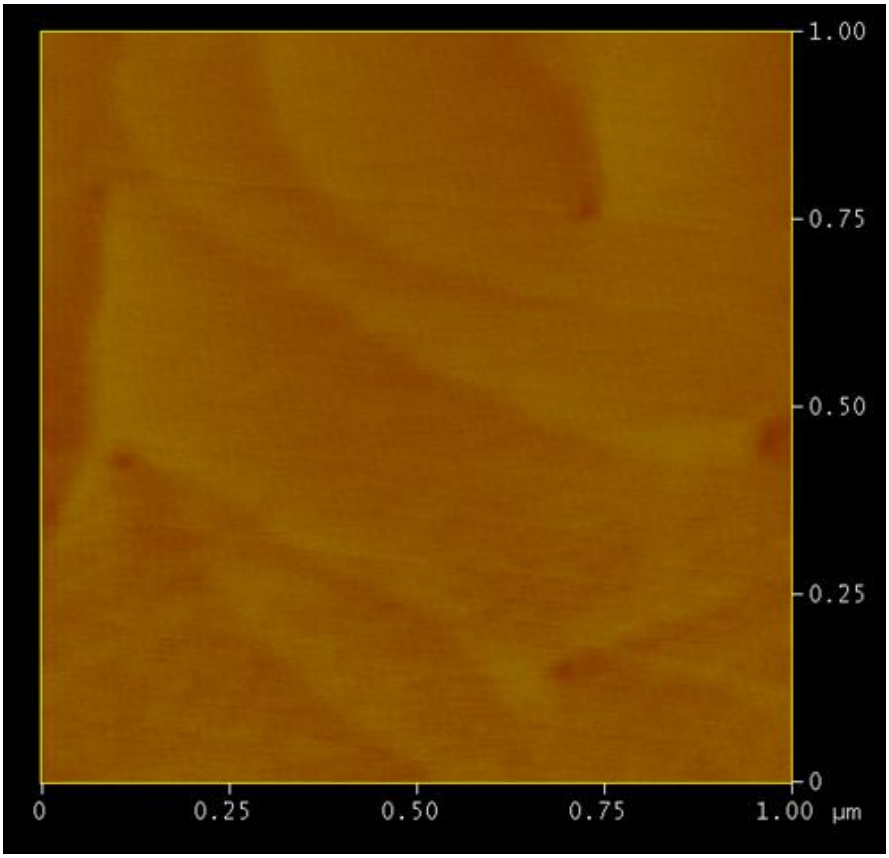

Figure 32. 1 µm x 1 µm AFM scan of the first GaN growth surface. The Z range is 1.057 nm; the root mean square roughness is 1.15 Å.

The SEM cross section shows the measured thicknesses of the layers. These approximate thicknesses have been shown, in practice, to provide a good underlying structure for the successful growth of relaxed GaN and good quality superficial device structures. The rough surface appearance of the AlN (deepest measured layer) in Figure 31 serves to mitigate stress at that interface more gradually that a planar interface could. This roughness serves to eliminate some threading dislocations generated at the heteroepitaxial AlN/Si interface and spread out compositionally induced strain over a larger area which allows for a relatively drastic compositional change between AlN and the first AlGaN transition layer. This large compositional change is tolerated in the overall structure by the distance between the interface in question with the superficial

device layers and the more superficial, less strained, material interfaces. Strain in response to the roughly 1.2% lattice mismatch at this interface will generate relaxation events which could compromise the electrical properties of device layers. Again, the morphology of the AlN surface serves to spread out and effectively reduce the impact relaxation events will have on the overall structure. The efficacy of this structure and its compositions to grow relaxed GaN and high quality device layers is validated by the AFM scan in Figure 32. This scan has a roughness of 1.15 Å which is on the order of an atomic plane thickness. This is an extremely good surface roughness for a GaN HEMT structure and is indicative of high quality material.

With the underlying growth layers established, repetitive growths of AlGaN/GaN HEMT structures would serve to confirm the quality of the baseline for future research. Figure 33 shows five such growths of the AlGaN/GaN baseline. Each peak is mostly coincident with the analogous peaks from the other wafers. As the reactor conditions reach a steady state, slight thermal differences from run to run will be present. This is typical of a growth sequence following a major shutdown. The evidence of slight thermal variations is seen in the overlaid HEMT XRD scans in the slight offset between the AlGaN peak positions. This is within tolerable ranges as the compositions remain effective to mitigate heteroepitaxial strain and provide a functional template for relaxed GaN growth even as the chamber conditions reach a steady state.

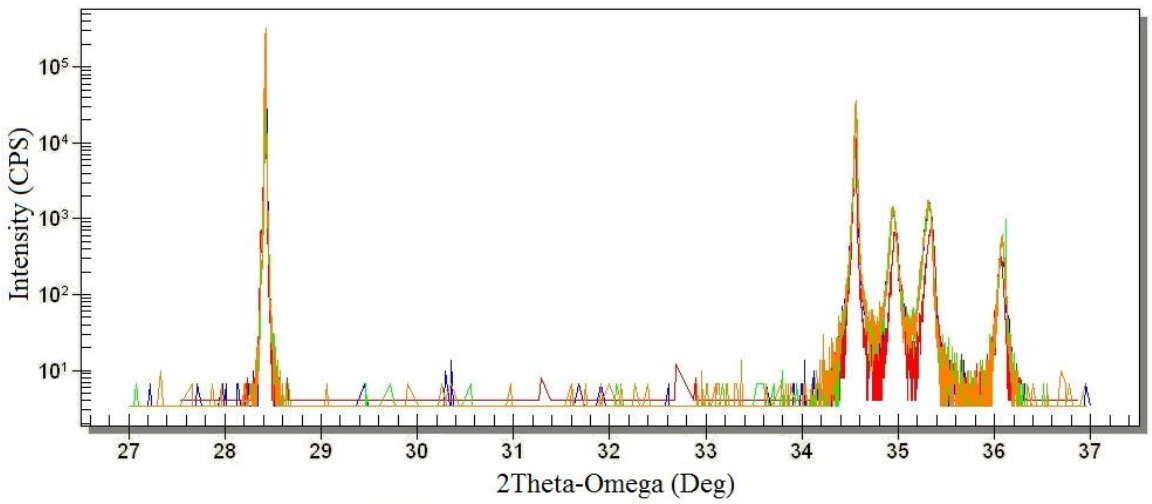

Figure 33. Repeated growth of AlGaN/GaN HEMT structures to establish the baseline growth process. The left-most peak is from the silicon substrate, the right four peaks are from the epitaxial layers. From left to right: GaN, AlGaN 2, AlGaN 1, and AlN

Experimentation of an AlGaN/AlN/GaN HEMT structure was instituted with the aim to provide a more advanced state-of-the-art baseline, in terms of 2DEG characteristics, for comparison of the BN-based HEMT structures researched here, as well as for other advanced studies. The experimental AlGaN/AlN/GaN recipe was updated with controlled growth conditions for the AlN nucleation, transition, GaN, and AlGaN barrier layers and a study of AlN profile layer growth times was performed. The initial recipe prescribed specific TMA and ammonia flows with a layer growth time of 60 seconds. These parameters were not altered for the first growth run. The results of this study are detailed in Figure 34.

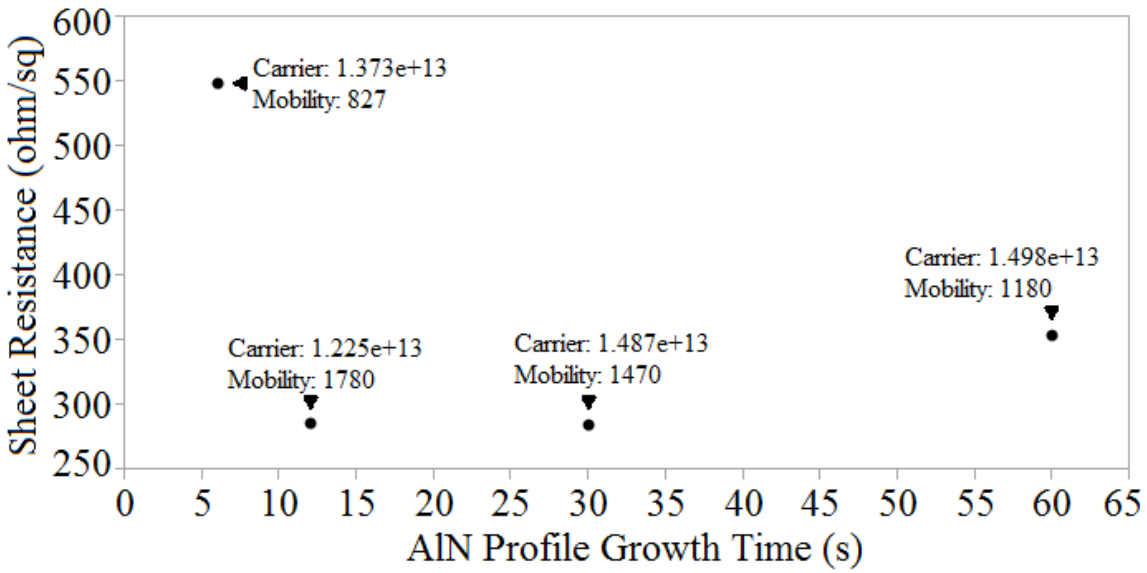

Figure 34. Sheet resistance vs profile layer growth times for AlGaN/AlN/GaN HEMT structures to establish research baseline. Carrier concentration measurements in cm^{-2} and mobility in $cm^2/V\text{-}s$ are displayed next to the corresponding data points.

The results indicate an optimal range between comparable growth times of 12 and 30 seconds. The data differ in measured mobility and carrier concentration, but produce identical sheet resistances. This study is consistent with the critical thickness discussion of an optimal thickness existing between incomplete coverage (retaining some degree of alloy scattering) and strain-induced morphology changes which are likely apparent in the significantly reduced mobility of the 60 second data point. The optimal region between 12 and 30 seconds would serve as a foundation for the boron-containing barrier interface layer experiments.

Alteration of the AlN profile recipe to include TEB flow in place of TMA for the profile layer was implemented and initial growth runs under identical ammonia flows began. The first BN-based HEMT growth followed the 12 second AlGaN/AlN/GaN recipe with double the TEB flow concentration relative to the TMA flows of the parent

recipe. The rational for this initial experiment was, matching the AlN flow directly was not possible as the prescribed flow rate for flow matching was not capable of maintaining pressure through the TEB pressure controller into the vent / run manifold (as determined by separate flow rate and stability experiments). This initial experiment, discussed in detail later, did not produce a measurable 2DEG.

The second experiment aimed to match the AlGaN/AlN/GaN 12 second layer, molecule for molecule. To address the hardware limitations, this was achieved by halving the flow rate through the bubbler, halving the bubbler pressure, and halving the profile layer growth time. Halving the bubbler pressure alleviated the hardware's inherent pressure building limitation and effectively doubled the molecular flows. This doubling, combined with the halved growth time and halved bubbler flows, effectively halved the molecular flow into the vent / run manifold (2 x ½ x ½ = ½) allowing the exact match of total molecules to the reactor of the 12 second AlN/GaN recipe over a shortened 6 second growth time. (In retrospect, this approach was an inefficient way to reduce the molecules to the reactor, though it was effective in doing so.) This growth attempt also failed to produce a measurable 2DEG. XRD scans from the first two experiments are shown in Figure 35.

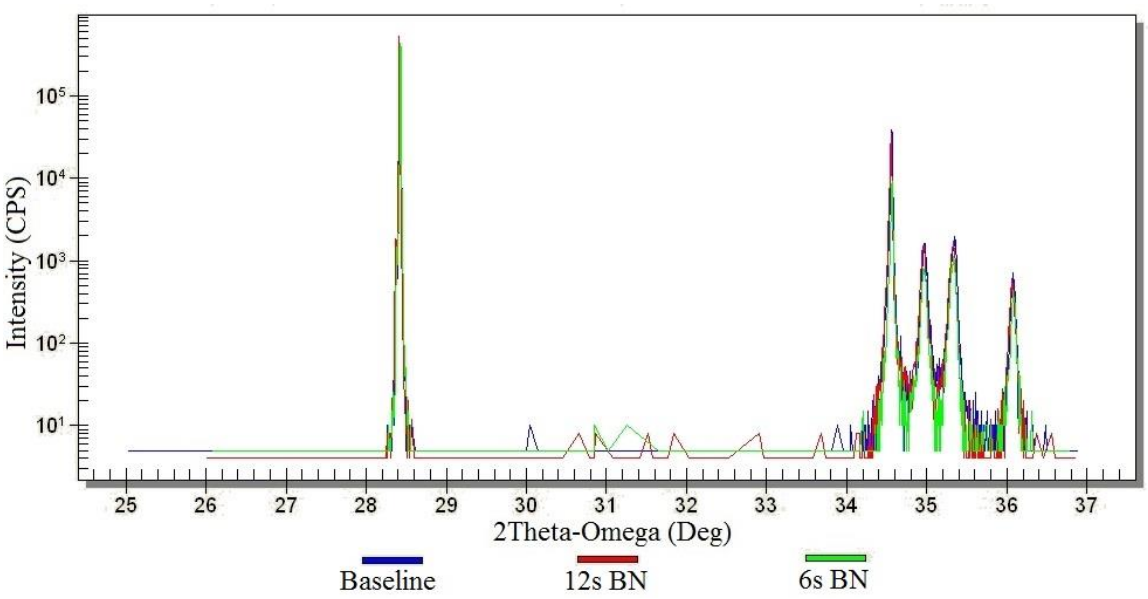

Figure 35. XRD scans of initial BN containing HEMT structures. The baseline structure is the standard AlGaN/GaN, the 12s BN growth is the first BN HEMT experiment, and the 6s BN is the halved TEB bubbler pressure / halved carrier gas flow / halved growth time flow-matched experiment. Boron inclusion did not shift the peaks of the underlying layers as compared to an AlGaN/GaN baseline, in blue.

Peaks from the BN HEMT growth attempts within Figure 35 are coincident with the AlGaN/GaN baseline. This is as expected as it would be abnormal for a superficial thin layer to compromise the crystalline integrity of the underlying layers, but this evidence absolves the overall material quality of culpability for the lack of a measurable 2DEG. With good material quality leading up to the BN layer and normal AlGaN barrier layer growth afterwards (which would induce a 2DEG) the logical conclusion is the impact of BN growth and the resulting strain, and/or the exposure to TEB and its reaction intermediaries, have degraded the GaN surface and superficial materials sufficiently so to diminish the 2DEG on the scale of a normal Hall sample (1 x 1 cm). Complementary AFM scans are shown in Figure 36.

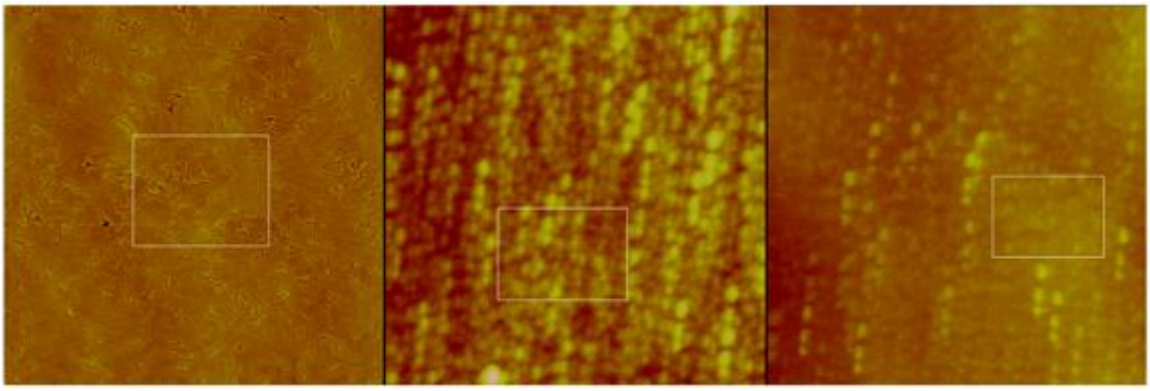

Figure 36. 5 µm x 5 µm AFM scans of BN containing HEMT surfaces. Left: baseline surface for comparison. Middle: 12s BN profile stack indicating significant surface abnormalities. Right: 6s BN profile stack with similar surface features to 12s BN, though significantly less pronounced. All surfaces consist of a thin GaN cap on AlGaN barrier atop the BN (Middle and Right data).

The morphology of the left AFM scan, the baseline surface, is typical for an AlGaN/GaN HEMT surface from the baseline process. It is exceptionally planar with a few surface features resulting from incomplete coalescence, or surface dissociation, of the GaN cap as a result of the high aluminum content barrier layer's preferred growth morphology. The morphology of the 12s (middle) and 6s (right) BN growth surface structures are irregular for a single-phased single crystal III-N film, which tend to have trigonal or hexagonal features when strained. The streaky non-planar nodule-like features indicate deviation from ideal material growth such as: incomplete layer coalescence, non-wurtzite growth phase, mixed phases, or boron precipitation induced by BN layers surpassing their critical thicknesses. The surface features, while unlike most GaN and AlN surfaces, are similar in appearance to non-ideal InN layer growth surfaces which deviate from optimized growth conditions. AFM scans of non-optimized InN surfaces are shown in Figure 37 for comparison. The island-like nodules are evidence of incomplete coalescence likely due to InN decomposition. The similarities between these

surface features and the BN HEMT surface features support that BN growth conditions are significantly non-optimized, or the BN thicknesses grown in the two experiments were considerably beyond the critical thickness allowed by the BN/GaN strained interface which would alter their morphology and that of the more superficial layers.

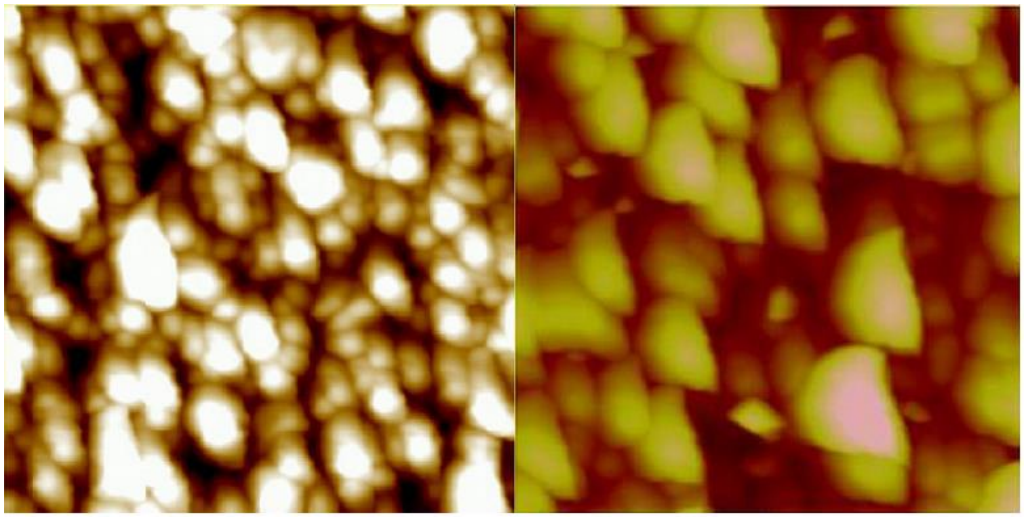

Figure 37. 2 x 2 μm AFM scans of InN surfaces grown under non-optimized growth conditions [170].

The initial AlGaN/BN/GaN growth experiments provided evidence that a lower molar flow concentration was necessary for successful BN-based HEMT growth which would require TEB manifold hardware changes as the TEB bubbler cooling bath was already at its lowest sustainable temperature setting of -10 °C and the carrier gas flows, as required to maintain TEB bubbler pressure, were already minimized. Such hardware changes required redesign of the TEB manifold from the standard (MFC and pressure controller) manifold to a more intricate, larger dynamic range, dilution manifold. Both configurations are shown for comparison in Figure 38.

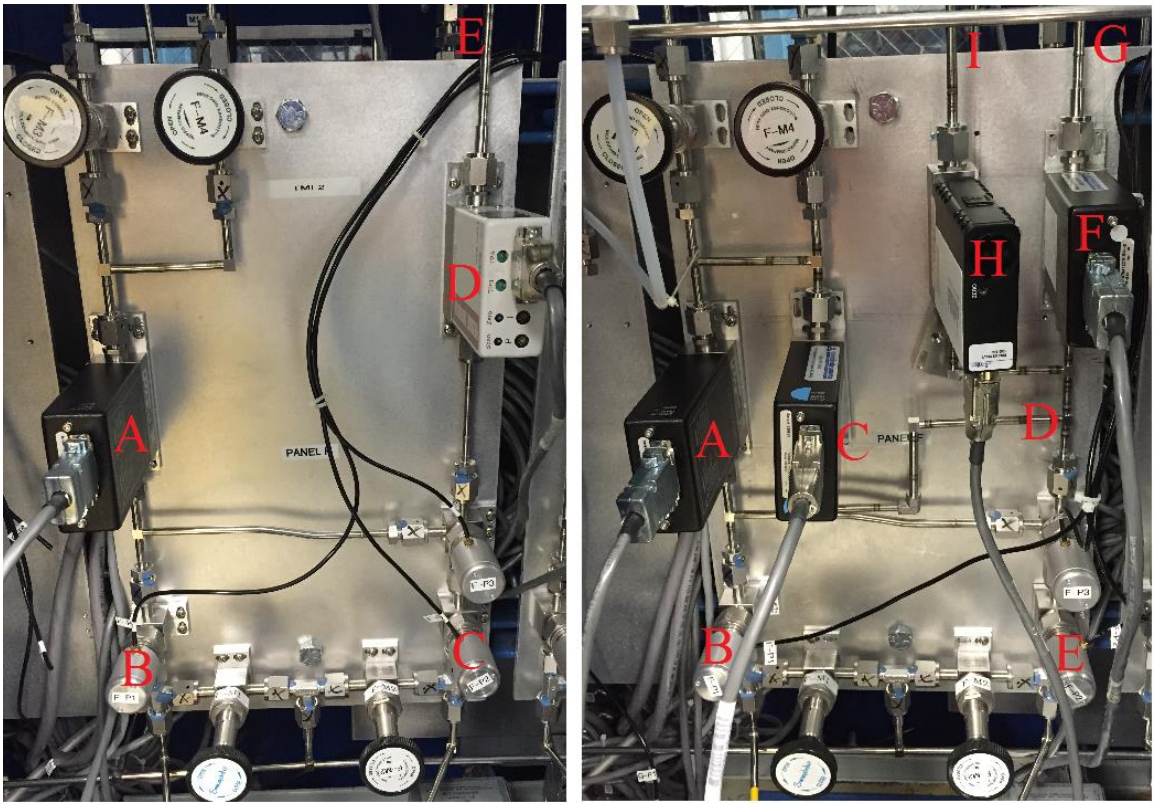

Figure 38. Triethylboron manifold and installed dilution manifold. Left: a single MFC (A) feeds the bubbler inlet (B). Bubbler outlet (C) flow goes through a pressure controller (D) to the vent / run line (E). Right: a single MFC (A) feeds the bubbler inlet (B), a second MFC (C) inserts diluent hydrogen (D) into the bubbler outlet stream (E), while a third MFC (F) delivers a diluted concentration of TEB into the vent/run line (G), and a pressure controller (H) expels excess gas volume to exhaust (I).

The purpose of the hardware changes was to increase the functional range of TEB concentrations available for BN growth by reducing the minimum TEB concentration which could be put into the vent / run manifold and still maintain TEB bubbler pressure. This was achieved primarily by the addition of a 500 sccm MFC to add diluent hydrogen after the bubbler outlet. The bubbler input 20 sccm MFC was not changed. The additional functional change to the manifold is the pressure controller no longer outputs to the vent / run manifold, but instead dumps excess volume directly to the exhaust. The output to the vent / run manifold is controlled more effectively by a 200 sccm MFC. The new configuration results in a functional concentration range increase by over two orders

of magnitude allowing for a much more thorough study of BN growth within a HEMT structure.

Reactor Troubleshooting

Reactor process development continued during the hardware fabrication for the new dilution manifold for the TEB lines. This process development suffered from abnormal inconsistencies and an absence of repeatable electrical data from the baseline HEMT structures. The variables impacting the electrical data were convoluted. A switch to lower resistivity silicon substrates altered measured electrical data to the point of preventing reliable characterization via the contactless mobility measurement due to the presence of charge carriers at the AlN nucleation interface with silicon in the form of diffused aluminum within the substrate acting as dopants. Evidence of a foreign contaminant came from visual inspection of the backside of the wafers to find white hazy areas along the periphery of the wafer. The growth surface above those same hazy sections commonly had cracking along their entire surface area.

Aside from the new group III element's introduction to the growth chamber, a newly implemented platter cleaning process was also a possible source of contamination. Given the low concentrations and very short time periods the chamber was exposed to boron, platter cleaning experimentation seemed like a reasonable problem solving prioritization. Nitronex cleaned their platters with commercial equipment which was used for other processes and not donated with the reactor. Beakers and platter carriers were donated and utilized to the best of our ability. The fundamental difference between the Nitronex platter cleaning procedure and the best available cleaning procedure in the

Texas State nanofabrication facility was the deionized water rinsing equipment. Nitronex used a water circulator which cascaded fresh hot deionized water over the treated susceptors allowing for the surfaces to be aggressively purged of residual reactant byproducts. The best option for rinsing with our available equipment was a relatively stagnant heated beaker for soaking and a large tank for a secondary room temperature soak. While this procedure was not identical, nor on the same level of potential efficacy as the Nitronex methods, it should be effective given the tendency of the cleaning species to be solvated by water.

Given the differences of the cleaning procedures, contamination had to be given the highest priority for problem solving efforts to resolve the absence of HEMT electrical properties grown by the reactor at that time. A susceptor was examined by SEM and EDAX to show small concentrations of contaminants at rough points along the internal edge. This led to experiments to remove unwanted contaminants that ranged from increased deionized water soaking to carbon dioxide blasting to acid etching to electrocleaning. The productive methods led to increased soak times in the deionized water baths to successful absolution of the hazy appearance and cracking during growth. While a few of the methods were equally successful at preventing the backside discoloration and the corresponding epitaxial layer cracking, the most reasonable method to integrate into the normal platter cleaning procedure was prolonged deionized water soak times. This method was entirely effective and required no extra equipment or process steps, just an increase to an established step's time.

Another issue involved the reactor exhaust system. The reactor's primary pump experienced electrical overload that was discovered to be due to water in the exhaust line,

thought to result from the intense flooding rains in central Texas during May of 2015. The entire exhaust system, including the original donated pump, had been compromised by the significant amount of water. Despite the preventative structures in the exhaust systems of the building, it was found that the facility contractors who installed the reactor exhaust line effectively and unintentionally created a drain at the lowest point of the vent on the lowest floor of the building. Facility alterations and preventative exhaust structures were put in place to hopefully eliminate this possibility in the future. After replacement of the local exhaust lines, repair or replacement of the valves between the reactor and the pump, and installation of a new pump, the system was again functional. During the time the pump was non-operational, software updates and hardware fabrication for the installation of the TEB dilution manifold were also implemented.

Miscellaneous unexpected reactor maintenance included repairing the Eurotherm temperature readout due to a communication card issue, replacing heater coil tie-downs, replacing faulty TMA and TMG pressure controllers, and trouble-shooting an event that involved consistently abnormally thin aluminum nitride, roughly half of the expected thickness, with poor uniformity. It was determined that the TMA pressure controller had been misconfigured since the system's creation. The underlying issue was that the pressure controller expected an input range of 0-10 volts which would correspond to a range of full open to full close of the pressure controlling mechanism. The system was providing a range of 0-5 volts which naturally elicited half the desired pressure from the TMA dilution manifold. This essentially doubled the concentration of TMA into the vent/run line as would be expected with a halved bubbler pressure, due to the consistency of the bubbler temperature and therefore a doubled contribution to the total pressure by

the temperature-dependent TMA vapor's partial pressure. When the growth recipe pressure set point for the bubbler was dropped to half of their previous values and the normal flows were restored after the efforts to troubleshoot the problem, the AlN layer thicknesses were back to normal. The root cause of the issue is presumed to have occurred during the software updates for the installation of the boron dilution manifold which shares a single pneumatic connection with the aluminum dilution manifold.

Finally, the H_2 purifying palladium cell experienced a catastrophic failure. The palladium cell is responsible for purifying the incoming hydrogen gas by only letting the small hydrogen pass through a thin palladium membrane interstitially which must be held at approximately 400 °C. The catastrophic failure was apparent due to the lack of pressure drop across this membrane. Usually, a pressure differential provides motive for the interstitial diffusion and resulting purification, so the lack of pressure drop implies a free path through the palladium membrane: i.e., a crack. Palladium cells are quite expensive and repair of the unit would cost practically the same as its replacement. The solution to the problem came through consultation with MOCVD and purification experts at Matheson. A resin based chemical purifier was installed to getter non-hydrogen species in the gas feed. This was a cost- and time-effective means to solve the hydrogen purification issue.

Following this period of reactor troubleshooting, normal material growth was reinstated. While reestablishing the baseline AlGaN/GaN HEMT structure, the barrier composition and thickness was observed to have drifted from target values. The data suggested that the aluminum composition was too high and that the thickness was too low. A common solution of increasing the TMG flow for the alloy growth would

simultaneously dilute the aluminum content and increase the thickness. The initial increase in TMG flows exceeded the critical thickness of the barrier layer causing cracking. The next step decreased the overall flow of both the TMG and TMA while maintaining the relative increase of TMG flow to TMA from the first growth attempt. This configuration would prove successful and the baseline AlGaN/GaN HEMT was reestablished after a roughly nine-month hiatus opening the door once again for research driven growth.

Research Structures

BN and BAlN films were grown within Ga-polar (0001) GaN-based HEMT structures using MOCVD growth techniques on silicon (111) substrates. Triethylboron (TEB) and ammonia were utilized as precursor molecules for B and N inclusion, respectively. The TEB manifold was kept at -10 °C, 760 Torr. TEB was brought into the reaction chamber with a hydrogen carrier gas. The silicon substrates were loaded into the reaction chamber, heated to a temperature sufficient for homogenous hydrogen etch of the native oxide (>1000 °C) clearing the growth surface of oxygen. The surface was then exposed to ammonia for a brief period followed by introduction of trimethylaluminum (TMA) for a high temperature AlN nucleation layer growth upon which a two-step transition AlGaN was grown for transition of material properties for GaN growth. Growth proceeded until a single-crystalline GaN layer of sufficient thickness with a planar surface was achieved. TEB was introduced directly to the GaN surface with or without TMA for ternary BAlN or binary BN, respectively. An AlGaN barrier layer was grown on the boron-containing layer and a thin GaN cap was grown to planarize the

growth surface. The chamber was then cooled and the substrate and newly grown epitaxial layers were extracted for characterization.

A representative HEMT material stack is illustrated in Figure 39. The figure generalizes the AlN nucleation and AlGaN transition layers and emphasizes the barrier layers. To properly diagnose the impact of boron inclusion on 2DEG properties, experimental AlGaN barrier layers (above the BAlN layer in Figure 39) were grown using the same growth parameters for all samples in this work. Relative to the AlGaN/GaN baseline using the recently updated barrier composition and thickness, the barrier layers used are identical in composition and were grown for 91% of the normal time. The deviation in time is to lessen critical thickness issues caused by a thicker barrier layer. This encourages, if only slightly, the boron-containing barrier interface layer to have a more appreciable impact on the properties of the 2DEG and epitaxial surface architecture. For the majority of growth, a twelve second pause in growth, or "growth stop," was employed to adjust ammonia flows in preparation for TEB introduction and another twelve second growth stop was used, as needed, to adjust ammonia flows for the barrier AlGaN growth after TEB flow terminated. Each experiment's defining differences are found in the input ranges for TEB flow (0.04 – 1.7 µmol/min), ammonia flow (0.002 – 0.1 mol/min), and BN layer growth time (1 – 60 sec) which were used in the AlGaN/BN/GaN study and ranges of TEB flow (0.008 – 0.032 µm/min), ammonia flow (0.03 mol/min), TMA flow (0.6 µmol/min) and BAlN layer growth time (12 – 20 sec) used in the AlGaN/BAlN/GaN study. The values for molecular flow rates are calculated as molecules entering the chamber per minute which necessarily deviates from the output from the OM bubblers due to the reactor and gas line

configuration. The growth pressure for all barrier layers was 100 Torr and the temperature was roughly 1012 °C

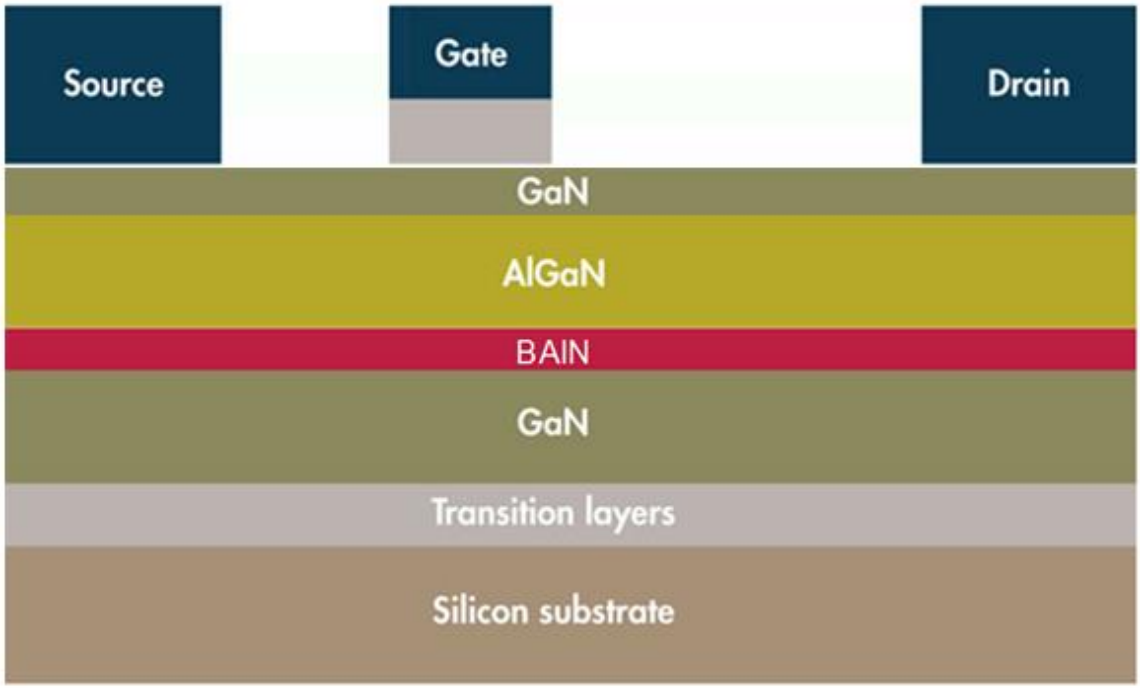

Figure 39. Generalized GaN HEMT structure with the barrier AlGaN and barrier interface BAlN layer thicknesses greatly exaggerated.

1 x 1 cm Hall devices were fabricated from each wafer to measure the two-dimensional electron gas (2DEG) properties by Hall measurements utilizing metallic indium for ohmic contact to the 2DEG. Hall data is presented as an average of all samples from a given wafer unless specified otherwise. The morphology of the epitaxial surface was characterized by atomic force microscopy (AFM) in both 5 x 5 μm and 1 x 1 μm areas to quantify the surface root mean square (RMS) roughness. X-ray diffraction (XRD) was utilized to diagnose structural differences between the as-grown boron containing films in comparison with the parent (boron-free) HEMT structures. Advanced characterization of select samples utilized scanning transmission electron microscopy

(STEM) producing high-angle annular dark field (HAADF) images. STEM samples were produced via a focused ion beam (FIB) sample preparation process within the scanning electron microscope (SEM). Additional samples were characterized by secondary ion mass spectroscopy (SIMS) for compositional depth profiling.

VI. RESULTS AND DISCUSSION

AlGaN/BN/GaN HEMT – Establishing a 2DEG

The experimental process to establish a 2DEG within an AlGaN/BN/GaN structure which began prior to the installation of the dilution manifold but was limited by the TEB concentration allowed by the hardware was initiated with growths utilizing reduced TEB flows. A BN layer growth time of 6 seconds was used and the ammonia flows matched the baseline AlGaN/AlN/GaN recipe. TEB flows were reduced within the experiment by steps of 50% total flow resulting in the successful growth of an AlGaN/BN/GaN HEMT structure with a measurable 2DEG. The summary of results of this experiment are presented in Table 5.

Table 5. Hall measurements from AlGaN/BN/GaN HEMTs. Experiment aim: establish upper TEB concentration limit for 2DEG generation.

TEB Flow (µmol/min)	Carrier Concentration (cm^{-2})	Mobility ($cm^2/V*s$)	Sheet Res (ohm/sq)	RMS Roughness (nm)
1.276	N/A	N/A	N/A	5.462
1.276	N/A	N/A	N/A	1.217
0.318	8.141E+12	929	825.2	2.070
0.159	1.018E+13	1202	511.5	0.611

It is important to note that the two highest TEB flow runs may have been compromised by oxygen contamination from the previously discussed system exhaust issues, though the overall experiment was successful to establish an upper TEB flow range for 2DEG generation. Ideally the correlation between TEB flow rate and BN layer growth rate follows the traditional direct dependence as observed in GaN and AlN,

previously discussed. However, the layer strain and resulting critical thickness may hinder such a relationship. The oxygen contamination scenario is the likely culprit to explain the comparison of roughness values for the two HEMT structures with RMS roughness values of and 1.217 and 2.070 nm. HEMT structure surface roughness should follow directly with morphology changes brought on by strained layers. Though these two wafers are a limited data set, the trend of decreasing roughness with decreasing strained layer thickness should still exist. Since this relationship is not true for these two, assuming the correlation between flows and layer thickness is true, the natural conclusion, based on the information associated with the contamination event and RMS roughness value, is that the 1.217 nm roughness wafer should have a 2DEG.

No BN signal from this experimental set was detected in XRD scans. Traditional XRD efforts utilizing signals from layers satisfying Bragg's law [229] to look for HEMT layers produced baseline-identical results. This could be a result of a few scenarios: perhaps the layer is so thin its signal is not appreciable due to overlap with another peak, or the growth preference of BN under these experimental conditions does not favor wurtzite growth, as such the material transitions quickly from the wurtzitic surface of the GaN to another phase which does not satisfy the same Bragg conditions as a concise wurtzite material so that the signal is so broad as to not be recognizable as a peak, a similar mechanism could be at play from the perspective of strain given the large mismatch between BN and GaN, or the possibility that BN was not grown and the degradation to the 2DEG is simply from an etch-like damage mechanism from exposing the GaN surface to the TEB or one of its decomposition or ammonia reaction products.

Thick BN Growth – XRD Evaluation of BN

An experiment designed to grow sufficiently thick BN so to be detectable by XRD was conducted using BN growth times of 60 seconds in the AlGaN/BN/GaN HEMT structure. The TEB flows were doubled for each sequential run within the experiment. No Hall sample from the experiment had a measurable 2DEG. The total TEB moles to the reactor (the product of molar flow rate and layer growth time) plotted against the average surface roughness for the three growth runs from this experimental set are presented in Figure 40, discussed in detail below, with the two 2DEG-containing AlGaN/BN/GaN HEMT wafers from the flow establishment experiment for comparison.

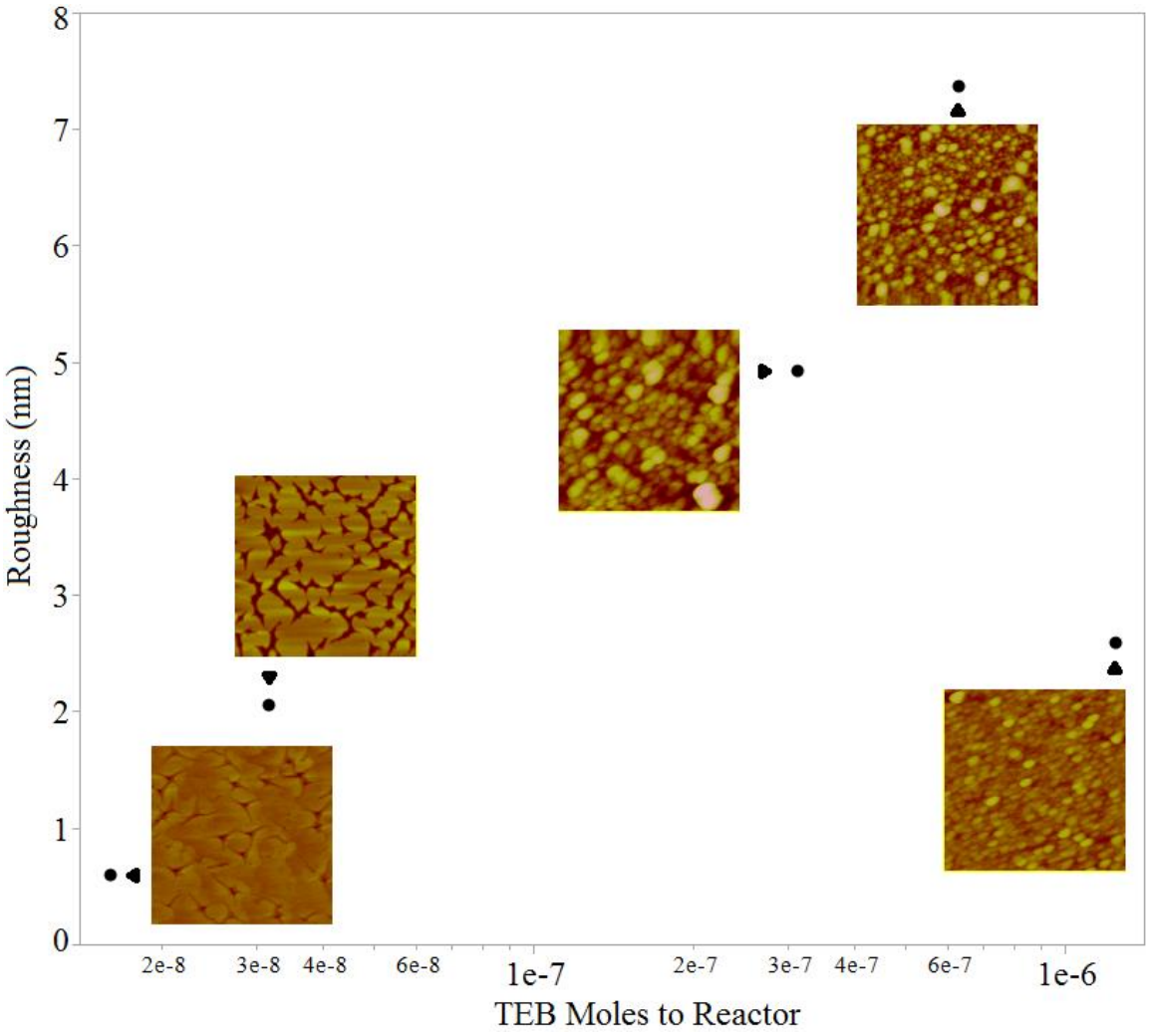

Figure 40. Plot of average surface roughness vs total TEB moles to reactor. The right-most three data points are from this experimental set and did not contain measurable 2DEGs. The left-most two are from the flow establishment experiment and both contained 2DEGs. Inlaid images are 1 x 1 µm AFM scans from the corresponding wafers illustrating the morphology changes responsible for the roughness measurements. Z-ranges for the AFM scans are, from left to right: 6.5, 21.3, 42.3, 36.9, 27.2 nm.

Ω - 2θ XRD scans from this experimental set are presented in Figure 41. No peaks are apparent which would not otherwise be expected in the baseline AlGaN/GaN HEMT structure. An Ω - 2θ scan of such an AlGaN/GaN HEMT is included for comparison in Figure 41.

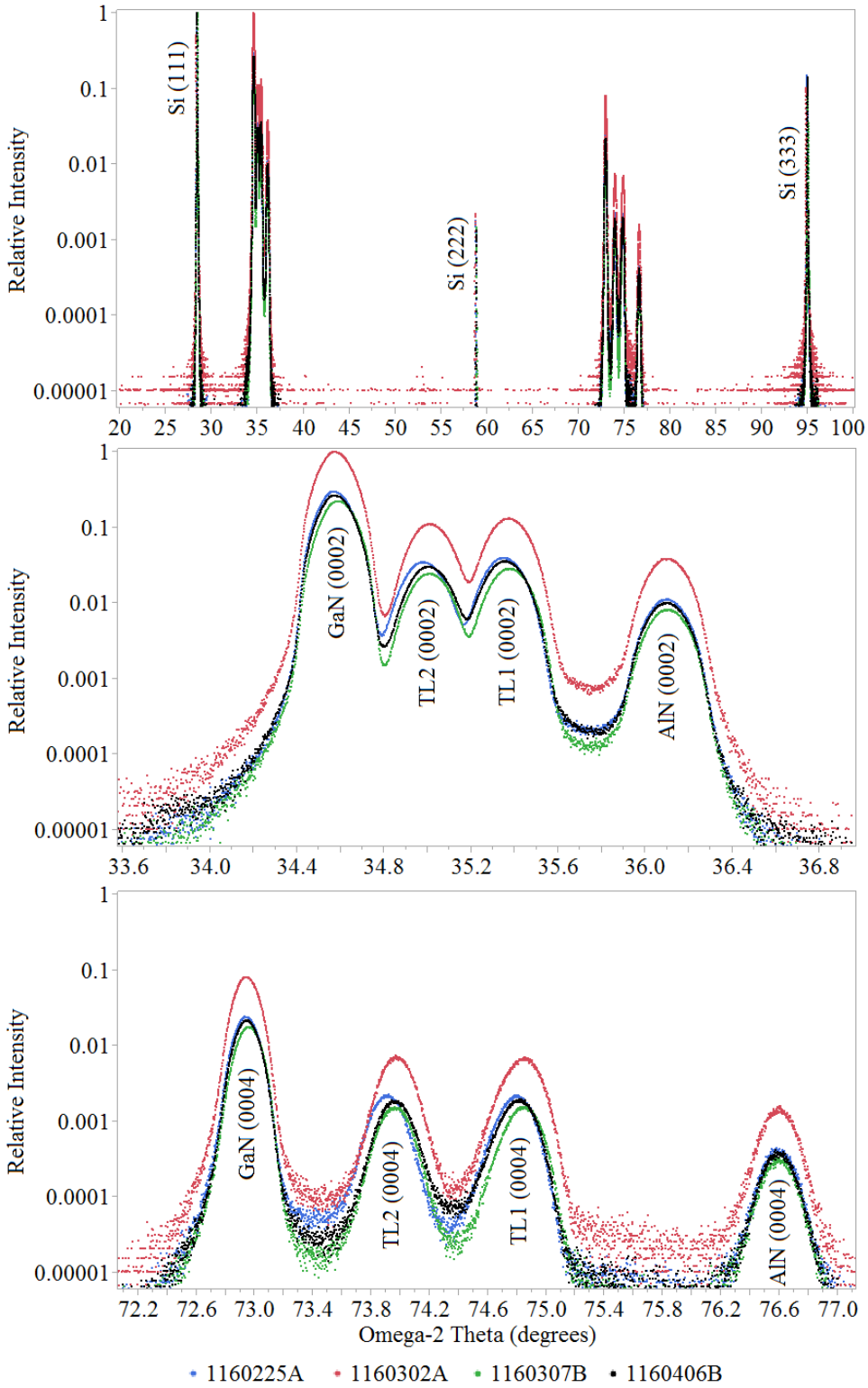

Figure 41. Omega – 2 Theta scans for thick BN experiment with a baseline AlGaN/GaN HEMT scan for comparison. Samples are designated by the total TEB moles delivered to the reactor. The upper graph shows the entirety of the range scanned, the middle and lower graphs show expanded views of the epitaxial layer peaks.

The excessively rough and non-planar surface apparent in the inlaid AFM images of Figure 40 are indicative of severe stress in the underlying layers. The surface morphology of the higher TEB flow wafers is nodular with coarsely segregated islands. The lack of hexagonal or trigonal crystallographic surface features, common to wurtzite materials, suggests the growth of alternative phase or phases within the crystal. Given that the primary change in the growth of each sample is the addition of TEB, and the increase in severity of the nodular appearance with increased TEB flows, the conclusion is that the critical thickness of a strained boron-containing layer, be it BN or a B alloy with surrounding layers or a combination of the two, has been exceeded. This is further supported by the absence of a measurable 2DEG in the heavily affected HEMT structures which indicates either a severely non-planar barrier layer / GaN interface or the accumulation of relaxation events sufficient to eliminate the strain necessary for the piezoelectric contribution to the 2DEG combined with the generation of electron states at relaxation sites eliminating 2DEG integrity by producing trap states.

The XRD scans in Figure 41 suggest there are slight compositional variations between the AlGaN transition layers of the various HEMT epiwafers. These compositional differences are insignificant in the growth and identification of BN within these epitaxial structures. The compositional variation is evident from the small shifts between analogous peaks in the lower two scans in the figure. As an example, the second peak of the middle scan (the second AlGaN transition layer) in the figure contains peaks whose maxima are not aligned to one another, specifically the blue data set (0.318 μmol TEB) is shifted towards the GaN peak indicating a higher gallium content within the second transition layer of that wafer. Every other wafer's second transition layer had an

identical composition of $Al_{0.24}Ga_{0.76}N$ while the shifted peak indicates an $Al_{0.12}Ga_{0.87}N$ composition for that single wafer. Every other peak position for that wafer's discreet layers were identical to the others in the set. This single layer deviation could be due to a decreased deposition temperature for that layer which would decrease the aluminum incorporation of an AlGaN layer. If the presence of TEB in the material stack were to blame for the shift, it would be expected that the GaN peak would also be shifted as it is between the BN layer and the AlGaN layer in question, but the exact alignment and congruency of the GaN peaks from wafer to wafer suggests that the GaN material quality is comparable for each HEMT structure. Additionally, if TEB were culpable for the shift, it would be expected that the other, higher TEB concentrated samples, would experience a similar or even more severe shift, but their peaks are aligned perfectly with the baseline. The barrier layers are not represented in the figure due to their peak overlap with the underlying thicker AlGaN barrier layer and overall low relative diffraction signal. While it could be assumed that the BN peak will be similarly masked by the other epitaxial layers, the presence of such a markedly different lattice spaced material grown under these conditions may still have been evident in these scans, validating the experiment.

The expected relaxed w-BN (0002) peak location from reported positions in the literature is 43° on a 2θ scan [230]–[233]. BN layers producing these peaks are not directly comparable to these experimental wafers due to the high likelihood of strain in the MOCVD-grown AlGaN/BN/GaN structures. BN layer peak positions under these conditions should reside somewhere between their relaxed peak position and alignment with GaN due to the intended lattice matched periodicity at the interface. As such, the BN signal may indeed be convoluted with other III-N peak positions or may be spread

over a large area due to the reduction in perceived tensile strain of progressive monolayers away from the GaN surface. In comparison with the baseline AlGaN/GaN in Figure 41 (black data), the AlGaN/BN/GaN samples with the intentionally thick BN do not have an appreciable BN signal in the previously defined range between the GaN peak and the literature reported position of w-BN of 43°. Additional explanations for the absence of an appreciable BN peak are: the BN signal is too weak relative to the other layers indicating these BN layers are still overly thin, or BN was not deposited but instead the surface roughness and 2DEG degradation are due to an etch-like behavior by TEB or one of its reaction byproducts roughening the GaN surface and the AlGaN/GaN interface.

To help identify the presence of BN in these AlGaN/BN/GaN with thick BN layers, a STEM sample was prepared from the wafer with the thickest intended BN layer (1.272 µmol TEB) along the [11$\bar{2}$0] zone axis by focused ion beam milling with final polishing done at 2 kV. HAADF images were then collected using a JEOL ARM 200F STEM operating at 200 kV. In this technique the image intensity varies approximately with the square of the atomic number allowing discrimination of compositional variations within a region. Images of the sample using this HAADF technique are presented in Figure 42. The images depict the superficial-most layers of the HEMT structure.

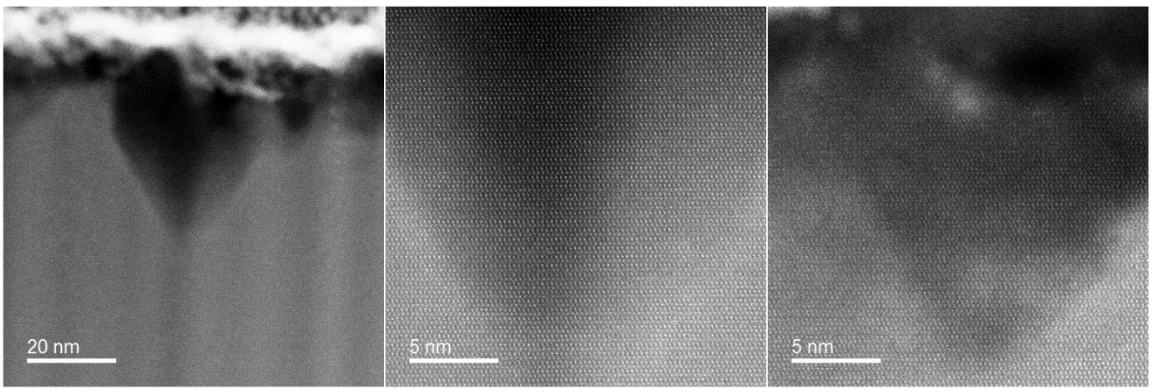

Figure 42. STEM HAADF images of AlGaN/BN/GaN HEMT structure with thick BN. 1.272 µmol of TEB was provided for BN growth within the HEMT structure. Darker regions indicate atoms with lower atomic numbers and lighter regions indicate those with higher atomic numbers.

In the left image of the figure, brightly colored platinum can be seen at the top. Platinum is used to protect the epitaxial regions of interest during sample preparation and is not involved in HEMT growth. Also visible in the image is a large pocket or crater of lower atomic numbered material atop and protruding into the GaN buffer. The same contrast can be seen in the other two images. The center image is a magnified view of the region in the left image. In these images, the darker material is still single crystalline as evidenced by the lattice periodicity within the region. The right image is of an accompanying region which contains compositionally segregated areas of irregularly light and dark materials. This technique does not provide an image of the cross-sectional surface but instead it provides an image of a given thickness of the sample. Accordingly, some areas of the imaged regions seem to be intermediately shaded as if they were composed of an intermediately atomic numbered element. These regions should be interpreted as areas of differing thicknesses of mixed composition. As an example, the middle image in the figure should be interpreted as an inverted cone-like shape of a low atomic numbered element supported on all sides by a higher atomic number element as if

the lighter atomic element were somewhat transparent towards the periphery of the one and the thicker central region is more opaque. This lighter material was positively identified within this sample as BN by electron energy loss spectroscopy (EELS) within the same STEM system. Secondary Ion Mass Spectrometry was used to confirm the presence of boron within this HEMT structure. The SIMS depth profile is seen in Figure 43.

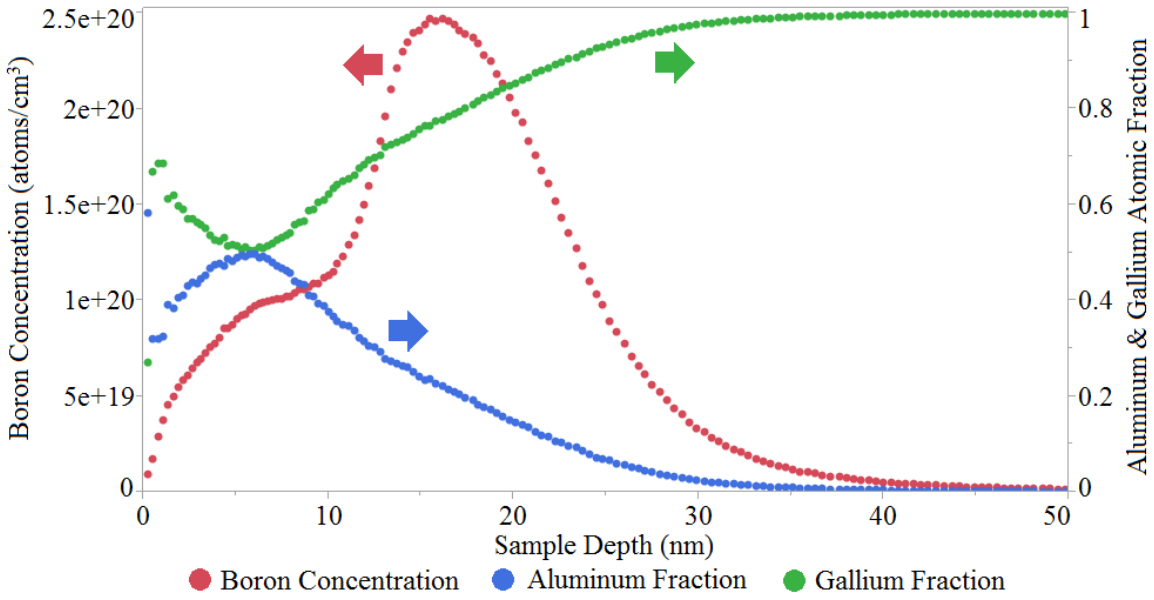

Figure 43. SIMS depth profile of the wafer grown with the highest TEB concentration of the thick BN experiment. Red data is boron concentration in atoms/cm^3 and corresponds to the left axis. Blue and green data are aluminum and gallium atomic fractions, respectively, which correspond to the right axis. Aluminum and gallium are used as markers to identify the boron location within the HEMT structure.

The total probed depth of the SIMS technique was ~100 nm. After the first 50 nm, the signals remain unchanged and were not included in the figure. The first 50 nm, however, are quite informative as to the behavior of the boron within the HEMT structure. The reported boron background level was ~5e14 atoms/cm^3. The first observation from the data, beginning at the epilayer surface; at 0 nm, is the appearance of

the AlGaN barrier layer. The roughly equal atomic fractions of aluminum and gallium in the first few nanometers of the sample, combined with the relatively shallow region of higher aluminum concentration, is evidence that the barrier layer growth in this sample did not conform to typical AlGaN growth behavior. The prescribed composition of the AlGaN barrier layer is roughly 26% aluminum and 74% gallium and the prescribed thickness is 19 nm. The large discrepancy between this ratio and thickness from that seen in the SIMS depth profile is due to the impact BN has on the growth of more superficial materials, specifically the increased relative composition of aluminum. A possible explanation for this increase is the decrease of gallium incorporation into the film due to unfavorable surface conditions from the high mismatch of BN with GaN. AlN would have a less severe mismatch, though the degree to which the aluminum composition is increased is still surprising. This deviation from the expected thickness and appearance was also apparent in the STEM images of Figure 42.

The shoulder on the boron concentration peak below 10 nm indicates a significant concentration within the AlGaN barrier layer which would be expected to alter typical (boron-free) AlGaN growth behavior. The boron concentration begins to significantly reduce at 20 nm depth providing further evidence of deviation of the AlGaN growth behavior from the expected thickness. The concentration levels off just beyond 40 nm which is consistent with the STEM images in Figure 42. Given the mixed phases seen in the right-most image of Figure 42 and the general appearance of the BN layer in those images, the boron concentration profile in Figure 43 represents an overall concentration from the various phase “pockets” in the region, per profiled depth over the area sampled. The underlying mechanism for this abnormal growth and phase segregation is the large

miscibility gap between BN, AlN and GaN. While this anticipated consequence of the large lattice mismatch of the three materials played a significant role in the growth of this sample, the TEB concentration used in its growth was substantially higher than the previously established upper range limits responsible for measurable 2DEG generation.

This thick BN layer growth experiment was unsuccessful in identifying a BN XRD peak but served to confirm the successful MOCVD growth of BN on GaN under the prescribed growth conditions. Confirmation came from STEM images, verified by EELS, and SIMS depth profiling.

AlGaN/BN/GaN HEMT Growth Optimization

AlGaN/BN/GaN HEMT optimization focused on three variables: TEB flow, ammonia flow, and BN layer growth time. 2DEG quality, as measured on Hall devices, was the primary feedback response for process improvements. Figure 44 compares Hall sheet resistance with total TEB molecules to the reactor from all the AlGaN/BN/GaN HEMTs grown in this study which produced a measurable 2DEG. As the total TEB molecules for a given wafer is the product of growth time and TEB molar flow, it is a good discriminating metric from wafer to wafer.

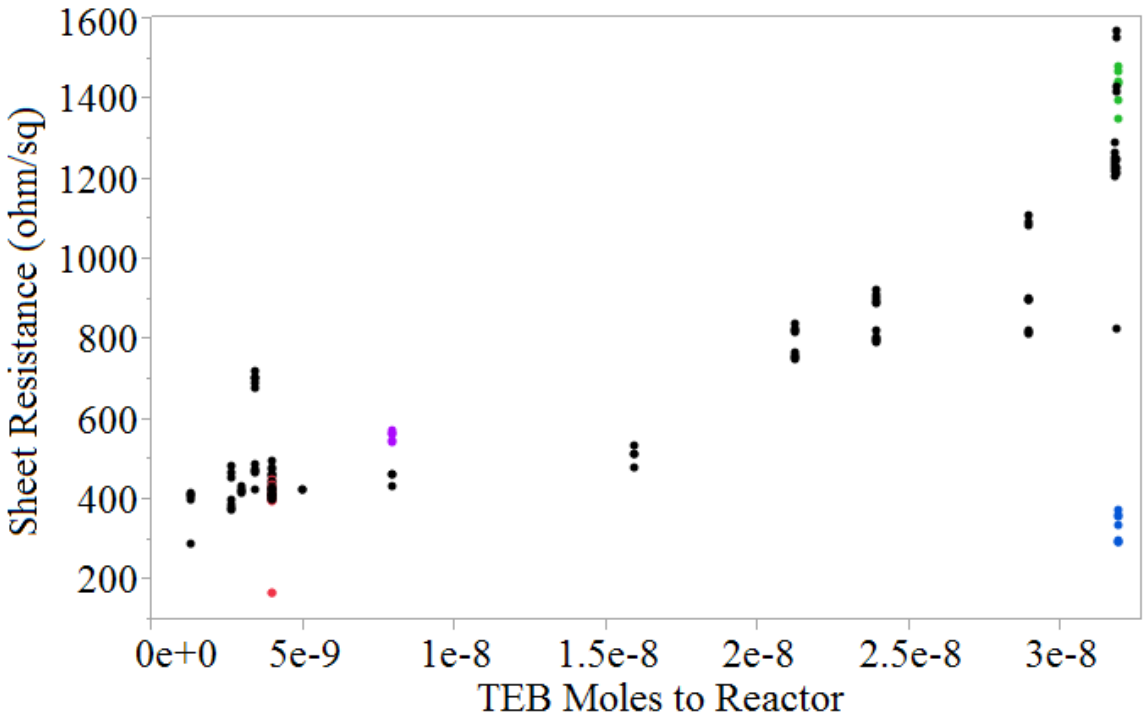

Figure 44. Hall sheet resistance vs total TEB molecules to the reactor for AlGaN/BN/GaN HEMTs. Each point is a single Hall measurement. Most wafers contributed multiple points using different Hall measurement settings and multiple Hall samples per wafer.

The data in the figure indicates a general trend of improved 2DEG properties (i.e., lower sheet resistance) with decreasing TEB molecules to the reactor. The degradation of 2DEG properties at higher TEB concentrations was an expected consequence and is consistent with literature examples of 2DEG-inducing layers which approach or exceed their critical thicknesses [205]. The outliers to this general trend will be discussed in due course. Various wafers which have received special characterization attention are colored for ease of identification in future discussion.

The most severe outliers in the data are the blue colored points in the lower right corner of the graph representing a very low sheet resistance produced with a high TEB concentration. These data are from three Hall samples from one wafer. This wafer was

laden with particles, and is the only such wafer that did not have a pristine or near-pristine surface in the data set in Figure 44, but a measurable 2DEG was present despite the heavy concentration of particles. The Hall data from this growth were impressive. The carrier concentration from three areas of the wafer sampled varied between 2.997e13 to 4.153e13 cm^{-2} with a mobility on the order of 510-555 $cm^2/V\text{-}s$. These remarkable results for carrier concentration; three to four times the normal AlGaN/GaN HEMT 2DEG value (1.0 – 1.1e13 cm^{-2}), warranted detailed investigation. STEM HAADF images of the BN/GaN interface were without an apparent BN layer. Figure 45 shows a representative HAADF STEM image of the GaN surface and barrier layers.

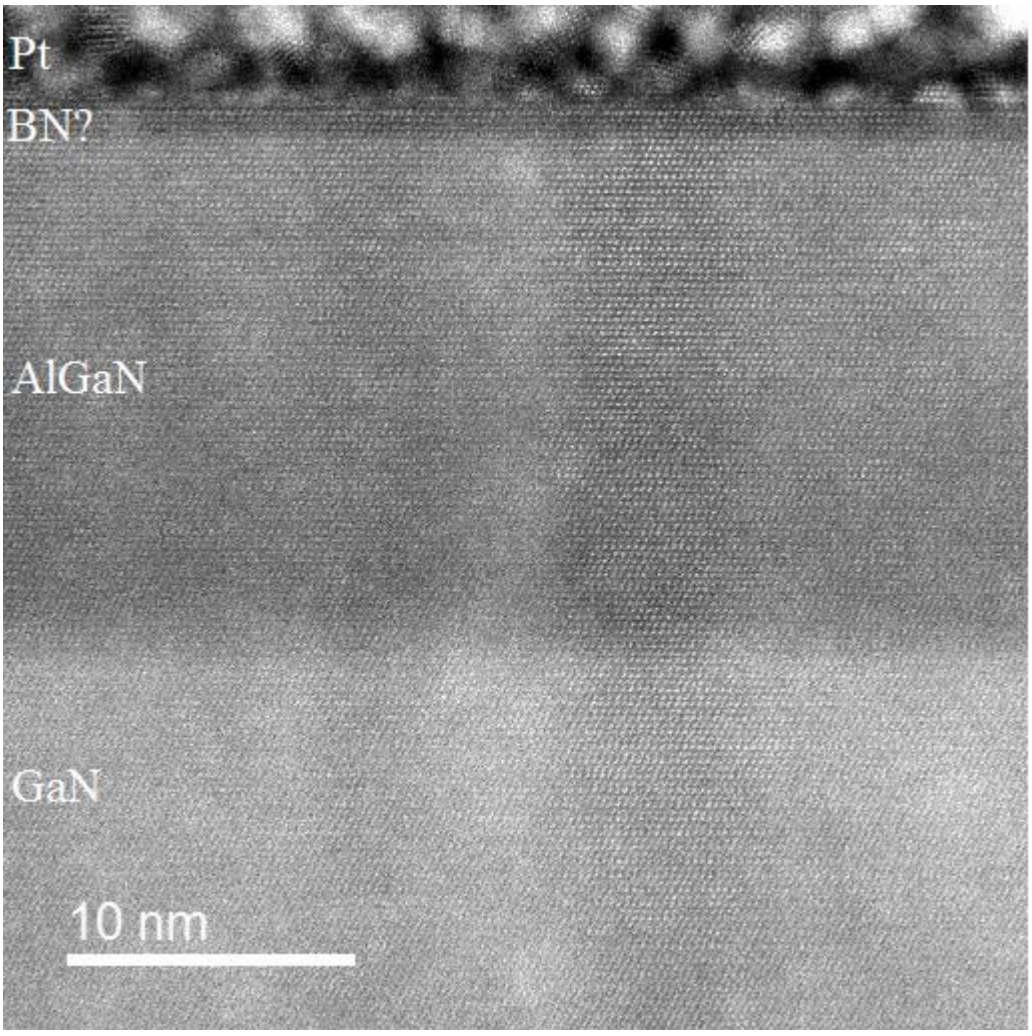

Figure 45. HAADF STEM image of AlGaN/BN/GaN HEMT structure GaN buffer and barrier layers. Platinum is the uppermost (mottled appearance) layer, followed by barrier layers and lighter GaN buffer at the bottom.

Notable in this image is the lack of a contrast region at the AlGaN/GaN interface that would indicate the presence of a BN-containing layer. Boron nitride is expected to be darker in appearance under this dark field Z-contrast image due to the high angle incoherent scattering of electrons defining the HAADF imaging technique. This scattering is highly sensitive to the physical size (and electron density) of a given atom which is directly related to its atomic number, a very discriminating metric for elements from the same periodic column.

A curious observation; the region in the image which should be a GaN cap atop the AlGaN barrier layer is contrarily dark and could indicate the presence of BN on the surface of the wafer. This BN layer, if correctly identified, would indicate that BN exhibits a material growth phenomenon similar to surfactant-mediated epitaxy [184] as has been seen in III-V growth, and other material growth on III-V surfaces, using In [165], [219], [234], Mg [21], [22], Sb [186], and other atomic and molecular species [184], [186]. The governing principle behind this epitaxial phenomenon is the miscibility gap between the so called surfactant and the bulk of the epitaxy surface. The result of the surfactant behavior is a constant segregation of the species in question to the epitaxial growth front. The general impact of this surfactant on the surface is a change in the growth behavior of incoming material. This change can range from an alteration of surface mobility effecting local composition or surface morphology, or the preferred incorporation of a given material at the surfactant site to the extent of enabling some material deposition that is otherwise not favored or even allowed. In this case, the BN would have formed on the GaN surface and then preferentially remained at the growth front during the incorporation of the barrier AlGaN and GaN cap. If this is the situation, the explanation of the remarkable 2DEG carrier concentration could be the existence of a double 2DEG; one created by the normal AlGaN/GaN interface, and another created by a BN/AlGaN interface. If the latter were to exist, its mobility would undoubtedly be poor due to the bond alternation of its ternary host material with the addition of significant strain at that interface given that the AlGaN is experiencing both tensile and compressive strain from its proposed interfaces with GaN and BN (or high boron concentrated layer), respectively. Figure 46 offers a magnified view of the superficial layer which could be

the surfactant BN. Given that the layer is in the expected location of the GaN cap, it may be an abnormal appearing GaN layer instead, though the possibility for it being BN or a BGaN alloy must be acknowledged. SIMS analysis of this wafer was not pursued due to the high concentration of particles which would have convoluted meaningful results.

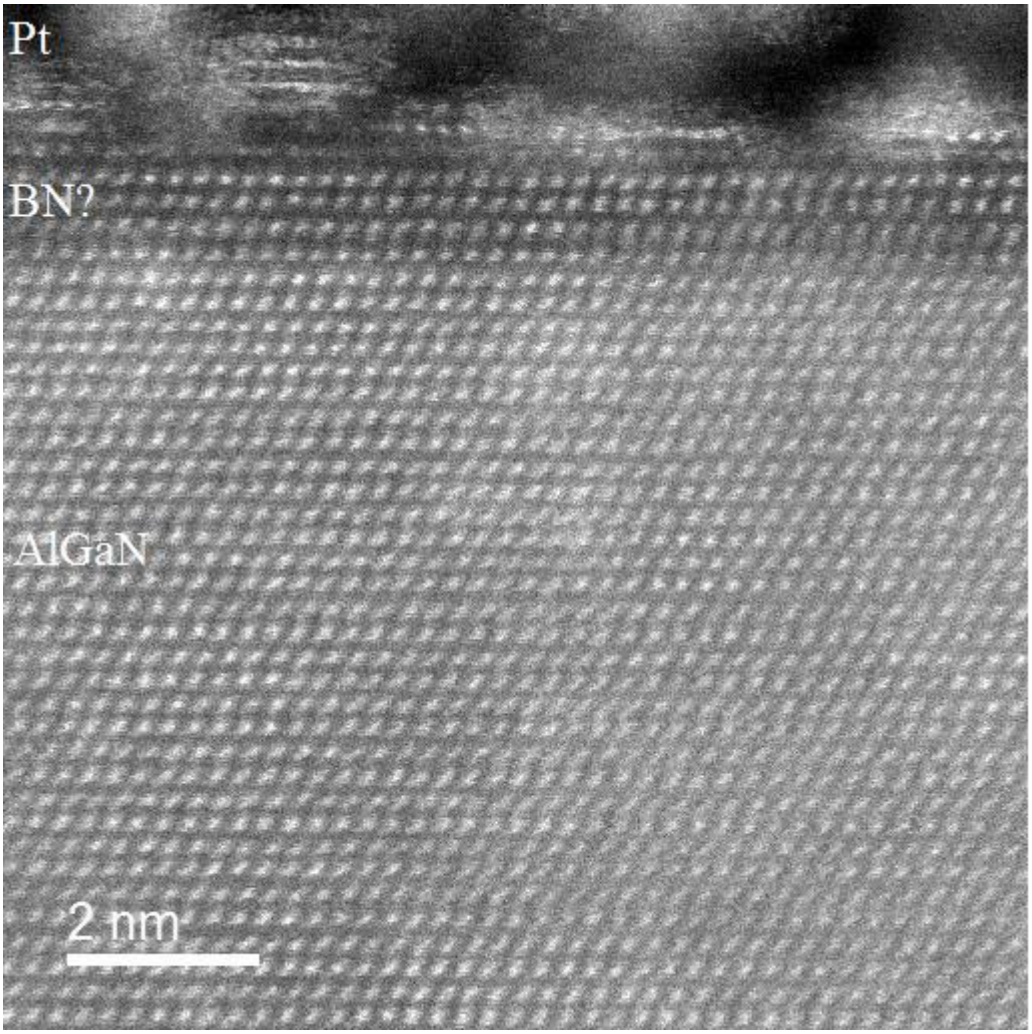

Figure 46. HAADF STEM image of the first few atomic layers of a BN-based HEMT structure. The uppermost region is platinum followed by what is considered to be a high boron content layer followed by the AlGaN barrier layer. The GaN buffer is not visible in this image.

Comparatively, Figure 47 shows a HAADF STEM image of a traditional AlGaN/GaN HEMT with SiNx passivation layer (not clearly visible). This image illustrates the typical appearance of a GaN cap layer.

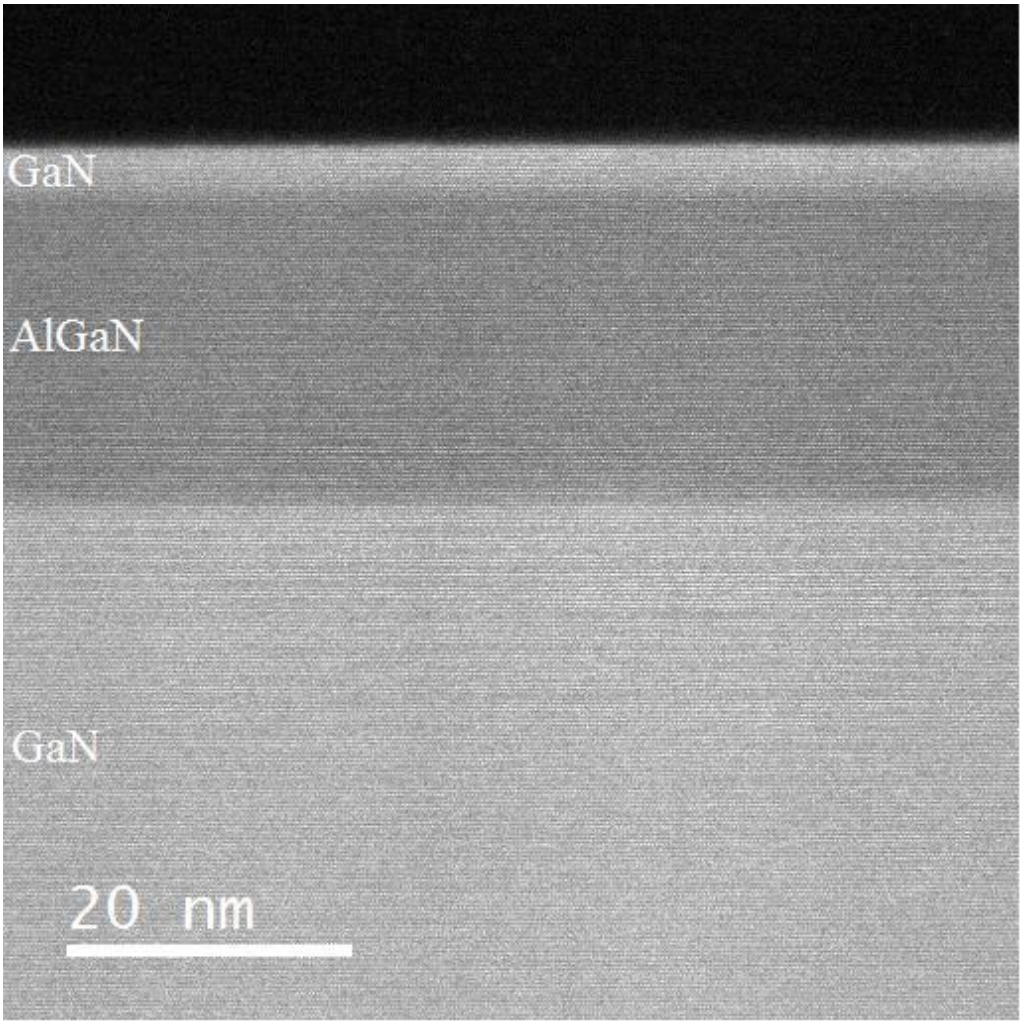

Figure 47. HAADF STEM image of superficial AlGaN/GaN HEMT layers. From top to bottom, SiNx passivation layer, GaN cap, AlGaN barrier, and GaN.

Ideally, a GaN cap layer should have the same contrast as the bulk GaN, as is apparent in this image. The HAADF STEM images in Figure 45 and Figure 46 show a GaN cap region whose appearance is darker than all other III-N layers in the images,

when compared to the traditional, boron-free, HEMT structure in Figure 47 the possibility of the surfactant behavior of BN is very likely.

A repeat of the same recipe, with preventative methods to discourage particle formation, resulted in an AlGaN/BN/GaN HEMT which conformed to the expected 2DEG properties per the total TEB molecules to the chamber and the sheet resistances reported in Figure 44. Data from the repeat sample are colored green and are in-line with the overall trend from the total data set in regards to the expected sheet resistance per the total TEB molecules to the reactor. STEM analysis of this wafer produced the images shown in Figure 48.

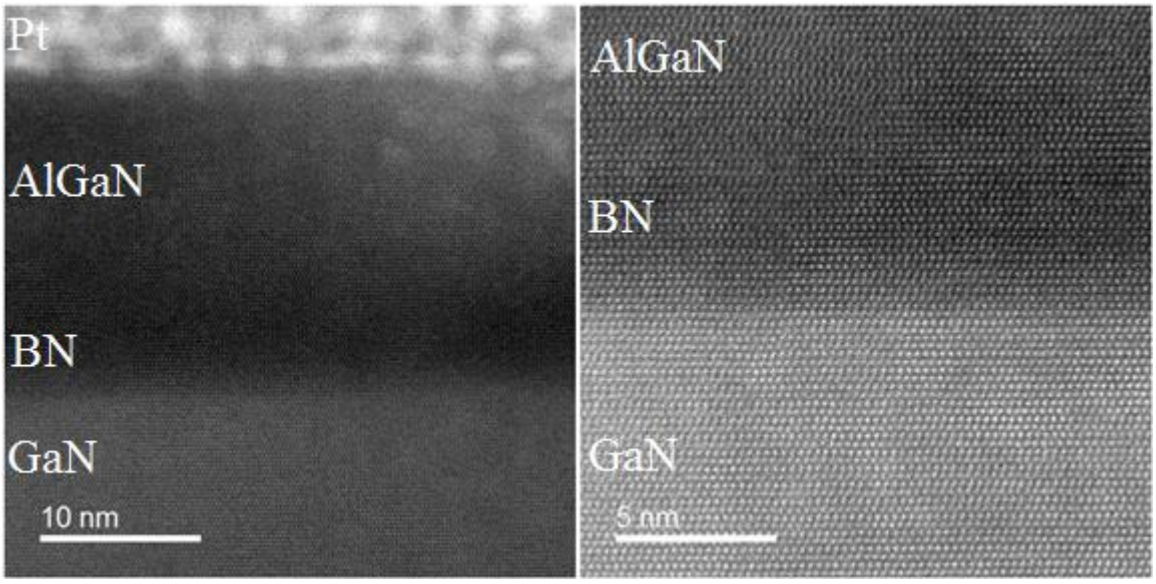

Figure 48. HAADF STEM images of AlGaN/BN/GaN HEMT structure. Platinum is visible in the top image along with a faint GaN cap layer. Images indicate the AlGaN barrier layer containing a darker BN layer of approximately 5-8 nm directly above the underlying GaN buffer layer.

The images show a markedly darker region above the GaN buffer. This region was confirmed to contain BN by EELS. The layer's BN/GaN interface is well-defined but the AlGaN/BN interface is not well defined. This is likely a result of the strain

induced morphology changes of the BN layer comparable to those reported for thin AlN layers on GaN surfaces [205]. The averaged Hall data (green data in Figure 44) from this wafer are: 6.140e12 cm^{-2} carrier concentration, 713 cm^2/Vs mobility and 1431 ohm/sq sheet resistance. These data indicate a lower quality 2DEG compared to the baseline structure which is exactly what one would expect from the measured thickness and apparent morphological changes to the BN barrier interface layer.

SIMS analysis of this wafer is presented in Figure 49. This graph indicates that the desired AlGaN/BN/GaN material stack contains an intermixed AlGaN & BN region.

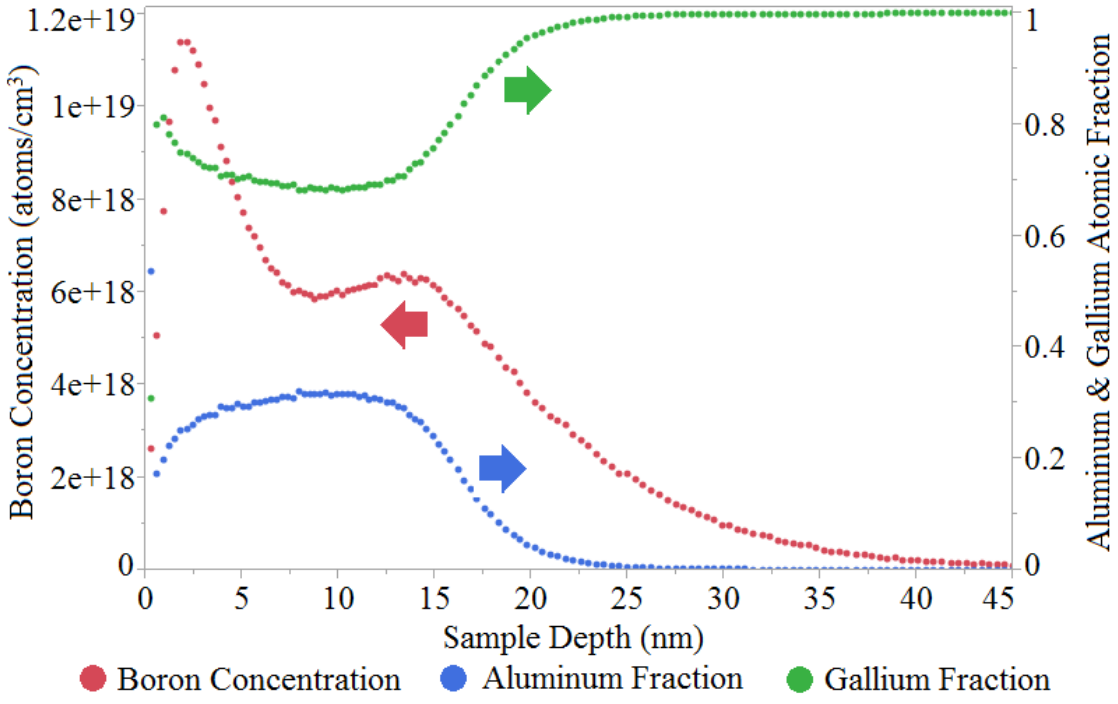

Figure 49. SIMS depth profile of the AlGaN/BN/GaN wafer from Figure 48. The left axis is boron concentration in atoms/cm^3. The right axis is the relative aluminum and gallium atomic fractions used as HEMT structure depth markers. The increased boron signal located just prior to the sharp increase in gallium concentration indicates the presence of BN/GaN interface, though the concentration of boron within the depth of the AlGaN region along with the presence of aluminum up to the increased boron-concentrated region indicates an overall poor definition of the prescribed AlGaN/BN/GaN HEMT structure.

A high concentration of boron within the first few monolayers is seen, similar to the layer that was visualized in the STEM images of the parent wafer in Figure 45 and Figure 46. The irregular thickness of the regrowth BN layer evident in the STEM images in Figure 48 also supports this intermixing hypothesis, either from a severely non-planar AlGaN/BN interface, a quaternary BAlGaN with a significant boron gradient which increases with depth, or a combination of the two. The latter option is supported by the combined STEM images and SIMS data, though given the techniques' relative contrast and depth profiling methods, it is not conclusive.

The comparison of this sample with its particle-laden analog presents a curious case of the unknown impact of particles on the epitaxial process. With the preferential surfactant behavior observed in the parent wafer's BN layer and the apparent absence of boron at its GaN surface combined with the observed presence of higher boron concentrations within the prescribed BN/GaN interface of the regrowth wafer, and their markedly different Hall measurements, one can conclude that the impact of the particles on the grown layers was very significant to the overall growth process, or the less likely, and poorly supported, possibility that the reactor conditions, despite their exact duplication, were somehow different resulting in different BN growth behavior for identical recipe executions.

Another interesting outlier to the AlGaN/BN/GaN HEMT population trend of decreasing sheet resistance with increasing TEB molecules to the chamber presented in Figure 44 is the wafer whose data is represented by the red data points. Four out of five of the Hall samples from this wafer align with the expected sheet resistance / TEB concentration trend. The fifth sample produced the separated red data points, well below

the general population. What appears as a single point is actually multiple measurements from the same sample over different sessions to check for instrument error. Hall data from this wafer is averaged in Table 6.

Table 6. Quantified Hall data of AlGaN/BN/GaN wafer represented in Figure 44 by the red data set.

	Carrier Concentration (10^{13} cm^{-2})	Mobility ($cm^2/V*s$)	Sheet Res (ohm/sq)
Single Sample	2.106 ± .04	1780 ± 25	167 ± 1
Rest of Samples	1.147 ± .05	1316 ± 71	415 ± 18

The remarkable data from this sample are competitive with the best state-of-the-art 2DEGs in the world, presently. A SIMS depth profile for this wafer, taken from a radially symmetric location as the Hall sample, is presented in Figure 50 along with a

reference SIMS depth profile from the previously discussed “regrowth sample” which had a BN profile layer of 5-8 nm as measured by STEM.

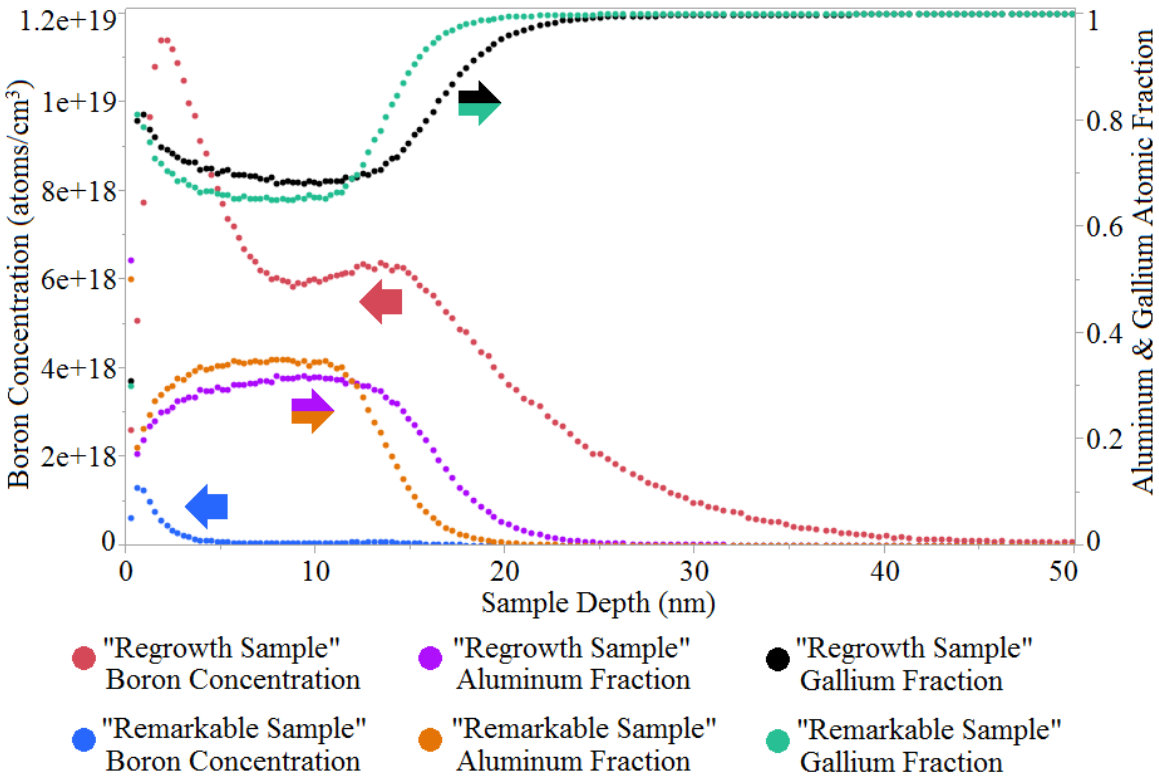

Figure 50. SIMS depth profile comparison of AlGaN/BN/GaN wafers. “Regrowth Sample” corresponds to the green data points in Figure 44 and “Remarkable Sample” corresponds to that figure’s red data points, currently under discussion. The regrowth sample had a STEM measured BN profile layer of 5-8 nm.

The figure suggests that the boron concentration distribution is not at all similar between the two displayed samples, aside from the consistent higher concentration near the surface. The same non-boron barrier layer parameters were used for both growth structures. The deeper offset of the increase in gallium fraction, indicating penetration of the GaN buffer, of the regrowth sample relative to the remarkable sample indicates a thicker depth contribution by the BN of the regrowth sample. The growth parameters used for these BN layers should have produced a BN profile layer thickness of the

remarkable sample which is 1/8th the thickness of the regrowth sample's, which was measured at ~5 – 8 nm. The relative growth parameters of TEB flow rate and layer growth time are ½ and ¼ smaller, respectively, in the remarkable sample relative to the regrowth sample, effectively reducing the TEB molecules delivered to the chamber by 1/8th for the former. This 1/8th difference is not apparent in the SIMS data, in fact, the boron concentration of the regrowth sample is, on average, 100.67x higher than the remarkable sample over the ~19 nm that the two have an appreciable SIMS signal. This large discrepancy between the prescribed growth recipe difference and the SIMS measured concentrations is another example of the curious behavior of BN within the GaN HEMT structure.

STEM images of the remarkable wafer are shown in Figure 51.

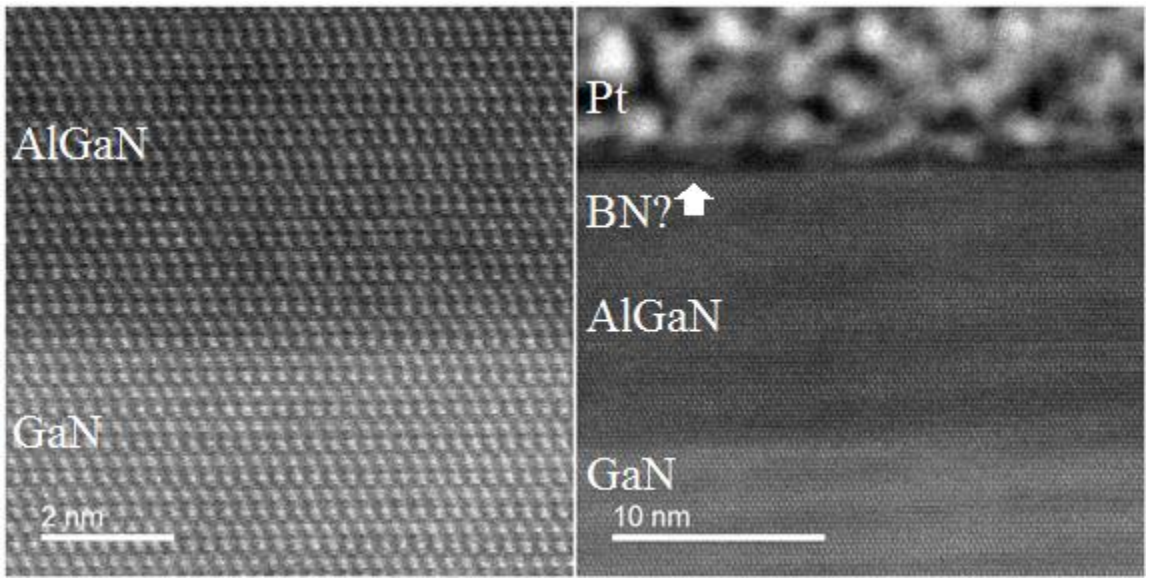

Figure 51. STEM HAADF images of AlGaN/BN/GaN wafer producing the "remarkable" measurements (red data points from Figure 44). BN is not readily apparent at the AlGaN/GaN interface magnified in the left image. The right image shows the surface platinum above what may be a thin BN layer with AlGaN and GaN underneath.

The images show an AlGaN/GaN interface, without a darker region near the interface. This data indicates that a concentrated BN layer is not present at this interface. The right image of the figure has what may be indicative of a BN or BGaN layer on top the AlGaN barrier layer. The thickness of this layer is approximately identical to the target BN layer thickness of 1 nm. If this layer is BN, or a high boron concentration layer, then it may be responsible for the improved 2DEG measurements as would be similar to the particle-laden sample previously discussed.

The Hall data from this region of the wafer contain a very high electron mobility which is contradictory to the particle-laden wafer's relatively low mobility. One explanation for the disconnect between the high quality 2DEG and the characterization efforts is that the characterization missed the structure responsible for inducing the 2DEG. A potential AlGaN/BN/GaN layer structure employing this ~1 nm BN layer could indeed be responsible for the Hall data, but the conditions necessary for its stable growth are either not uniformly met across the wafer or are so restrictive in their functional window that only a small portion of the wafer satisfied them. Without direct evidence of this layer configuration, results remain inconclusive. Though a possible explanation, following the surfactant-like behavior seen in both wafers, is that the latter example contains a much thinner boron-containing layer and may not suffer from critical thickness induced degradation of the 2DEG. This scenario is consistent with previously defined behavior of thin AlN on GaN layers which exceeded their critical thicknesses [205]. 2DEGs induced by such layers contain significantly enhanced carrier concentrations and reduced mobilities due to the morphological changes associated with critical thickness strain at the interface. If this scenario is accurate for the particle-laden

2DEG which exceeded a carrier concentration of 4e13 cm^{-2} in one Hall sample, then the potential for a BN induced 2DEG far exceeds that of other III-N HEMT configurations.

The wafer labeled the regrowth sample visually contained the prescribed AlGaN/BN/GaN configuration while the remarkable sample did not, despite similar growth conditions. The primary difference between the two is growth time. Another sample, represented by the purple data points in Figure 44 was grown with the same growth time with ¼ less TEB flows, relative to the regrowth sample, with all other parameters unchanged. SIMS depth profiling of this ¼ flow wafer is shown in Figure 52 along with the regrowth sample for direct comparison.

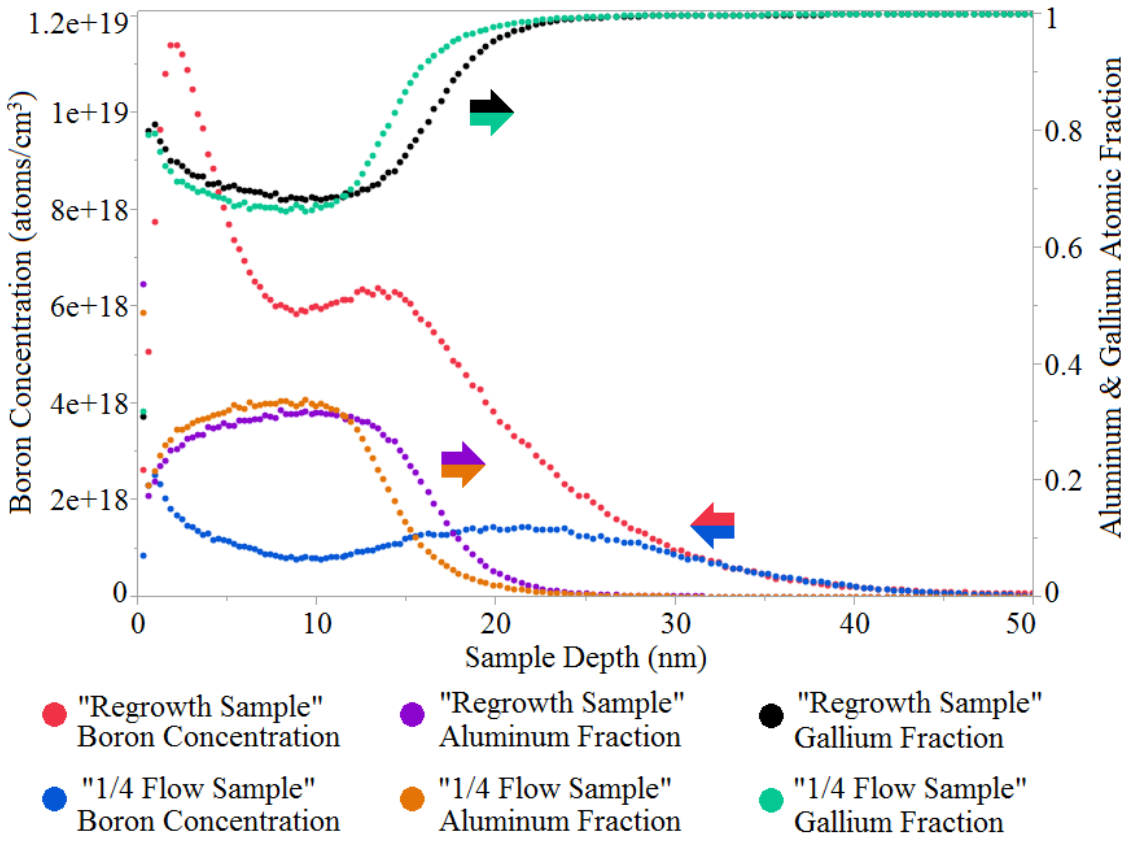

Figure 52. SIMS depth profiling of AlGaN/BN/GaN HEMT structures. The "1/4 flow sample" corresponds to the purple data points in Figure 44 and the "regrowth sample" corresponds to the green data points from that figure.

The figure indicates that the boron concentration of the ¼ flow wafer follows a similar distribution with maxima at the surface and near the AlGaN/GaN interface. The offset of the aluminum and gallium fraction curves for the two wafers indicate that the GaN surface for the ¼ flow sample is not as deep within the structure as the regrowth sample. This would indicate a smaller BN thickness contribution. The maximum near the AlGaN/GaN interface of boron concentration for the ¼ flow structure is deeper than its counterpart, even more so considering the offset of the GaN surface. This may be misleading and simply a product of the concentration which was allowed to diffuse relative to the total boron concentration. While the maxima of the two samples near their respective GaN surfaces are offset, there is still a greater concentration in the regrowth sample which has the greater overall boron concentration. The two recipes differed, as the moniker would suggest, by ¼ the TEB flow rate with the same growth time. Intuitively this should reduce the boron concentration in the ¼ flow wafer by ¼ relative to its counterpart structure. Statistically, over the ~19 nm depth over which the two have significant boron concentrations, the concentration of the regrowth sample is on average 6.15x that of the ¼ flow sample. Again, diffusive processes may be more appreciable relative to the overall boron population in the latter sample. Mechanistically, diffusion within a solid solution will be limited by compositional restraints of a given medium. In this case, the boron of the higher concentrated sample would have been restricted in its diffusive options by this compositional restraint into the GaN forcing some boron atoms into a higher concentrated alloy or binary BN providing a more stable solid solution, discouraging diffusion into other layers. Accordingly, the lower concentration sample may have experienced less a restraint and accumulated less concentrated material

proportionately. The discrepancy between the prescribed 4x to the measured 6.15x greater boron concentrations within the barrier layer regions of the two structures is likely due to diffusion and the 19 nm sample size used for the calculation.

TEB Molecules to the Chamber: Time vs Flow

The two routes of manipulating the total TEB molecules to the reactor for a given AlGaN/BN/GaN growth process include altering the growth time while maintaining the flows, or reducing the flows while maintaining the growth time. The existence of barriers to BN nucleation would favor the latter option, while minimizing structural rearrangement of a strained layer would favor the former. Comparative AlGaN/BN/GaN HEMT wafers within the experimental set (shown in Figure 44) allow for a direct comparison of the impact of these two alternative routes. Maintaining the TEB flow rate and adjusting the layer growth time presents a direct analysis on the thickness of a prescribed layer with a consistent growth rate from sample to sample. Figure 53 shows the sheet resistances of Hall samples from three studies of constant TEB flow rate with varied BN layer growth times for AlGaN/BN/GaN HEMTs.

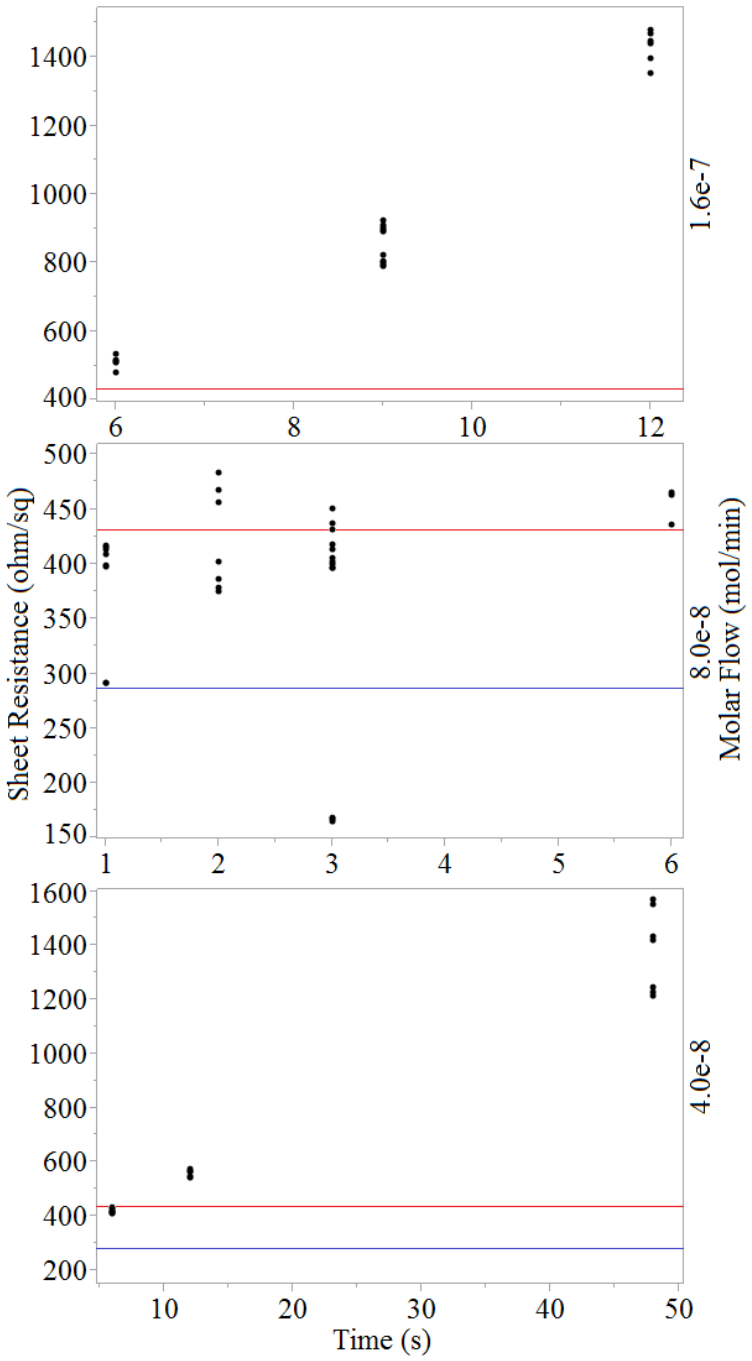

Figure 53. Sheet resistance vs growth time for AlGaN/BN/GaN HEMT structures with matched TEB flows. Note the three graphs have differently scaled axes. Averaged baseline sheet resistances are included for comparison. AlGaN/GaN baseline sheet resistance is marked in red, AlGaN/AlN/GaN baseline sheet resistance is marked in blue. Each data point represents one Hall measurement. Clustered points are from the same Hall sample, columnar points are from the same wafer. The general trend of an improved sheet resistance with lower growth time is observed. The middle graph deviates slightly with the significantly improved Hall sample measurements, previously discussed.

The figure suggests a trend of improved sheet resistance for lower growth times with the same TEB flow rate. This supports the overall trend from this work of improved 2DEG quality for reduced total TEB molecules to the growth surface. As previously discussed and seen in other results, the impact TEB exposure has on the growth structure is not necessarily the growth of a concise BN layer, but instead a contribution of diffused or surfacted boron into the more superficial layers of the HEMT structure. It can be safely assumed that with the identical flow regimes of the experiments presented in Figure 53, the diffusive behavior of the boron into the surrounding layers will also be identical, as allowed by the BN layer growth time.

Important observations from the comparison of the experiments, most notably the comparison of the two 12 second growth time wafers which are found in both the top and bottom graphs of the figure, reveal the impact of higher flow rates at the same growth times. Increased strain within the structure decreases the 2DEG quality, once sufficiently beyond the critical layer thickness. This is seen in the comparison of the 4x flow rate difference of the two 12 second data sets. The higher flow rate produced a measured sheet resistance of ~1400 ohm/sq while the ¼ reduced flow rate produced a sheet resistance of ~550 ohm/sq. The middle graph which represents the intermediate TEB flow rate, but substantially reduced growth times, contains the best AlGaN/BN/GaN HEMT measurements from this research. The "remarkable sample," is found at the three second column. To reiterate the discussion, a single Hall sample contained the remarkable results while the remainder of the Hall samples tested fall in line with the bulk of the data and do not so substantially deviate from the AlGaN/GaN baseline HEMT 2DEG properties. Not to be overlooked, the intermediate 2 second BN layer wafer

contained larger regions of better-than-baseline measurements. This non-uniformity, while not ideal, still serves to illustrate the benefit of an AlGaN/BN/GaN HEMT structure.

Altering the flow rate with a constant growth time is a useful method to observe the impact of growth rate, given the same time-sensitive opportunities of nucleation, diffusion and structural rearrangement of the BN layer. Figure 54 shows the sheet resistances of Hall samples from four experiments of constant BN layer growth times within AlGaN/BN/GaN HEMT structures with varied TEB flow rates.

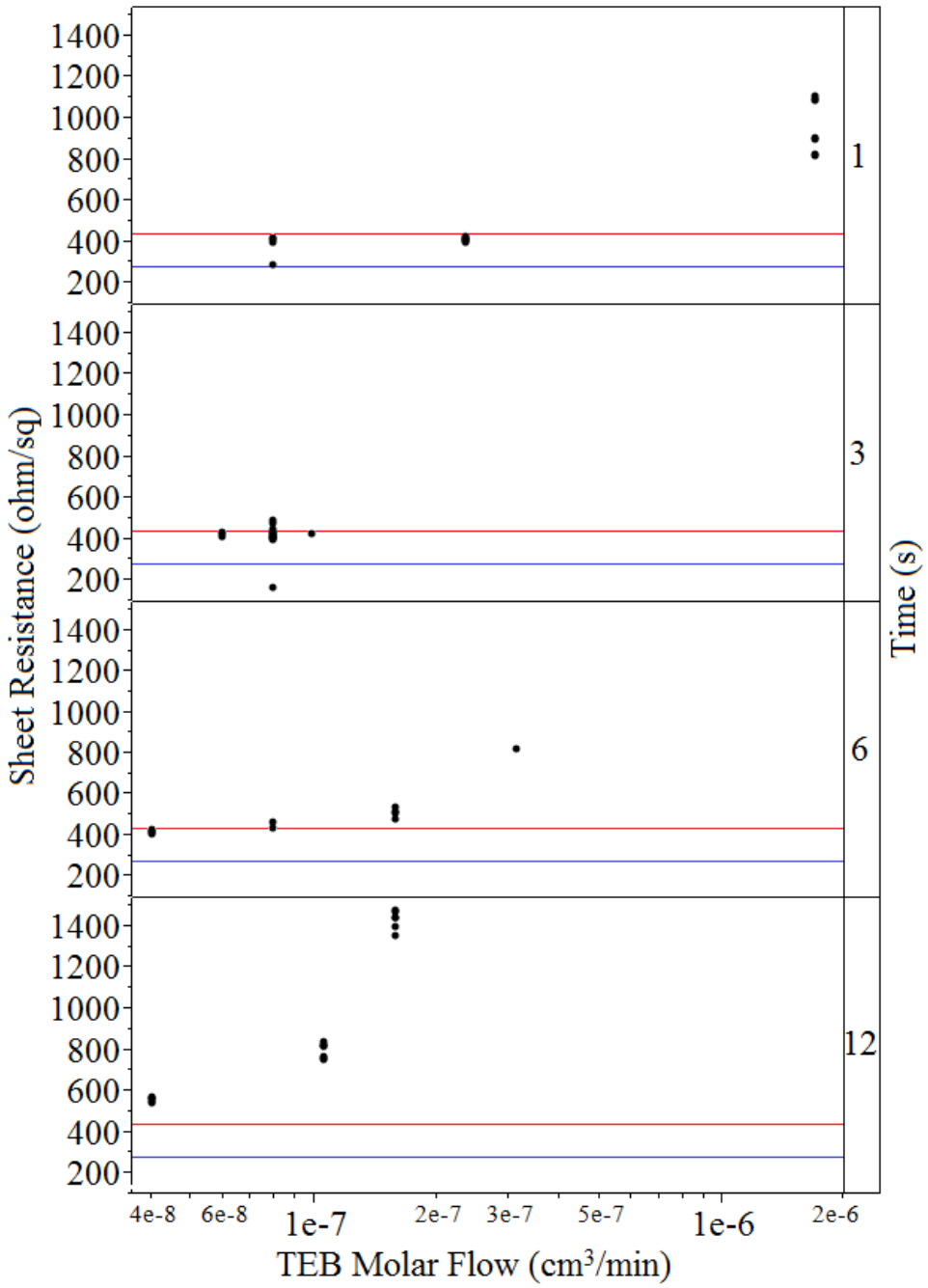

Figure 54. Sheet resistance vs TEB molar flow for AlGaN/BN/GaN HEMT structures with matched BN layer growth times. Averaged baseline sheet resistances are included for comparison. AlGaN/GaN baseline sheet resistance is marked in red, AlGaN/AlN/GaN baseline sheet resistance is marked in blue. The general trend of improved 2DEG quality with reduced TEB is evident in the majority of these data sets with exception of the second graph from the top is likely due to the smaller range of TEB flows within the study.

The figure supports the overall trend of better 2DEG properties with reduced total TEB molecules to the growth surface. The upper flow (total TEB concentration) tolerance ranges for the AlGaN/GaN heterostructure are apparent in most of the data sets. The higher data points (> 600 ohm/sq) are significantly beyond typical 2DEG quality in device-quality structures. The lower flow ranges for each set are competitive or better than standard commercial AlGaN/GaN HEMT structure 2DEGs. The comparison between the shorter and higher growth time studies shows a greater tolerance for higher flow rates for the lower growth times. This is a natural consequence of a reduced total TEB concentration within the structure. This is most appreciable in the extrema of the study in the comparison of the 1 second and 12 second graphs. The intermediate point of the 1 second graph is from a higher flow rate than the highest point of the 12 second study, yet the 1 second data point is from a very good 2DEG while the 12 second growth is a very poor 2DEG measurement. Again, this is a natural consequence of the total TEB concentration within the HEMT structure.

Comparing BN profile layer growth times between AlGaN/BN/GaN HEMT structures with identical total delivered TEB molecules, and necessarily different flows to accommodate this relationship, will determine the impact of layer growth time between these similar structures. The Figure 44 data set contains three such groupings, presented in Figure 55.

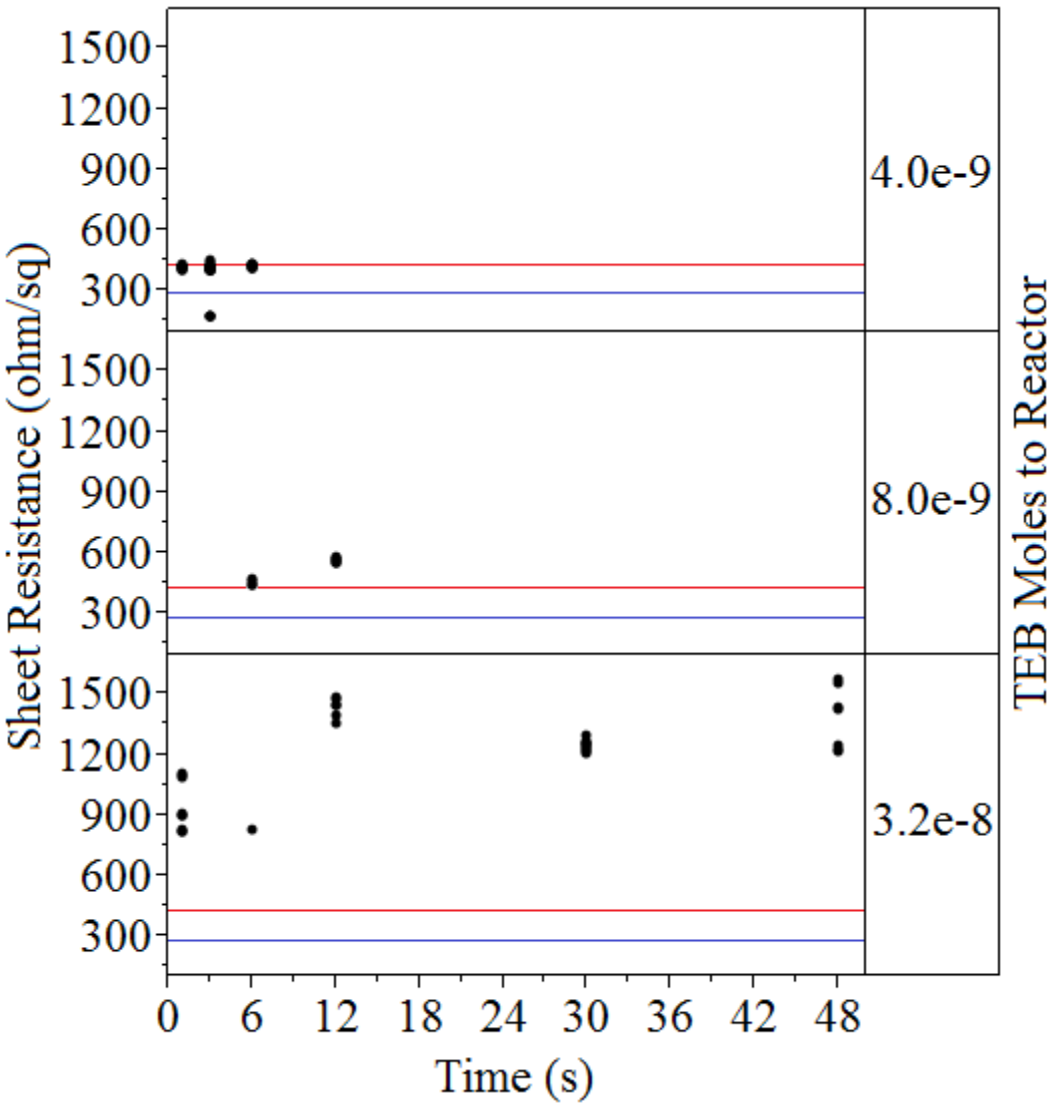

Figure 55. Sheet resistance vs BN layer growth time for AlGaN/BN/GaN HEMT structures with matched total TEB molecules delivered to the reactor. Averaged baseline sheet resistances are included for comparison. Each data point is from a single Hall measurement, columnar data sets of each graph come from the same wafer. The trend of reduced profile layer growth times producing better quality 2DEGs is loosely supported.

The figure suggests that a reduced growth time is best for a higher quality 2DEG. The lower graph contains data from five wafers, but the inconsistency of the lowest growth time samples and the higher sheet resistances of the 12 second BN layer's Hall measurements relative to its 30 second counterpart diminish its contribution to a general trend. Consistent within the data of Figure 55 is the overall trend of reduced total TEB

molecules producing better quality 2DEG measurements. This is most notable when comparing the highest TEB concentration graph to the other two, which are closer in concentration to one other. The impact of BN profile growth time within AlGaN/BN/GaN HEMT structures on the overall 2DEG properties, when compared between wafers of identical TEB concentrations, is somewhat inconclusive but the trend of reduced growth times producing better 2DEGs is suggested. This is likely due to the impact of structural rearrangement in response to layer strain in the form of relaxation events and morphology changes as has been seen in previously discussed samples.

V/III Ratio

Following the general trend in group III element reactivity and the resulting solid stability of III-N compound semiconductors, BN is expected to be very stable and require a relatively low V/III ratio for successful growth from TEB and ammonia under typical MOCVD conditions. While the larger group III elements, specifically indium and gallium, require higher V/III ratios due to their tendency to decompose, the more stable BN and AlN do not require such high ammonia concentrations to maintain their composition. The corresponding effect on growth parameter changes is a slight to absent change of material properties with relatively large changes in V/III ratio, provided that a minimum threshold for reactivity, determined by the activation rate of ammonia, is met. Figure 56 summarizes the bulk of AlGaN/BN/GaN HEMT structures used in this work.

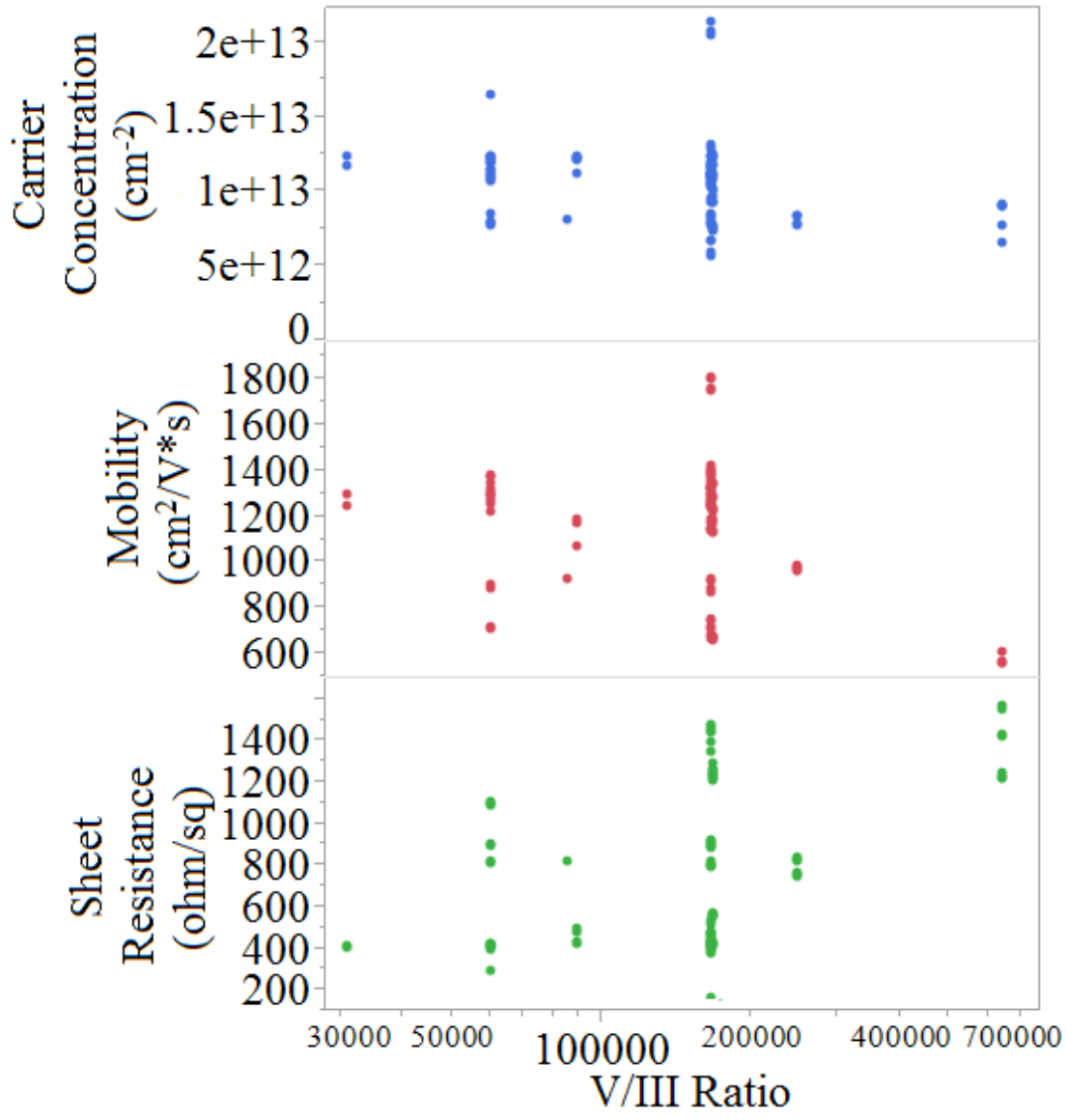

Figure 56. V/III ratio vs Hall measurements for BN profile layers within AlGaN/BN/GaN HEMT structures. No definitive trends are apparent between Hall measured 2DEG metrics and the V/III ratio of these BN profile layer induced 2DEGs.

The figure compares the Hall measured 2DEG carrier concentration, mobility and corresponding sheet resistance with the V/III ratio used in each AlGaN/BN/GaN HEMT structure's BN layer. Each structure's AlGaN barrier layer is identical, though a variety of flows and growth times are included in the data. No strong trend is apparent within the data for any 2DEG metric. This supports the general idea that the minimum ammonia

concentration has been met for every BN sample. Extremely low V/III ratios are not attainable with the hardware used to grow these samples. A lower flow ammonia MFC than is currently employed on the MOCVD reactor would be necessary to reliably maintain the very small flows needed to push the lower limits of BN reactivity and solid stability should they exist at typical MOCVD temperatures and pressures. To compare the behavior of HEMT structures within the more populated columns of Figure 56, studies of constant V/III ratio with varied BN layer TEB flows and growth times are presented in Figure 57.

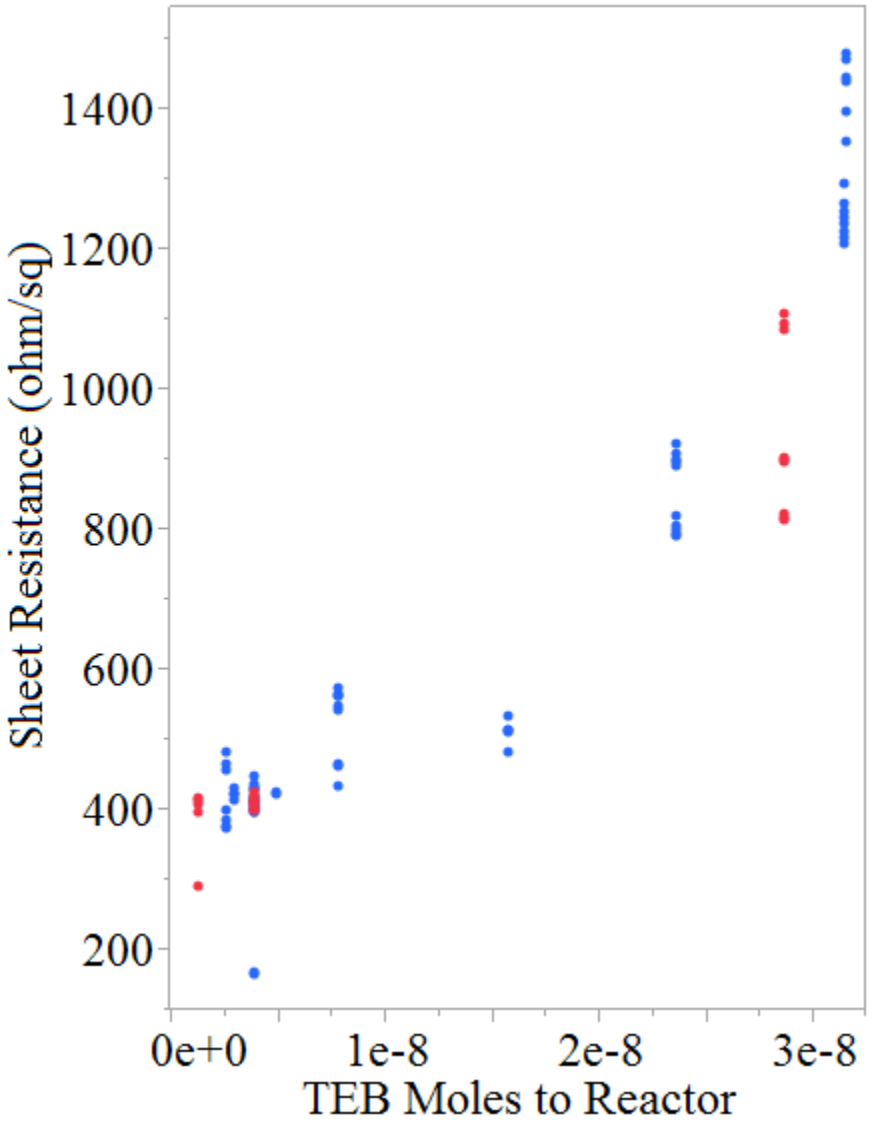

Figure 57. Sheet resistance vs TEB moles to reactor for BN layer growth within AlGaN/BN/GaN HEMT structures. BN layers producing blue data points were grown with a calculated V/III ratio of ~174,000 and those represented by red data points were grown with a calculated V/III ratio of ~60,000. No apparent difference is observed for either V/III ratio.

The two constant V/III ratio studies are not appreciably different from one another. The larger blue data set in the figure is partially defined by the standard ammonia flow employed for every AlGaN barrier layer used in this research, which is also used in the baseline AlGaN/AlN/GaN recipe which was used as a template and is

responsible for the large data set size. The majority of the samples use a lower ammonia flow corresponding to their low TEB flows. The consistency between the two V/III ratios used in this study supports that the ammonia concentration threshold is met. While an optimal V/III ratio range is likely to exist for these growth conditions, the ratios used in these data are either both within or outside that range. Further evidence is needed to identify V/III ratios which are not conducive for BN growth. A study of constant growth parameters with varied V/III ratios is presented in Figure 58.

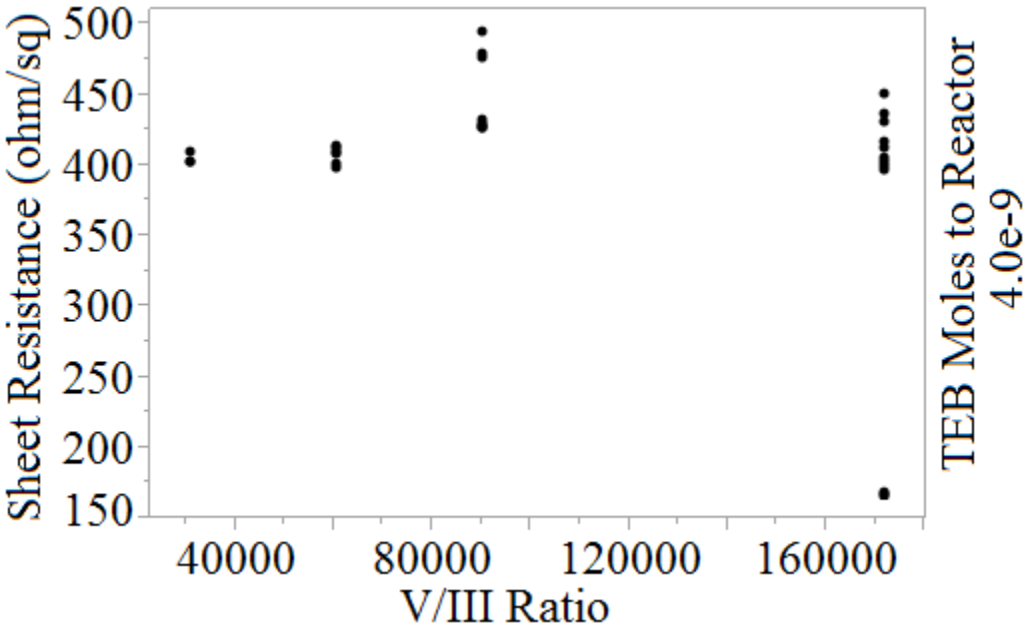

Figure 58. Sheet resistance vs V/III ratio for BN layer growth within AlGaN/BN/GaN HEMT structures. This study varied V/III ratio while maintaining all other growth parameters to isolate the impact of ammonia concentration on the growth of BN layers and the resulting consequences to 2DEG properties.

The study suggests a relatively flat relationship between sheet resistance and V/III ratio under these BN layer growth conditions. The greatest impact to 2DEG measurements from changes to V/III ratios in this study is the difference in uniformity of measured Hall samples from each wafer. Each column of data points within the figure

come from the same wafer. The left most data set came from a single Hall sample but the next set, still at a relatively low V/III, is from across its wafer and is more uniform than the higher V/III ratio data sets with similar sampling areas. This is a small sample size and may not portray an accurate consequence of changing V/III ratios.

Overall the effect of V/III ratio changes on BN layer growth within AlGaN/BN/GaN HEMT structures over the ranges used in this work does not seem significant. The theory of a minimum ammonia threshold needed to satisfy BN layer growth from the reaction of TEB and ammonia under MOCVD conditions is supported, though more evidence is needed to define such a threshold.

AlGaN/BAlN/GaN HEMT Growth

Figure 59 shows AlGaN/AlN/GaN HEMT AlN profile layer growth times and the resulting Hall-measured 2DEG sheet resistances. Table 7 quantifies the Hall measurements for the AlGaN/AlN/GaN HEMTs with varied AlN profile growth times.

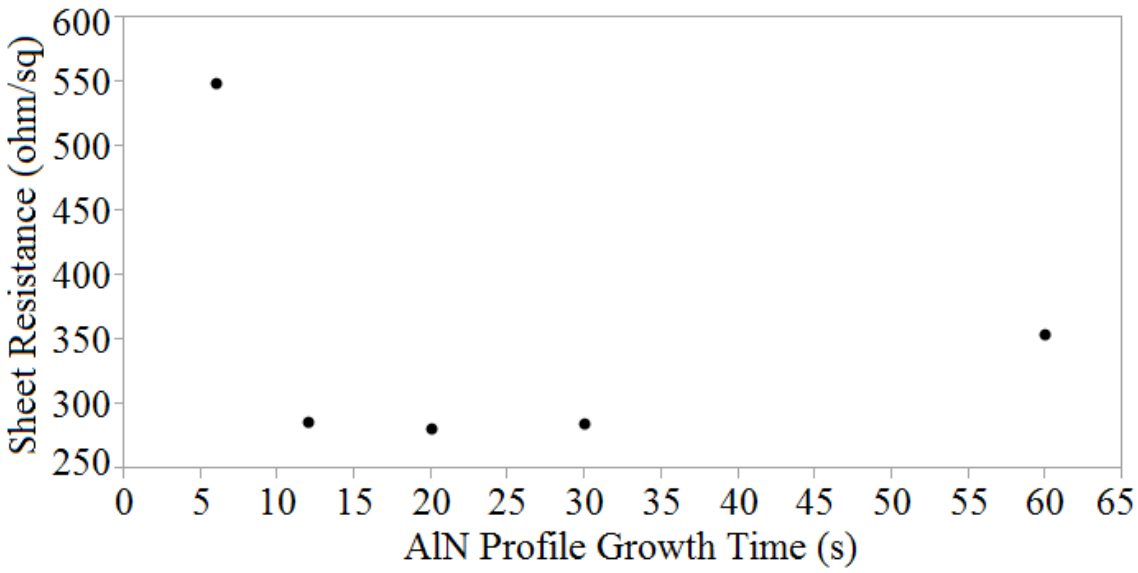

Figure 59. Sheet resistance vs AlN profile growth time for AlGaN/AlN/GaN HEMTs.

Table 7. Hall measurements for AlGaN/AlN/GaN HEMTs with varying AlN profile growth times.

Profile Growth Time (s)	Carrier Concentration (cm-2)	Mobility (cm2/V*s)	Sheet Res (ohm/sq)
6	1.373E+13	827	549.3
12	1.225E+13	1780	286
20	1.286E+13	1727	281.4
30	1.487E+13	1470	285.1
60	1.498E+13	1180	353.9

The AlGaN/AlN/GaN HEMT structure with the 20 second AlN growth time has the lowest sheet resistance, albeit comparable to the 12 and 30 second growth times. This AlN growth condition was the basis for a set of AlGaN/BAlN/GaN HEMT structures with TEB added to the AlN profile layer with gas phase TEB/TMA ratios of 1.25%, 2.50%, and 5.00%. All other growth conditions were unchanged. The resulting sheet resistance measurements per gas phase TEB/TMA ratio are presented in Figure 60.

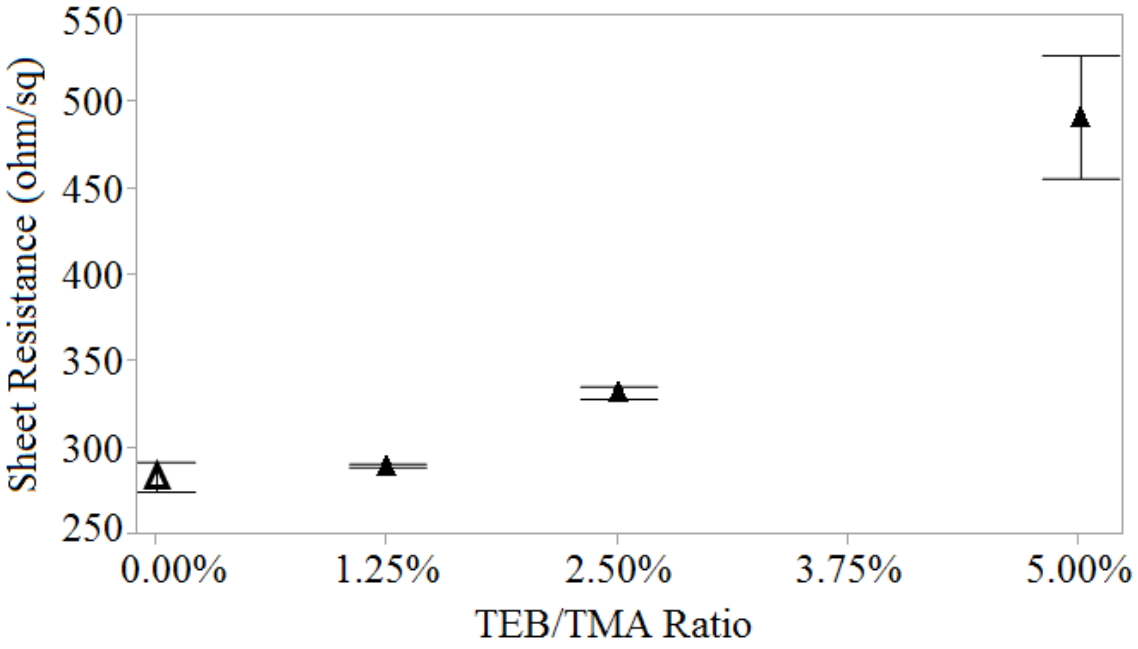

Figure 60. Sheet resistance vs TEB/TMA gas phase ratio for AlGaN/BAlN/GaN HEMTs grown with a 20 second BAlN growth time. Error bars represent the standard deviation of the averaged data for each wafer. The hollow triangle data set at TEB/TMA = 0.00% represents the AlGaN/AlN/GaN HEMT structure with 20 second AlN profile growth time for a direct comparison of the effect TEB has on 2DEG sheet resistance.

The 1.25% and 2.5% TEB/TMA growth runs were examined by STEM. Comparative HAADF images are shown in Figure 61. The images support that boron incorporation into the growth structure was successful through the appearance of a darker contrast layer at the AlGaN/GaN interface. The presence of BN was confirmed by EELS in these two samples. The BAlN/GaN interface appears planar and well-defined while the AlGaN/BAlN appears very poorly defined as the frequency of compositional irregularities, even in this small sampling, are significant.

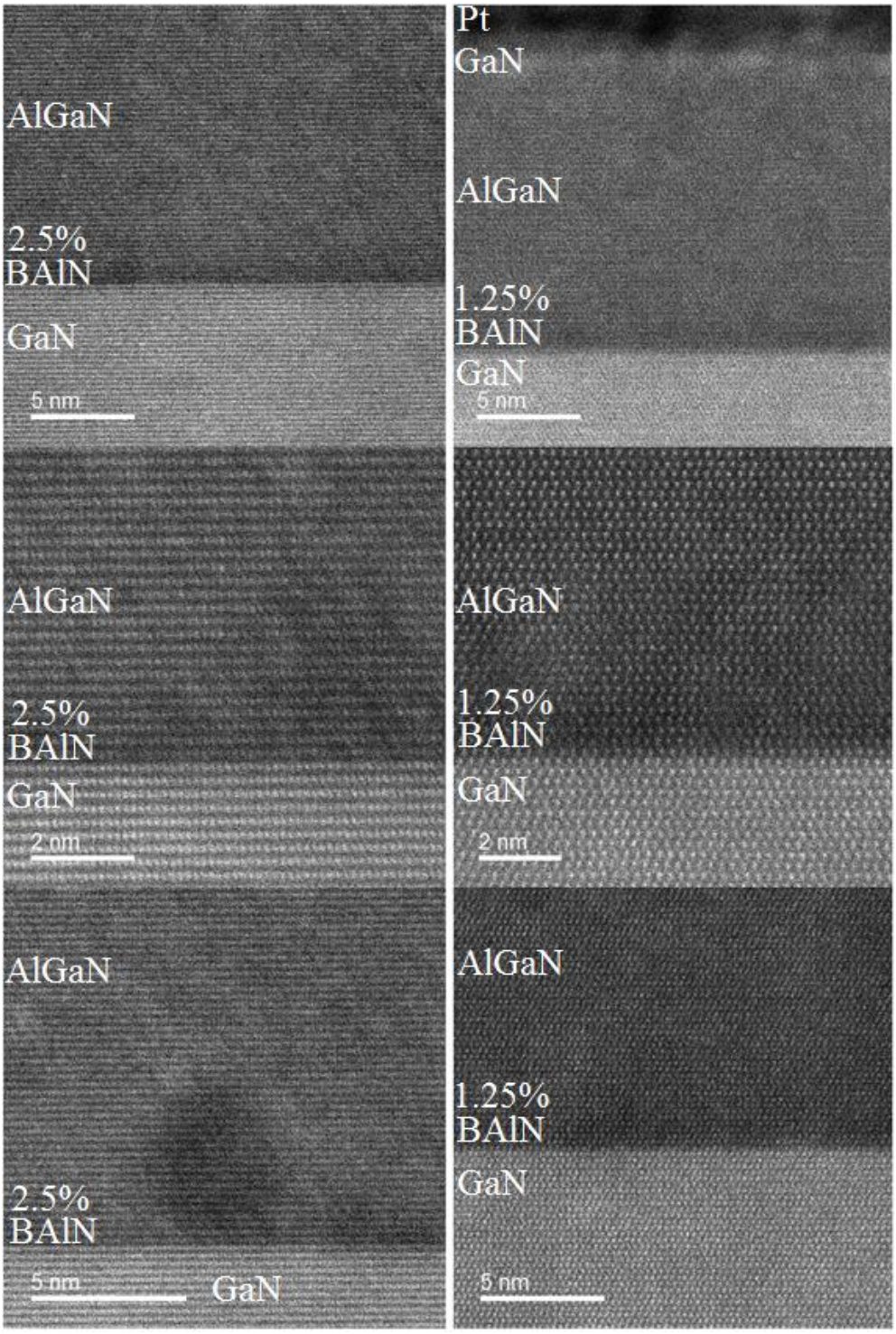

Figure 61. STEM HAADF images of AlGaN/BAlN/GaN HEMT structures. The left three images are from the BAlN layer grown with a 2.50% TEB/TMA gas phase ratio. The right three images are from the 1.25% TEB/TMA wafer. The images show a well-defined BAlN/GaN interface with a poorly defined AlGaN/BAlN interface. The latter interface exhibits compositional irregularities that extend several atomic layers into the AlGaN, most notable in the lower images.

SIMS depth profiling of the 1.25% and 2.50% TEB/TMA grown BAlN layers within the AlGaN/BAlN/GaN HEMT structures confirmed the presence of boron well into the AlGaN barrier layer. Figure 62 shows the overlaid data from the SIMS depth profiling of the two wafers.

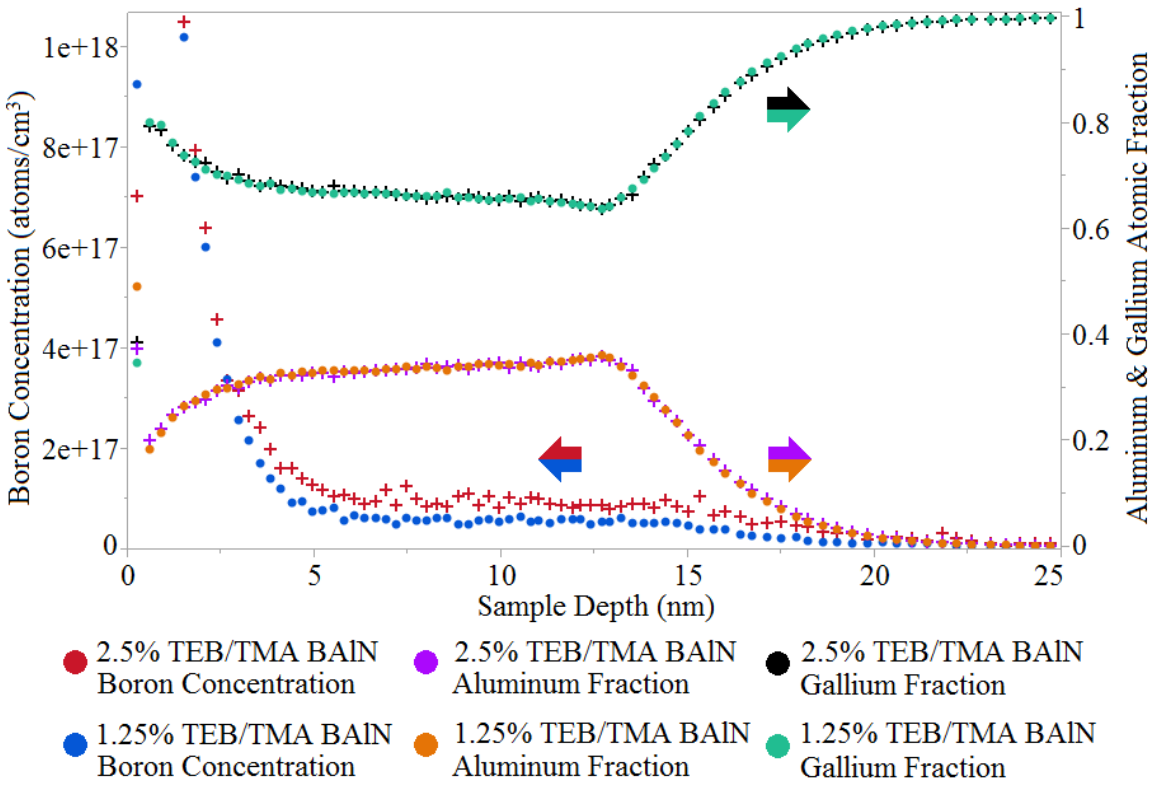

Figure 62. Overlaid SIMS depth profiles of AlGaN/BAlN/GaN HEMT structures. The left axis is boron concentration in atoms/cm^3. The right axis is the relative atomic fraction of aluminum and gallium to serve as a depth marker with in the HEMT structure for the boron concentration. The 2.50% TEB/TMA wafer has an average boron concentration (between 3 – 25 nm depth) 1.89x that of the 1.25% TEB/TMA wafer.

The AlGaN/BAlN/GaN structure is well defined by the aluminum and gallium atomic fraction contours, with the aluminum concentration increasing gradually towards the BAlN/GaN interface with a small increased fraction at ~13 nm. Ideally, the boron would be localized and confined to the region defined by the (small) aluminum increase, however it is seen in both structures that there is no preference for this interface and the

boron is almost ubiquitously populating the barrier layer and protrudes into the GaN buffer with a preference for the more superficial AlGaN barrier. This general distribution, in addition to the sharply increased boron concentration of both samples close to the surface, can be interpreted as a general diffusion mechanism (supported by the presence of boron in GaN and the well-defined BAlN/GaN interface) with an added surfactant-like growth behavior of the BN within the structure as was seen in AlGaN/BN/GaN HEMT structures.

The boron concentration produced by the doubled (2.50% vs 1.25%) TEB/TMA concentration is roughly doubled (1.89x) throughout the boron-concentrated region. Interestingly, the boron distribution of the more concentrated sample seems more irregular in the SIMS profile indicating the increased preference of compositional phase segregation with higher boron concentrations. This is supported visually by the large dark pocket in the lowest (bottom left) STEM image from this same wafer in Figure 61. This is as would be expected for higher concentrations of a minority species within a solid solution where a miscibility gap is prominent. As the concentration of the minority species with poor miscibility is increased beyond solubility limits within the solution, the increased tendency for phase segregation will increase the proportionate volume of mixed compositional phase regions. Given the severity of the miscibility gap between both AlN and GaN with BN, it is not surprising to observe a marked difference even at small concentration differences. Following the same principles of phase segregation, the approximately doubled boron concentration in Figure 62 for the 2.50% TEB/TMA combined with very good 2DEG properties in Figure 60 suggest that the critical thickness, as it relates to relaxation events at the GaN surface, of the overall barrier layers

was not reached, though phase segregation of the boron species suggests further efforts are needed to confine boron to the GaN interface to improve this potential device structure.

The preference for boron to diffuse from the designed BAlN layer may have contributed to avoiding the critical thickness as the strain due to the boron content would be evenly spread over many nanometers instead of being concentrated within a thin BAlN ternary. At higher boron concentrations, even with the diffusivity of the species within the HEMT structure, a critical thickness will undoubtedly be reached. Literature evidence has shown a compositional tolerance of BAlN of 11% boron within an epitaxial thickness of 5 nm [197]. The STEM images of Figure 61 provide evidence that the 20 second BAlN growth time did not exceed (or even approach) this 5 nm thickness. Some assumption must be made for boron vs aluminum solid incorporation efficiency from the relative gas phase composition of the reactant TEB and TMA molecules, but exceeding 11% boron in a BAlN alloy produced with a 2.50% TEB/TMA ratio seems unlikely. As such, it can be concluded that the phase separation of the boron species is not from traditional phase segregation due to a miscibility gap and critical thickness limitations, but instead can be attributed to the diffusive / surfactant-like growth behavior of BN under the reaction conditions used and the energetic preference to avoid internal strain within the crystal via segregation.

VII. CONCLUSIONS

AlGaN/BN/GaN HEMT structures were grown to provide a proof of concept for the generation of a functional 2DEG at a BN/GaN interface. The additional goal of this body of work was to enhance the 2DEG beyond currently available GaN HEMT platforms, in that regard, the work was minimally successful. Multiple grown structures provided excellent, even world record competitive, 2DEG sheet resistances. The uniformity, repeatability and consistency across the wafer, and from run to run, was not on par with the expectations and requirements of a production-worthy process. The primary barrier to success is the diffusivity of boron within the structure as is evident from SIMS depth profiling. The potential of this novel HEMT structure has been established in the many low sheet resistances measured. These exemplary 2DEG measurements do not represent the majority of 2DEGs measured which follows a general trend of 2DEG degradation from boron inclusion by exposure to TEB. Continued efforts to optimize the growth conditions of the BN profile layer and its underlying GaN surface and superficial barrier layer composition and thickness with the goal of discouraging boron diffusion and encouraging BN material quality improvements and BN layer confinement and thickness uniformity will build on the consistency and overall quality of the induced 2DEGs at the BN/GaN interface within these HEMT structures established by this work.

The inclusion of boron into the AlGaN/AlN/GaN HEMT structure in the form of a BAlN alloy was not successful to improve on the 2DEG properties beyond the baseline structure per the hypothesis of this work though the results are quite comparable. Barriers for success of the 2DEG improvement include diffusivity of the boron species

within the HEMT structure as evidenced by SIMS depth profiling and STEM images, and undesirable phase segregation within the barrier layers due to the inherent consequences of the large lattice mismatch between the alloying species and general high diffusivity rates of boron as evidenced by segregated regions within STEM images. Further optimization of relative boron and aluminum concentrations and layer growth conditions to support the growth of a homogeneous confined BAlN layer is warranted as well as efforts to minimize the diffusivity and general phase segregation by employing alternative reaction conditions during BAlN growth and growth of the surrounding material.

This work has provided a proof of concept for the inclusion of boron into traditional GaN HEMT structures and has shown the potential for 2DEG enhancement and the platform's inclusion into competitive devices. Further process development is warranted to address the barriers for success identified by this work, most notably the preferential diffusion and phase segregation of the boron species and its resulting III-N alloys.

Future Work

Experimentation focused on optimizing the GaN material quality and barrier layer composition, thickness, and material quality over a range of chamber conditions varying temperature and pressure so to minimize or eliminate growth stoppage time facilitating the growth of improved material quality and interface quality of the BN and BAlN profile layers and their interfacial surfaces established by this work is recommended for future

studies. These efforts will provide a foundation for addressing the barriers for success identified by this work.

The effective growth by MOCVD, or comparable methods, of boron nitride and its alloys utilizing nitrogen as a carrier gas for the boron precursor is present in the literature [145], [195], [200], [201], [235]. Hydrogen was used in all HEMT growth efforts of this work and was effective to grow BN and its various alloys. The possibility for alternative growth behavior using nitrogen as a carrier gas for TEB is an appealing avenue for future experimentation and is warranted based on the success of research efforts in the literature to grow these materials.

Experimentation designed to keep the boron species isolated and confined to the prescribed layers within the HEMT structure would be a worthwhile pursuit as it would address the keystone barrier for success of this technology and its application in GaN based HEMT devices. As discussed, these efforts could include optimization of the surrounding material growth conditions so to maximize the material quality of the boron containing layers and their interfaces with the surrounding material. Additional efforts could include an encapsulating layer or layers designed to restrict boron diffusivity. Discouraging diffusivity by reducing growth temperature may also encourage 2DEG enhancement.

Experimentation into altering the AlGaN portion of the barrier layers could provide improvement to the 2DEG properties as both the composition and thickness of this layer contribute to the stress of the crucial 2DEG inducing interface of the HEMT structure. Studies to reduce the thickness of the AlGaN portion of the barrier layers

would provide a more direct impact of the boron-containing barrier interface layer on the resulting 2DEG properties. This experimentation avenue will be an iterative process necessitating optimization of the boron containing layer thickness and growth conditions in conjunction with efforts to improve 2DEG quality through AlGaN material growth so to maximize the overall value of the technology.

In addition to the barrier layer alterations, the expanded experimentation of a BAlN induced 2DEG is very appealing. Maximizing the boron content while minimizing the thickness so to avoid phase separation and surpassing the critical thickness will provide a spectrum of 2DEG properties which will better define the potential for this technology. This will complement the efforts to adjust and likely reduce the thickness of the more superficial AlGaN barrier layer.

Given the relatively high diffusivity of the boron species within the device layers, experimentation into exploiting this behavior in the HEMT structure is warranted. Specifically, the intentional growth of a BAlGaN quaternary in place of the traditional AlGaN within the AlGaN/GaN or AlGaN/AlN/GaN or a boron-containing version of either could produce a more stable and reliably grown HEMT structure with 2DEG properties well beyond the currently commercialized structures. Experimental efforts will include various gas phase compositional ranges and various growth condition changes such as pressure, temperature and material growth rate.

Lattice matched barrier layers such as AlInN or the quaternary AlInGaN would be interesting additions to a high strain boron-containing barrier interface layer as the impact to the 2DEG environment could be very appealing. The addition of boron to either of the

lattice matched materials would be challenging as the presence of indium would further discourage boron incorporation, but would present an academically interesting structure.

The significant lattice differences between BN and the other III-Ns open the door to other novel device structures. The two most interesting opportunities for novel structures are a BN/AlN 2DEG interface, which could find use in higher temperature applications and could be grown on silicon with very few underlying layers, and a superlattice structure containing high boron concentrated layers aimed to eliminate or reduce the strain and thickness limitations brought on by CTE mismatches between GaN and its heteroepitaxial substrates opening the door for thicker GaN growth and more robust device performance.

Alternative substrates which could eliminate the need for such substantial transition layers as are needed for silicon could provide the means to detect BN, or its alloys, XRD signals to monitor and characterize material quality. Such substrates include sapphire and SiC which require less underlying layer growth for relaxed GaN.

REFERENCES

[1] U. K. Mishra, L. Shen, T. E. Kazior, and Y. F. Wu, "GaN-based RF power devices and amplifiers," *Proc. IEEE*, vol. 96, no. 2, pp. 287–305, 2008.

[2] J. E. Lilienfeld, "Methods and apparatus for controlling electric currents," 1,745,175, 1930.

[3] D. Kahng, "Electric Field Controlled Semiconductor Device," 3,102,230, 1963.

[4] F. M. Wanlass, "Low stand-by power complementary field effect circuitry," 3,356,858, 1967.

[5] T. P. Chow and R. Tyagi, "Wide bandgap compound semiconductors for superior high-voltage unipolar devices," *IEEE Trans. Electron Devices*, vol. 41, no. 8, pp. 1481–1483, 1994.

[6] H. M. Macksey and F. H. Doerbeck, "GaAs FETs having high output power per unit gate width," *IEEE Electron Device Lett.*, vol. 2, no. 6, pp. 147–148, Jun. 1981.

[7] B. M. Green, E. Lan, P. Li, O. Hartin, C. A. Gaw, M. CdeBaca, E. M. Johnson, L. S. Klingbeil, P. Fisher, J. Kim, D. Maurer, B. Knappenberger, M. Miller, and C. H. Weitzel, "A high power density 26 V GaAs pHEMT technology," in *2004 IEEE MTT-S International Microwave Symposium Digest (IEEE Cat. No.04CH37535)*, 2004, vol. 2, pp. 817–820.

[8] D. Fanning, A. Balistreri, E. Beam Iii, K. Decker, S. Evans, R. Eye, W. Gaiewski, T. Nagle, P. Saunier, and H.-Q. Tserng, "High Voltage GaAs pHEMT Technology for S-band High Power Amplifiers."

[9] J. Brown, R. Borges, E. Piner, A. Vescan, S. Singhal, and R. Therrien, "AlGaN/GaN HFETs fabricated on 100-mm GaN on silicon (111) substrates," *Solid. State. Electron.*, vol. 46, no. 10, pp. 1535–1539, 2002.

[10] Y.-F. Wu, M. Moore, A. Saxler, T. Wisleder, and P. Parikh, "40-W/mm Double Field-plated GaN HEMTs," *2006 64th Device Res. Conf.*, pp. 151–152, 2006.

[11] U. K. Mishra, "Status of AlGaN/GaN HEMT technology– A UCSB perspective," in *Proceedings of the IEEE Gallium Arsenide Other Semiconductor Application Symposium*, 2005, pp. 21–27.

[12] D. W. Runton, B. Trabert, J. Shealy, and R. Vetury, "History of GaN: High-power RF gallium nitride (GaN) from infancy to manufacturable process and beyond," *IEEE Microw. Mag.*, vol. 14, no. 3, pp. 82–93, 2013.

[13] H. P. Maruska and J. J. Tietjen, "The preparation and properties of vapor-deposited single-crystal-line GaN," *Appl. Phys. Lett.*, vol. 15, no. 10, pp. 327–329, Oct. 1969.

[14] H. M. Manasevit, F. M. Erdmann, and W. I. Simpson, "The Use of Metalorganics in the Preparation of Semiconductor Materials," *J. Electrochem. Soc.*, vol. 118, no. 11, pp. 1864–1868, 1971.

[15] H. Amano, S. N., I. Akasaki, and Y. Toyoda, “Metalorganic vapor phase epitaxial growth of high quality GaN film using AlN buffer layer,” *Appl. Phys. Lett.*, vol. 48, no. 5, pp. 353–355, 1986.

[16] B. Gil, *Physiscs of wurtzite nitrides and oxides*. Springer International Publishing Switzerland, 2014.

[17] L. Liu and J. H. Edgar, “Substrates for gallium nitride epitaxy,” *Mater. Sci. Eng. R Reports*, vol. 37, no. 3, pp. 61–127, 2002.

[18] M. H. Wong, F. Wu, J. S. Speck, and U. K. Mishra, “Polarity inversion of N-face GaN using an aluminum oxide interlayer,” *J. Appl. Phys.*, vol. 108, no. 12, p. 123710, 2010.

[19] M. H. Wong, F. Wu, T. E. Mates, J. S. Speck, and U. K. Mishra, “Polarity inversion of N-face GaN by plasma-assisted molecular beam epitaxy,” *J. Appl. Phys.*, vol. 104, no. 9, 2008.

[20] J. E. Northrup, “Magnesium incorporation at (0001) inversion domain boundaries in GaN,” *Appl. Phys. Lett.*, vol. 82, no. 14, p. 2278, 2003.

[21] V. Ramachandran, R. M. Feenstra, W. L. Sarney, L. Salamanca-Riba, J. E. Northrup, L. T. Romano, and D. W. Greve, “Inversion of wurtzite GaN(0001) by exposure to magnesium,” *Appl. Phys. Lett.*, vol. 75, no. 6, p. 808, 1999.

[22] E. Monroy, M. Hermann, E. Sarigiannidou, T. Andreev, P. Holliger, S. Monnoye, H. Mank, B. Daudin, and M. Eickhoff, “Polytype transition of N-face GaN:Mg from wurtzite to zinc-blende,” *J. Appl. Phys.*, vol. 96, no. 7, pp. 3709–3715, 2004.

[23] O. Ambacher, J. Smart, J. R. Shealy, N. G. Weimann, K. Chu, M. Murphy, W. J. Schaff, L. F. Eastman, R. Dimitrov, L. Wittmer, M. Stutzmann, W. Rieger, and J. Hilsenbeck, “Two-dimensional electron gases induced by spontaneous and piezoelectric polarization charges in N- and Ga-face AlGaN/GaN heterostructures,” *J. Appl. Phys.*, vol. 85, no. 6, p. 3222, 1999.

[24] M. H. Wong, S. Keller, N. Dasgupta, D. J. Denninghoff, S. Kolluri, D. F. Brown, J. Lu, N. a Fichtenbaum, E. Ahmadi, U. Singisetti, A. Chini, S. Rajan, S. P. DenBaars, J. S. Speck, and U. K. Mishra, “N-polar GaN epitaxy and high electron mobility transistors,” *Semicond. Sci. Technol.*, vol. 28, no. 7, p. 074009, 2013.

[25] P. M. Asbeck, E. T. Yu, S. S. Lau, G. J. Sullivan, J. Van Hove, and J. Redwing, “Piezoelectric charge densities in AlGaN/GaN HFETs,” *Electron. Lett.*, vol. 33, no. 14, p. 1230, Jul. 1997.

[26] F. Bernardini, V. Fiorentini, and D. Vanderbilt, “Spontaneous polarization and piezoelectric constants of III-V nitrides,” *Phys. Rev. B*, vol. 56, no. 16, p. 4, 1997.

[27] E. S. Hellman, “The Polarity of GaN a Critical Review,” *Mater. Res. Soc. Internet J. Nitride Semicond. Res.*, vol. 2, no. January 1998, pp. 1–10, 1999.

[28] T. Sasaki and T. Matsuoka, “Substrate-polarity dependence of metal-organic vapor-phase epitaxy-grown GaN on SiC,” *J. Appl. Phys.*, vol. 64, no. 9, p. 4531, Nov. 1988.

[29] M. Asif Khan, J. N. Kuznia, D. T. Olson, and R. Kaplan, “Deposition and surface characterization of high quality single crystal GaN layers,” *J. Appl. Phys.*, vol. 73, no. 6, p. 3108, Mar. 1993.

[30] M. Seelmann-Eggebert, J. L. Weyher, H. Obloh, H. Zimmermann, A. Rar, and S. Porowski, “Polarity of (00.1) GaN epilayers grown on a (00.1) sapphire,” *Appl. Phys. Lett.*, vol. 71, no. 18, p. 2635, Nov. 1997.

[31] F. Ponce, Van de Walle CG, and J. Northrup, “Atomic arrangement at the AlN/SiC interface.,” *Phys. Rev. B. Condens. Matter*, vol. 53, no. 11, pp. 7473–7478, 1996.

[32] R. Di Felice and J. E. Northrup, “Energetics of AlN thin films on the Al2O3(0001) surface,” *Appl. Phys. Lett.*, vol. 73, no. 7, pp. 936–938, 1998.

[33] J.-L. Rouviere, M. Arlery, A. Bourret, R. Niebuhr, and K.-H. Bachem, “Understanding the Pyramidal Growth of GaN,” *MRS Proc.*, vol. 395, p. 393, Feb. 2011.

[34] M. Volmer and A. Weber, “No Title,” *Z. Phys. Chemie*, no. 119, p. 277, 1925.

[35] K. Volz, W. Stolz, A. Dadgar, and A. Krost, *Growth of III/Vs on Silicon: Nitrides, Phosphides, Arsenides and Antimonides*, Second Edi., vol. 3. Elsevier B.V., 2014.

[36] R. Liu, F. A. Ponce, A. Dadgar, and A. Krost, “Atomic arrangement at the AIN/Si (111) interface,” *Appl. Phys. Lett.*, vol. 83, no. 5, pp. 860–862, 2003.

[37] S. Changchun, P. M. Asbeck, and E. T. Yu, “Piezoelectric polarization associated with dislocations in wurtzite GaN,” *Appl. Phys. Lett.*, vol. 74, no. 4, pp. 573–575, 1999.

[38] T. S. Zheleva, O.-H. Nam, M. D. Bremser, and R. F. Davis, “Dislocation density reduction via lateral epitaxy in selectively grown GaN structures,” *Appl. Phys. Lett.*, vol. 71, no. 17, p. 2472, 1997.

[39] D. S. Wuu, W. K. Wang, K. S. Wen, S. C. Huang, S. H. Lin, S. Y. Huang, C. F. Lin, and R. H. Horng, “Defect reduction and efficiency improvement of near-ultraviolet emitters via laterally overgrown GaN on a GaN/patterned sapphire template,” *Appl. Phys. Lett.*, vol. 89, no. 16, p. 161105, Oct. 2006.

[40] F. A. Ponce, *Group III Nitride Semiconductor Compounds: Physics and Applications*. Clarendon Press, 1998.

[41] J. Kuzmík, P. Javorka, a. Alam, M. Marso, M. Heuken, and P. Kordoš, “Determination of channel temperature in AlGaN/GaN HEMTs grown on sapphire and silicon substrates using DC characterization method,” *IEEE Trans. Electron Devices*, vol. 49, no. 8, pp. 1496–1498, 2002.

[42] J. Kim, B. K. Kang, S.-N. Lee, J. Choi, and K. M. Song, “Improved light-output power of InGaN-based multiple-quantum-well light-emitting diodes by GaN/InAlGaN/GaN multi-barrier,” *Curr. Appl. Phys.*, Nov. 2015.

[43] J. E. Van Nostrand, J. Solomon, A. Saxler, Q.-H. Xie, D. C. Reynolds, and D. C. Look, "Dissociation of Al[sub 2]O[sub 3](0001) substrates and the roles of silicon and oxygen in n-type GaN thin solid films grown by gas-source molecular beam epitaxy," *J. Appl. Phys.*, vol. 87, no. 12, p. 8766, Jun. 2000.

[44] R. Gaska, Q. Chen, J. Yang, a. Osinsky, M. Asif Khan, and M. S. Shur, "High-temperature performance of AlGaN/GaN HFET's on SiC substrates," *IEEE Electron Device Lett.*, vol. 18, no. 10, pp. 492–494, 1997.

[45] L. Belyaev, *Ruby and sapphire Rubin i sapfir*. New Delhi: Amerind publishing for the National Bureau of Standards United States Department of Commerce and the National Science Foundation, 1980.

[46] H. Morkoç, S. Strite, G. B. Gao, M. E. Lin, B. Sverdlov, and M. Burns, "Large-band-gap SiC, III-V nitride, and II-VI ZnSe-based semiconductor device technologies," *J. Appl. Phys.*, vol. 76, no. 3, pp. 1363–1398, 1994.

[47] H. Lahrèche, P. Vennéguès, O. Tottereau, M. Laügt, P. Lorenzini, M. Leroux, B. Beaumont, and P. Gibart, "Optimisation of AlN and GaN growth by metalorganic vapour-phase epitaxy (MOVPE) on Si(111)," *J. Cryst. Growth*, vol. 217, pp. 13–25, 2000.

[48] H. Y. Shin, C. W. Yang, S. H. Jung, and J. B. Yoo, "A Study on Growth Characteristics of GaN Layers Grown by MOCVD on Si (111) Substrate," *J. Korean Phys. Soc.*, vol. 42, no. February, pp. 403–407, 2003.

[49] Y. Lu, X. Liu, D. C. Lu, H. Yuan, G. Hu, X. Wang, Z. Wang, and X. Duan, "The growth morphologies of GaN layer on Si(1 1 1) substrate," *J. Cryst. Growth*, vol. 247, no. 1–2, pp. 91–98, 2003.

[50] S. H. P.R. Hageman, "Growth of GaN epilayers on Si(111) substrates using multiple buffer layers," *Mater. Resour. soc.*, vol. 693, no. 111, pp. 1–6, 2002.

[51] E. Feltin, B. Beaumont, M. Laügt, P. De Mierry, P. Vennéguès, H. Lahrèche, M. Leroux, and P. Gibart, "Stress control in GaN grown on silicon (111) by metalorganic vapor phase epitaxy," *Appl. Phys. Lett.*, vol. 79, no. 20, pp. 3230–3232, 2001.

[52] S. Lawrence, T. Suzue, and T. Egawa, "Breakdown enhancement of AlGaN/GaN HEMTs on 4-in silicon by improving the GaN quality on thick buffer layers," *IEEE Electron Device Lett.*, vol. 30, no. 6, pp. 587–589, 2009.

[53] S. Strite, "An investigation of the properties of cubic GaN grown on GaAs by plasma-assisted molecular-beam epitaxy," *J. Vac. Sci. Technol. B Microelectron. Nanom. Struct.*, vol. 9, no. 4, p. 1924, Jul. 1991.

[54] H. Okumura, S. Misawa, and S. Yoshida, "Epitaxial growth of cubic and hexagonal GaN on GaAs by gas-source molecular-beam epitaxy," *Appl. Phys. Lett.*, vol. 59, no. 9, p. 1058, Aug. 1991.

[55] S. Miyoshi, K. Onabe, N. Ohkouchi, H. Yaguchi, R. Ito, S. Fukatsu, and Y. Shiraki, “MOVPE growth of cubic GaN on GaAs using dimethylhydrazine,” *J. Cryst. Growth*, vol. 124, no. 1–4, pp. 439–442, Nov. 1992.

[56] Y. Kumagai, M. Takemoto, H. Seki, and A. Koukitu, “Thick and high quality gan growth on GaAs (111)A surfaces for preparation of freestanding GaN substrates,” *Cryst. Ep. Growth, Vol 1*, vol. 246, pp. 39–47, 2002.

[57] M. Mizuta, S. Fujieda, Y. Matsumoto, and T. Kawamura, “Low Temperature Growth of GaN and AlN on GaAs Utilizing Metalorganics and Hydrazine,” *Jpn. J. Appl. Phys.*, vol. 25, no. Part 2, No. 12, pp. L945–L948, Dec. 1986.

[58] T. J. Anderson, M. J. Tadjer, J. K. Hite, J. D. Greenlee, A. D. Koehler, K. D. Hobart, and F. J. Kub, “Effect of Reduced Extended Defect Density in MOCVD Grown AlGaN/GaN HEMTs on Native GaN Substrates,” *IEEE Electron Device Lett.*, vol. 37, no. 1, pp. 28–30, 2016.

[59] Q. Bao, M. Saito, K. Hazu, Y. Kagamitani, K. Kurimoto, D. Tomida, K. Qiao, T. Ishiguro, C. Yokoyama, and S. F. Chichibu, “Ammonothermal growth of GaN on a self-nucleated GaN seed crystal,” *J. Cryst. Growth*, vol. 404, pp. 168–171, 2014.

[60] D. Ehrentraut, R. T. Pakalapati, D. S. Kamber, W. Jiang, D. W. Pocius, B. C. Downey, M. Mclaurin, and M. P. D’Evelyn, “High Quality, Low Cost Ammonothermal Bulk GaN Substrates,” *Jpn. J. Appl. Phys.*, vol. 52, pp. 1–4, 2013.

[61] R. Dwiliński, R. Doradziński, J. Garczyński, L. P. Sierzputowski, and Y. Kanbara, “Bulk Monocrystalline Gallium Nitide,” 6656615, 2003.

[62] T. Hashimoto, F. Wu, J. S. Speck, and S. Nakamura, “Ammonothermal growth of bulk GaN,” *J. Cryst. Growth*, vol. 310, pp. 3907–3910, 2008.

[63] R. Dwiliński, R. Doradziński, J. Garczyński, L. P. Sierzputowski, a. Puchalski, Y. Kanbara, K. Yagi, H. Minakuchi, and H. Hayashi, “Excellent crystallinity of truly bulk ammonothermal GaN,” *J. Cryst. Growth*, vol. 310, no. 17, pp. 3911–3916, 2008.

[64] K. Aarset, C. E. Beer, K. Hagen, E. M. Page, and D. a. Rice, “Organometallic Precursors for the Formation of GaN by MOCVD: Structural Characterization of (CH 3) 3 GaNH(CH 2 CH 3) 2 by Gas-Phase Electron Diffraction and ab Initio Molecular Orbital Calculations,” *J. Phys. Chem. A*, vol. 106, no. 37, pp. 8762–8768, 2002.

[65] G. B. Stringfellow, “Fundamental aspects of organometallic vapor phase epitaxy,” *Mater. Sci. Eng. B*, vol. 87, no. 2, pp. 97–116, 2001.

[66] D. a Neumayer and J. G. Ekerdt, “Growth of Group III Nitrides . A Review of Precursors and Techniques,” *Chem. Mater.*, no. 14, pp. 9–25, 1996.

[67] J. Shi, R. Zuo, and S. Meng, “DFT study on adduct reaction paths of GaN MOCVD growth,” *Sci. China Technol. Sci.*, vol. 56, no. 7, pp. 1644–1650, 2013.

[68] M. J. Almond, C. E. Beer, D. A. Rice, and K. Hagen, “Organometallic Precursors for the Formation of Gan By Mocvd - the Spectroscopic and Gas-Phase Electron-Diffraction Structural Characterization of Me(3)Ga Nhme(2) and Me(2)Ga(Mu-Nme(2)) (2),” *J. Mol. Struct.*, vol. 346, pp. 83–94, 1995.

[69] S. Ravasio, T. Momose, K. Fujii, Y. Shimogaki, M. Sugiyama, and C. Cavallotti, “Analysis of the gas phase kinetics active during GaN deposition from NH3 and Ga(CH3)3,” *J. Phys. Chem. A*, vol. 119, no. 28, pp. 7858–7871, 2015.

[70] C. Hemmingsson, P. P. Paskov, G. Pozina, M. Heuken, B. Schineller, and B. Monemar, “Growth of bulk GaN in a vertical hydride vapour phase epitaxy reactor,” *Superlattices Microstruct.*, vol. 40, no. 4–6, pp. 205–213, Oct. 2006.

[71] B. Łucznik, B. Pastuszka, I. Grzegory, M. Boćkowski, G. Kamler, E. Litwin-Staszewska, and S. Porowski, “Deposition of thick GaN layers by HVPE on the pressure grown GaN substrates,” *J. Cryst. Growth*, vol. 281, no. 1, pp. 38–46, 2005.

[72] H. Amano, “Progress and Prospect of the Growth of Wide-Band-Gap Group III Nitrides: Development of the Growth Method for Single-Crystal Bulk GaN,” *Jpn. J. Appl. Phys.*, vol. 52, no. 5R, p. 050001, 2013.

[73] R. P. Vaudo, X. Xu, C. Loria, A. D. Salant, J. S. Flynn, and G. R. Brandes, “GaN Boule Growth: A Pathway to GaN Wafers with Improved Material Quality,” *Phys. status solidi*, vol. 194, no. 2, pp. 494–497, Dec. 2002.

[74] M. Bockowski, “Review: Bulk growth of gallium nitride: challenges and difficulties,” *Cryst. Res. Technol.*, vol. 42, no. 12, pp. 1162–1175, 2007.

[75] G. Fiegl and W. Torbet, “Continuous replenishment of molten semiconductor in a Czochralski-process, single-crystal-growing furnace,” 4,282,184, 1981.

[76] R. Groh, G. Gerey, L. Bartha, and J. I. Pankove, “On the thermal decomposition of GaN in vacuum,” *Phys. Status Solidi*, vol. 26, no. 1, pp. 353–357, Nov. 1974.

[77] G. Jacob, R. Madar, and J. Hallais, “Optimized growth conditions and properties of N-type and insulating GaN,” *Mater. Res. Bull.*, vol. 11, no. 4, pp. 445–450, Apr. 1976.

[78] B. V L’vov, “Kinetics and mechanism of thermal decomposition of GaN,” *Thermochim. Acta*, vol. 360, no. 1, pp. 85–91, Aug. 2000.

[79] M. Furtado and G. Jacob, “Study on the influence of annealing effects in GaN VPE,” *J. Cryst. Growth*, vol. 64, pp. 257–267, 1983.

[80] Y. Morimoto, “Few Characteristics of Epitaxial GaN - Etching and Thermal Decomposition,” *J. Electrochem. Soc.*, vol. 121, no. 10, pp. 1383–1384, 1974.

[81] D. D. Koleske, A. E. Wickenden, R. L. Henry, J. C. Culbertson, and M. E. Twigg, “GaN decomposition in H2 and N2 at MOVPE temperatures and pressures,” *J. Cryst. Growth*, vol. 223, no. 4, pp. 466–483, 2001.

[82] J. Karpiński, J. Jun, and S. Porowski, “Equilibrium pressure of N2 over GaN and high pressure solution growth of GaN,” *J. Cryst. Growth*, vol. 66, no. 1, pp. 1–10, Jan. 1984.

[83] W. Utsumi, H. Saitoh, H. Kaneko, T. Watanuki, K. Aoki, and O. Shimomura, “Congruent melting of gallium nitride at 6 GPa and its application to single-crystal growth.,” *Nat. Mater.*, vol. 2, no. 11, pp. 735–738, 2003.

[84] R. A. Logan and C. D. Thurmond, “Heteroepitaxial Thermal Gradient Solution Growth of GaN,” *J. Electrochem. Soc.*, vol. 119, no. 12, p. 1727, Dec. 1972.

[85] M. Bockowski, “High pressure solution growth of GaN,” *Jpn. J. Appl. Phys.*, vol. 53, pp. 100203–1–100203–9, 2014.

[86] I. Grzegory, M. Bockowski, J. Jun, and P. Figurny, “On the liquidus curve for GaN,” *High Press. Res.*, vol. 7, no. 1–6, pp. 284–286, Dec. 1991.

[87] M. Boćkowski, I. Grzegory, G. Kamler, B. Łucznik, S. Krukowski, M. Wróblewski, P. Kwiatkowski, K. Jasik, and S. Porowski, “Platelets and needles: Two habits of pressure-grown GaN crystals,” *J. Cryst. Growth*, vol. 305, no. 2, pp. 414–420, Jul. 2007.

[88] H. Yamane and M. Shimada, “Preparation of GaN single crystals using a Na flux,” *Chem. Mater.*, vol. 1896, no. 1, pp. 413–416, 1997.

[89] Y. Mori, M. Imade, K. Murakami, H. Takazawa, H. Imabayashi, Y. Todoroki, K. Kitamoto, M. Maruyama, M. Yoshimura, Y. Kitaoka, and T. Sasaki, “Growth of bulk GaN crystal by Na flux method under various conditions,” *J. Cryst. Growth*, vol. 350, no. 1, pp. 72–74, 2012.

[90] F. Kawamura, H. Umeda, M. Kawahara, M. Yoshimura, Y. Mori, T. Sasaki, H. Okado, K. Arakawa, and H. Mori, “Drastic Decrease in Dislocations during Liquid Phase Epitaxy Growth of GaN Single Crystals Using Na flux Method without Any Artificial Processes,” *Jpn. J. Appl. Phys.*, vol. 45, no. 4A, pp. 2528–2530, 2006.

[91] H. Yamane, M. Shimada, T. Sekiguchi, and F. J. DiSalvo, “Morphology and characterization of GaN single crystals grown in a Na flux,” *J. Cryst. Growth*, vol. 186, no. 1–2, pp. 8–12, 1998.

[92] F. Kawamura, M. Morishita, M. Tanpo, M. Imade, M. Yoshimura, Y. Kitaoka, Y. Mori, and T. Sasaki, “Effect of carbon additive on increases in the growth rate of 2in GaN single crystals in the Na flux method,” *J. Cryst. Growth*, vol. 310, p. 3946, 2008.

[93] T. W. Weeks, E. L. Piner, T. Gehrke, and K. J. Linthicum, “Gallium nitride materials and methods,” 6617060, 2003.

[94] T. W. Weeks, E. L. Piner, T. Gehrke, and K. J. Linthicum, “Gallium nitride materials and methods,” 8,105,921, 2012.

[95] F. Bernardini, V. Fiorentini, and D. Vanderbilt, “Accurate calculation of polarization-related quantities in semiconductors,” *Phys. Rev. B*, vol. 63, p. 193201, 2001.

[96] J. P. Ibbetson, P. T. Fini, K. D. Ness, S. P. DenBaars, J. S. Speck, and U. K. Mishra, “Polarization effects, surface states, and the source of electrons in AlGaN/GaN heterostructure field effect transistors,” *Appl. Phys. Lett.*, vol. 77, no. 2, p. 250, 2000.

[97] O. Ambacher and B. Foutz, “Two dimensional electron gases induced by spontaneous and piezoelectric polarization in undoped,” *J. Appl. Phys.*, vol. 87, no. 1, p. 334, 2000.

[98] E. T. Yu, X. Z. Dang, P. M. Asbeck, S. S. Lau, and G. J. Sullivan, “Spontaneous and piezoelectric polarization effects in III–V nitride heterostructures,” *J. Vac. Sci. Technol. B Microelectron. Nanom. Struct.*, vol. 17, no. 4, p. 1742, 1999.

[99] D. Jena, J. Simon, A. Wang, Y. Cao, K. Goodman, J. Verma, S. Ganguly, G. Li, K. Karda, V. Protasenko, C. Lian, T. Kosel, P. Fay, and H. Xing, “Polarization-engineering in group III-nitride heterostructures: New opportunities for device design,” *Phys. Status Solidi Appl. Mater. Sci.*, vol. 208, no. 7, pp. 1511–1516, 2011.

[100] H. W. Jang, C. M. Jeon, K. H. Kim, J. K. Kim, S.-B. Bae, J.-H. Lee, J. W. Choi, and J.-L. Lee, “Mechanism of two-dimensional electron gas formation in Al[sub x]Ga[sub 1−x]N/GaN heterostructures,” *Appl. Phys. Lett.*, vol. 81, no. 7, p. 1249, 2002.

[101] J. M. Redwing, M. a. Tischler, J. S. Flynn, S. Elhamri, M. Ahoujja, R. S. Newrock, and W. C. Mitchel, “Two-dimensional electron gas properties of AlGaN/GaN heterostructures grown on 6H–SiC and sapphire substrates,” *Appl. Phys. Lett.*, vol. 69, no. 7, p. 963, 1996.

[102] P. Chavarkar, I. Smorchkova, S. Keller, U. K. Mishra, W. Walukiewicz, and Y. Wu, “Group-III nitride based high electron mobility transistor (HEMT) with barrier/spacer layer,” 6849882, 2005.

[103] M. Asif Khan, J. N. Kuznia, D. T. Olson, W. J. Schaff, J. W. Burm, and M. S. Shur, “Microwave performance of a 0.25 μm gate AlGaN/GaN heterostructure field effect transistor,” *Appl. Phys. Lett.*, vol. 65, no. 9, p. 1121, Aug. 1994.

[104] M. Asif Khan, J. N. Kuznia, A. R. Bhattarai, and D. T. Olson, “Metal semiconductor field effect transistor based on single crystal GaN,” *Appl. Phys. Lett.*, vol. 62, no. 15, p. 1786, Apr. 1993.

[105] Y. Wu and A. Agarwal, *Comprehensive Semiconductor Science and Technology*. Elsevier, 2011.

[106] M. A. Khan, J. M. VanHove, J. N. Kuznia, and D. T. Olson, “High electron mobility transistor with GaN/AlGaN heterojunctions,” 5192987, 1993.

[107] E. L. Piner, A. W. Hanson, J. C. Roberts, and P. Rajagopal, “III-Nitride material structures including silicon substrates,” 7247889, 2007.

[108] I. P. Smorchkova, S. Keller, S. Heikman, C. R. Elsass, B. Heying, P. Fini, J. S. Speck, and U. K. Mishra, "Two-dimensional electron-gas AlN/GaN heterostructures with extremely thin AlN barriers," *Appl. Phys. Lett.*, vol. 77, no. 24, p. 3998, 2000.

[109] S. Elhamri, W. C. Mitchel, R. Berney, M. Ahoujja, J. C. Roberts, P. Rajagopal, J. W. Cook, E. L. Piner, and K. J. Linthicum, "Impact of AlN interlayer on the transport properties of AlGaN/GaN heterostructures grown on silicon," *Phys. Status Solidi*, vol. 5, no. 6, pp. 1962–1964, 2008.

[110] M. Tabuchi, T. Kumamoto, and Y. Takeda, "Lattice accommodation in heteroepitaxial semiconductor layers grown beyond critical thickness," *J. Appl. Phys.*, vol. 77, no. 1, p. 143, 1995.

[111] a. D. Bykhovski, B. L. Gelmont, and M. S. Shur, "Elastic strain relaxation and piezoeffect in GaN-AlN, GaN-AlGaN and GaN-InGaN superlattices," *J. Appl. Phys.*, vol. 81, no. 9, p. 6332, 1997.

[112] I. P. Smorchkova, L. Chen, T. Mates, L. Shen, S. Heikman, B. Moran, S. Keller, S. P. DenBaars, J. S. Speck, and U. K. Mishra, "AlN/GaN and (Al,Ga)N/AlN/GaN two-dimensional electron gas structures grown by plasma-assisted molecular-beam epitaxy," *J. Appl. Phys.*, vol. 90, no. 10, pp. 5196–5201, 2001.

[113] A. M. Sanchez, F. J. Pacheco, S. I. Molina, J. Stemmer, J. Aderhold, and J. Graul, "Critical thickness of high-temperature AIN interlayers in GaN on sapphire (0001)," *J. Electron. Mater.*, vol. 30, no. 5, pp. L17–L20, 2001.

[114] A. Bourret, C. Adelmann, B. Daudin, J.-L. Rouvière, G. Feuillet, and G. Mula, "Strain relaxation in (0001) AlN/GaN heterostructures," *Phys. Rev. B*, vol. 63, no. 24, pp. 1–13, 2001.

[115] K. Jeganathan, T. Ide, M. Shimizu, and H. Okumura, "Strain relaxation correlated with the transport properties of AlN/GaN heterostructure grown by plasma-assisted molecular-beam epitaxy," *J. Appl. Phys.*, vol. 93, no. 4, pp. 2047–2050, 2003.

[116] A. E. Romanov, G. E. Beltz, P. Cantu, F. Wu, S. Keller, S. P. Denbaars, and J. S. Speck, "Cracking of III-nitride layers with strain gradients," *Appl. Phys. Lett.*, vol. 89, no. 16, pp. 23–25, 2006.

[117] J. W. Matthews and A. E. Blakeslee, "Defects in epitaxial multilayers * I. Misfit dislocations," *J. Cryst. Growth*, vol. 27, pp. 118–125, 1974.

[118] U. Jain, S. C. Jain, J. Nijs, J. R. Willis, R. Bullough, R. P. Mertens, and R. Van Overstraeten, "Calculation of critical-layer-thickness and strain relaxation in GexSi1-x strained layers with interacting 60 and 90 dislocations," *Solid. State. Electron.*, vol. 36, no. 3, pp. 331–337, 1993.

[119] M. Neuburger, T. Zimmermann, and E. Kohn, "Unstrained InAIN / GaN HEMT structure," *Int. J. High Speed Electron. Syst.*, vol. 14, no. 3, pp. 785–790, 2004.

[120] F. Medjdoub and J. Carlin, “Status of the emerging InAlN/GaN power HEMT technology,” *Open Electr. Electron. Eng. J.*, vol. 2, pp. 1–7, 2008.

[121] R. Tülek, A. Ilgaz, S. Gökden, A. Teke, M. K. Öztürk, M. Kasap, S. ÖzElik, E. Arslan, and E. Özbay, “Comparison of the transport properties of high quality AlGaN/AlN/GaN and AlInN/AlN/GaN two-dimensional electron gas heterostructures,” *J. Appl. Phys.*, vol. 105, no. 1, pp. 1–6, 2009.

[122] O. Ambacher, J. Majewski, C. R. Miskys, A. Link, M. Hermann, M. Eickhoff, M. Stutzmann, F. Bernardini, V. Fiorentini, V. Tilak, B. Schaff, and L. F. Eastman, “Pyroelectric properties of Al (In) GaN / GaN hetero- and,” *J. Phys. Condens. Matter*, vol. 14, pp. 3399–3434, 2002.

[123] T. Lim, R. Aidam, P. Waltereit, T. Henkel, R. Quay, R. Lozar, T. Maier, L. Kirste, and O. Ambacher, “GaN-Based Submicrometer HEMTs With Lattice-Matched InAlGaN Barrier Grown by MBE,” *IEEE Electron Device Lett.*, vol. 31, no. 7, pp. 671–673, 2010.

[124] N. Ketteniss, L. R. Khoshroo, M. Eickelkamp, M. Heuken, H. Kalisch, R. H. Jansen, and a Vescan, “Study on quaternary AlInGaN/GaN HFETs grown on sapphire substrates,” *Semicond. Sci. Technol.*, vol. 25, no. 7, p. 075013, 2010.

[125] R. Wang, G. Li, J. Verma, B. Sensale-rodriguez, T. Fang, J. Guo, Z. Hu, O. Laboutin, Y. Cao, W. Johnson, G. Snider, P. Fay, D. Jena, and H. G. Xing, “220-GHz Quaternary Barrier InAlGaN/AlN/GaN HEMTs,” *IEEE Electron Device Lett.*, vol. 32, no. 9, pp. 1215–1217, 2011.

[126] N. Ketteniss, a Askar, B. Reuters, a Noculak, B. Holländer, H. Kalisch, and a Vescan, “Polarization-reduced quaternary InAlGaN/GaN HFET and MISHFET devices,” *Semicond. Sci. Technol.*, vol. 27, no. 5, p. 055012, 2012.

[127] D. S. Lee, O. Laboutin, Y. Cao, W. Johnson, E. Beam, A. Ketterson, M. Schuette, P. Saunier, D. Kopp, P. Fay, and T. Palacios, “317 GHz InAlGaN/GaN HEMTs with extremely low on-resistance,” *Phys. Status Solidi*, vol. 10, no. 5, pp. 827–830, 2013.

[128] N. Kharche and S. K. Nayak, “Quasiparticle band gap engineering of graphene and graphone on hexagonal boron nitride substrate,” *Nano Lett.*, vol. 11, pp. 5274–5278, 2011.

[129] O. Fukunaga, “Science and technology in the recent development of boron nitride materials,” *J. Phys. Condens. Matter*, vol. 14, pp. 10979–10982, 2002.

[130] Y. Kobayashi, K. Kumakura, T. Akasaka, H. Yamamoto, and T. Makimoto, “Mechanical transfer of GaN-based devices using layered boron nitride as a release layer,” *Nature*, vol. 484, no. 7393, pp. 223–227, 2012.

[131] T. Makimoto, K. Kumakura, Y. Kobayashi, T. Akasaka, and H. Yamamoto, “A vertical InGaN/GaN light-emitting diode fabricated on a flexible substrate by a mechanical transfer method using BN,” *Appl. Phys. Express*, vol. 5, no. 7, p. 072102, 2012.

[132] H. X. Jiang and J. Y. Lin, “Hexagonal boron nitride for deep ultraviolet photonic devices,” *Semicond. Sci. Technol.*, vol. 29, no. 8, p. 084003, 2014.

[133] T. Matsuoka, N. Yoshimoto, T. Sasaki, and A. Katsui, “Wide-gap semiconductor InGaN and InGaAln grown by MOVPE,” *J. Electron. Mater.*, vol. 21, no. 2, pp. 157–163, 1992.

[134] G. Liu, J. Zhang, X. H. Li, G. S. Huang, T. Paskova, K. R. Evans, H. Zhao, and N. Tansu, “Metalorganic vapor phase epitaxy and characterizations of nearly-lattice-matched AlInN alloys on GaN/sapphire templates and free-standing GaN substrates,” *J. Cryst. Growth*, vol. 340, no. 1, pp. 66–73, 2012.

[135] I. M. Watson, “Metal organic vapour phase epitaxy of AlN, GaN, InN and their alloys: A key chemical technology for advanced device applications,” *Coord. Chem. Rev.*, vol. 257, no. 13–14, pp. 2120–2141, 2013.

[136] A. V. Lobanova, A. S. Segal, E. V. Yakovlev, and R. A. Talalaev, “AlInN MOVPE: Growth chemistry and analysis of trends,” *J. Cryst. Growth*, vol. 352, no. 1, pp. 199–202, 2012.

[137] C. F. Tseng, T. Y. Tsai, Y. H. Huang, M. T. Lee, and R. H. Horng, “Transport phenomena and the effects of reactor geometry for epitaxial GaN growth in a vertical MOCVD reactor,” *J. Cryst. Growth*, vol. 432, pp. 54–63, 2015.

[138] T. Momose, T. Kamiya, Y. Suzuki, S. Ravasio, C. Cavallotti, M. Sugiyama, and Y. Shimogaki, “Kinetic Analysis of GaN-MOVPE via Thickness Profiles in the Gas Flow Direction with Systematically Varied Growth Conditions,” *ECS J. Solid State Sci. Technol.*, vol. 5, no. 3, pp. P164–P171, 2016.

[139] Z. Zhang, H. Fang, H. Yan, Z. Jiang, J. Zheng, and Z. Gan, “Influencing factors of GaN growth uniformity through orthogonal test analysis,” *Appl. Therm. Eng.*, vol. 91, pp. 53–61, 2015.

[140] A. C. Jones, C. R. Whitehouse, and J. S. Roberts, “Chemical Approaches To the Metalorganic Cvd of Group-Iii Nitrides,” *Chem. Vap. Depos.*, vol. 1, no. 3, p. 65–&, 1995.

[141] O. Ambacher, “Growth and applications of Group III-nitrides,” *J. Phys. D. Appl. Phys.*, vol. 31, no. 20, pp. 2653–2710, 1998.

[142] C. H. Wei and J. H. Edgar, “Unstable composition region in the wurtzite B1-x-yGaxAlyN system,” *J. Cryst. Growth*, vol. 208, no. 1, pp. 179–182, 2000.

[143] a. Y. Polyakov, M. Shin, W. Qian, M. Skowronski, D. W. Greve, and R. G. Wilson, “Growth of AlBN solid solutions by organometallic vapor-phase epitaxy,” *J. Appl. Phys.*, vol. 81, no. 1997, p. 1715, 1997.

[144] T. Akasaka and T. Makimoto, “Flow-rate modulation epitaxy of wurtzite AlBN,” *Appl. Phys. Lett.*, vol. 88, no. 4, p. 041902, 2006.

[145] S. Gautier, G. Patriarche, T. Moudakir, M. Abid, G. Orsal, K. Pantzas, D. D. Troadec, a. Soltani, L. Largeau, O. Mauguin, and a. Ougazzaden, "Deep structural analysis of novel BGaN material layers grown by MOVPE," *J. Cryst. Growth*, vol. 315, no. 1, pp. 288–291, 2011.

[146] T. Honda, M. Shibata, M. Kurimoto, M. Tsubamoto, J. Yamamoto, and H. Kawanishi, "Band-gap energy and effective mass of BGaN," *Jpn. J. Appl. Phys.*, vol. 39, no. 4 B, pp. 2389–2393, 2000.

[147] M. Chubarov, H. Pedersen, H. Högberg, S. Filippov, J. A. A. Engelbrecht, J. O'Connel, and A. Henry, "Boron nitride: A new photonic material," *Phys. B Condens. Matter*, vol. 439, pp. 29–34, 2014.

[148] M. Chubarov, H. Pedersen, H. Högberg, J. Jensen, and A. Henry, "Growth of High Quality Epitaxial Rhombohedral Boron Nitride," *Cryst. Growth Des.*, vol. 12, no. 6, pp. 3215–3220, 2012.

[149] a. Ougazzaden, S. Gautier, T. Moudakir, Z. Djebbour, Z. Lochner, S. Choi, H. J. Kim, J. H. Ryou, R. D. Dupuis, and a. a. Sirenko, "Bandgap bowing in BGaN thin films," *Appl. Phys. Lett.*, vol. 93, no. 8, pp. 1–4, 2008.

[150] W. E. Fenwick, "Boron-containing buffer layer for growing gallium nitride on silicon," 8,916,906, 2014.

[151] T. Malinauskas, a. Kadys, S. Stanionytė, K. Badokas, J. Mickevičius, J. Jurkevičius, D. Dobrovolskas, and G. Tamulaitis, "Growth of BGaN epitaxial layers using close-coupled showerhead MOCVD," *Phys. Status Solidi*, vol. 252, no. 5, pp. 1138–1141, 2015.

[152] K. Nakamura, "Preparation and Properties of Boron Nitride Films by Metal Organic Chemical Vapor Deposition," *J. Electrochem. Soc.*, vol. 133, no. 6, p. 1120, 1986.

[153] M. J. Rand and J. F. Roberts, "Preparation and Properties of Thin Film Boron Nitride," *J. Electrochem. Soc.*, vol. 115, no. 4, p. 423, 1968.

[154] M. Chubarov, H. Pedersen, H. Högberg, V. Darakchieva, J. Jensen, P. O. Å. Persson, and A. Henry, "Epitaxial CVD growth of sp2-hybridized boron nitride using aluminum nitride as buffer layer," *Phys. status solidi - Rapid Res. Lett.*, vol. 5, no. 10–11, pp. 397–399, 2011.

[155] M. D. Bremser, W. G. Perry, T. Zheleva, N. V. Edwards, O. H. Nam, N. Parikh, D. E. Aspnes, and R. F. Davis, "Growth, Doping and Characterization of AlxGa1−xN Thin Film Alloys on 6H-SiC(0001) Substrates," *MRS Internet J. Nitride Semicond. Res.*, vol. 71, no. 6, pp. 800–803, Jun. 1997.

[156] W.-C. Huang, C.-M. Chu, Y.-Y. Wong, K.-W. Chen, Y.-K. Lin, C.-H. Wu, W.-I. Lee, and E.-Y. Chang, "Investigations of GaN growth on the sapphire substrate by MOCVD method with different AlN buffer deposition temperatures," *Mater. Sci. Semicond. Process.*, vol. 45, pp. 1–8, 2016.

[157] S. Jia, Y. Cai, D. Wang, B. Zhang, K. M. Lau, and K. J. Chen, "Enhancement-mode AlGaN/GaN HEMTs on silicon substrate," *IEEE Trans. Electron Devices*, vol. 53, no. 6, pp. 1474–1477, 2006.

[158] K. Wang, Y. Xing, J. Han, K. Zhao, L. Guo, Y. Zhang, X. Deng, Y. Fan, and B. Zhang, "Influence of the TMAl source flow rate of the high temperature AlN buffer on the properties of GaN grown on Si(111) substrate," *J. Alloys Compd.*, vol. 671, pp. 435–439, 2016.

[159] U. K. Mishra, P. Parikh, and Y. F. Wu, "AlGaN/GaN HEMTs: An overview of device operation and applications," *Proc. IEEE*, vol. 90, no. 6, pp. 1022–1031, 2002.

[160] X. G. Zhang, B. Soderman, E. Armour, and A. Paranjpe, "Investigation of MOCVD growth parameters on the quality of GaN epitaxial layers," *J. Cryst. Growth*, vol. 318, no. 1, pp. 436–440, 2011.

[161] R. M. Biefeld, D. D. Koleske, and J. G. Cederberg, *3 - The Science and Practice of Metal-Organic Vapor Phase Epitaxy (MOVPE)*, Second Edi. Elsevier B.V., 2015.

[162] N. Fujimoto, T. Kitano, G. Narita, N. Okada, K. Balakrishnan, M. Iwaya, S. Kamiyama, H. Amano, I. Akasaki, K. Shimono, T. Noro, T. Takagi, and a. Bandoh, "Growth of high-quality AlN at high growth rate by high-temperature MOVPE," *Phys. Status Solidi*, vol. 3, no. 6, pp. 1617–1619, 2006.

[163] M. Imura, K. Nakano, N. Fujimoto, N. Okada, K. Balakrishnan, M. Iwaya, S. Kamiyama, H. Amano, I. Akasaki, T. Noro, T. Takagi, and A. Bandoh, "High-temperature metal-organic vapor phase epitaxial growth of AlN on sapphire by multi transition growth mode method varying V/III ratio," *Japanese J. Appl. Physics, Part 1 Regul. Pap. Short Notes Rev. Pap.*, vol. 45, no. 11, pp. 8639–8643, 2006.

[164] J. Chen, S. M. Zhang, B. S. Zhang, J. J. Zhu, G. Feng, X. M. Shen, Y. T. Wang, H. Yang, and W. C. Zheng, "Effects of reactor pressure on GaN nucleation layers and subsequent GaN epilayers grown on sapphire substrate," *J. Cryst. Growth*, vol. 254, no. 3–4, pp. 348–352, 2003.

[165] S. Keller and S. P. DenBaars, "Metalorganic chemical vapor deposition of group III nitrides—a discussion of critical issues," *J. Cryst. Growth*, vol. 248, no. 0, pp. 479–486, 2003.

[166] H. Kim-Chauveau, P. de Mierry, J.-M. Chauveau, and J.-Y. Duboz, "The influence of various MOCVD parameters on the growth of Al1−xInxN ternary alloy on GaN templates," *J. Cryst. Growth*, vol. 316, no. 1, pp. 30–36, 2011.

[167] K. S. Kim, A. Saxler, P. Kung, M. Razeghi, and K. Y. Lim, "Determination of the band-gap energy of Al[sub 1−x]In[sub x]N grown by metal–organic chemical-vapor deposition," *Appl. Phys. Lett.*, vol. 71, no. 6, p. 800, 1997.

[168] J. W. Ho, L. Zhang, Q. Wee, A. A. O. Tay, M. Heuken, and S. J. Chua, "Structural and morphological qualities of InGaN grown via elevated pressures in MOCVD on AlN/Si(111) substrates," *J. Cryst. Growth*, vol. 383, pp. 1–8, 2013.

[169] M. Moret, S. Ruffenach, O. Briot, and B. Gil, “MOVPE growth and characterization of indium nitride on C-, A-, M-, and R-plane sapphire,” *Phys. Status Solidi Appl. Mater. Sci.*, vol. 207, no. 1, pp. 24–28, 2010.

[170] C. Yang, X. Wang, H. Xiao, X. Zhang, G. Hu, J. Ran, C. Wang, J. Li, J. Li, and Z. Wang, “Growth temperature dependences of InN films grown by MOCVD,” *Appl. Surf. Sci.*, vol. 255, no. 5 PART 2, pp. 3149–3152, 2008.

[171] B. Maleyre, O. Briot, and S. Ruffenach, “MOVPE growth of InN films and quantum dots,” *J. Cryst. Growth*, vol. 269, no. 1, pp. 15–21, 2004.

[172] N. Khan, A. Sedhain, J. Li, J. Y. Lin, and H. X. Jiang, “High mobility InN epilayers grown on AlN epilayer templates,” *Appl. Phys. Lett.*, vol. 92, no. 17, pp. 2006–2009, 2008.

[173] O. Tuna, H. Behmenburg, C. Giesen, H. Kalisch, R. H. Jansen, G. P. Yablonskii, and M. Heuken, “Dependence of InN properties on MOCVD growth parameters,” *Phys. Status Solidi Curr. Top. Solid State Phys.*, vol. 8, no. 7–8, pp. 2044–2046, 2011.

[174] S. Majety, J. Li, X. K. Cao, R. Dahal, B. N. Pantha, J. Y. Lin, and H. X. Jiang, “Epitaxial growth and demonstration of hexagonal BN/AlGaN p-n junctions for deep ultraviolet photonics,” *Appl. Phys. Lett.*, vol. 100, pp. 1–5, 2012.

[175] C. Kimura, T. Yamamoto, T. Hori, and T. Sugino, “Field emission characteristics of BN/GaN structure,” *Appl. Phys. Lett.*, vol. 79, no. 27, pp. 4533–4535, 2001.

[176] J. Boo, C. Rohr, and W. Ho, “Growth of Boron Nitride Thin Films on Silicon Substrates Using New Organoboron Precursors,” *Solid State Phys.*, vol. 705, pp. 705–710, 1999.

[177] J. H. Edgar, D. . T. Smith, C. . R. Eddy, C. . A. Carosella, and B. . D. Sartwell, “c-Boron–aluminum nitride alloys prepared by ion-beam assisted deposition,” *Thin Solid Films*, vol. 298, no. 1, pp. 33–38, 1997.

[178] D. D. Koleske, A. E. Wickenden, R. L. Henry, W. J. DeSisto, and R. J. Gorman, “Growth model for GaN with comparison to structural, optical, and electrical properties,” *J. Appl. Phys.*, vol. 84, no. 1998, p. 1998, 1998.

[179] A. Tripathi and D. Mazzarese, “A study of the OMVPE growth mechanisms using internal reflectance spectroscopy to examine adsorption of TMGa and NH3 and surface reactions between them,” *J. Electron. …*, vol. 18, no. 1, pp. 45–51, 1989.

[180] G. B. Stringfellow, *Organometallic Vapor-Phase Epitaxy*. Elsevier, 1999.

[181] D. Mazzarese, A. Tripathi, W. C. Conner, K. A. Jones, L. Calderon, and D. W. Eckart, “In situ {FTIR} and surface analysis of the reaction of trimethylgallium and ammonia,” *J. Electron. Mater.*, vol. 18, no. 3, pp. 369–377, 1989.

[182] Q. An, A. Jaramillo-Botero, W. G. Liu, and W. A. Goddard, “Reaction pathways of GaN (0001) growth from trimethylgallium and ammonia versus triethylgallium and hydrazine using first principle calculations,” *J. Phys. Chem. C*, vol. 119, no. 8, pp. 4095–4103, 2015.

[183] P. Zanella, G. Rossetto, N. Brianese, F. Ossola, M. Porchia, and J. O. Wiilliams, "Organometallic Precursors in the Growth of Epitaxial Thin Films of Groups III-V Semiconductors by Metal-Organic Chemical Vapor Deposition," *Chem. Mater.*, vol. 3, no. 1, pp. 225–242, 1991.

[184] T. F. Kuech, *21 - Metal Organic Vapor Phase Epitaxy Chemical Kinetics*, Second Edi. Elsevier B.V., 2015.

[185] I. Bryan, Z. Bryan, S. Mita, A. Rice, J. Tweedie, R. Collazo, and Z. Sitar, "Surface kinetics in AlN growth: A universal model for the control of surface morphology in III-nitrides," *J. Cryst. Growth*, vol. 438, pp. 81–89, 2016.

[186] G. B. Stringfellow, "Development and current status of organometallic vapor phase epitaxy," *J. Cryst. Growth*, vol. 264, no. 4, pp. 620–630, 2004.

[187] H. Tokoi, A. Ohtake, K. Tago, K. Watanabe, and T. Mishima, "Development of GaN Growth Reaction Model Using Ab Initio Molecular Orbital Calculation and Computational Fluid Dynamics of Metalorganic Vapor-Phase Epitaxy," *J. Electrochem. Soc.*, vol. 159, no. 5, p. D270, 2012.

[188] Q. Guo, O. Kato, and A. Yoshida, "Thermal stability of indium nitride single crystal films," *J. Appl. Phys.*, vol. 73, no. 11, pp. 7969–7971, 1993.

[189] E. L. Piner, M. K. Behbehani, N. a El-Masry, F. G. McIntosh, J. C. Roberts, K. S. Boutros, and S. M. Bedair, "Effect of hydrogen on the indium incorporation in InGaN epitaxial films," *Appl. Phys. Lett.*, vol. 70, no. 4, pp. 461–463, 1997.

[190] S. S. Liu and D. A. Stevenson, "Growth Kinetics and Catalytic Effects in the Vapor Phase Epitaxy of Gallium Nitride," *J. Electrochem. Soc.*, vol. 125, no. 7, p. 1161, 1978.

[191] Y. Yue, Z. Hu, J. Guo, B. Sensale-Rodriguez, G. Li, R. Wang, F. Faria, T. Fang, B. Song, X. Gao, S. Guo, T. Kosel, G. Snider, P. Fay, D. Jena, and H. Xing, "InAlN/AlN/GaN HEMTs with regrown ohmic contacts and f T of 370 GHz," *IEEE Electron Device Lett.*, vol. 33, no. 7, pp. 988–990, 2012.

[192] P. Kung, A. Saxler, X. Zhang, D. Walker, R. Lavado, K. S. Kim, and M. Razeghi, "Al {sub x} Ga {sub 1 {minus} x} N based materials and heterostructures," *Mater. Res. Soc.*, no. 449, p. 79, 1997.

[193] S. Ruffenach-Clur, O. Briot, B. Gil, R.-L. Aulombard, and J. L. Rouviere, "MOVPE growth and structural characterization of AlxGa1-xN," *MRS Internet J. Nitride Semicond. Res.*, vol. 2, no. 1997, p. 27(7pp), 1997.

[194] A. Sohmer, J. Off, H. Bolay, V. Härle, V. Syganow, J. S. Im, V. Wagner, F. Adler, A. Hangleiter, A. Dörnen, F. Scholz, D. Brunner, O. Ambacher, and H. Lakner, "GaInN/GaN-heterostructures and quantum wells grown by metalorganic vapor-phase epitaxy," *MRS Internet J. Nitride Semicond. Res.*, vol. 2, no. 1997, p. 14(10pp), 1997.

[195] S. Gautier, M. Abid, T. Moudakir, G. Orsal, A. En Naciri, K. Pantzas, F. Jomard, P. L. Voss, D. J. Rogers, F. H. Teherani, and A. Ougazzaden, "Application of dilute boron B(Al,In,Ga)N alloys for UV light sources," vol. 7940, no. 1, p. 79400X–79400X–7, 2011.

[196] S. Watanabe, T. Takano, K. Jinen, J. Yamamoto, and H. Kawanishi, "Refractive indices of BxAl1−xN (x= 0–0.012) and ByGa1−yN (y= 0–0.023) epitaxial layers in ultraviolet region," *Phys. Status Solidi*, vol. 2694, no. 7, pp. 2691–2694, 2003.

[197] X. Li, S. Sundaram, Y. El Gmili, F. Genty, S. Bouchoule, G. Patriache, P. Disseix, F. Réveret, J. Leymarie, J.-P. Salvestrini, R. D. Dupuis, P. L. Voss, and a. Ougazzaden, "MOVPE grown periodic AlN/BAlN heterostructure with high boron content," *J. Cryst. Growth*, vol. 414, pp. 119–122, 2015.

[198] T. L. Williamson, N. R. Weisse-Bernstein, and M. a. Hoffbauer, "Growth of ternary wurtzite BAlN and BGaN by ENABLE-MBE," *Phys. Status Solidi Curr. Top. Solid State Phys.*, vol. 2, no. 3, pp. 462–465, 2014.

[199] V. K. Gupta, C. C. Wamsley, M. W. Koch, and G. W. Wicks, "Molecular beam epitaxy growth of boron-containing nitrides," *J. Vac. Sci. Technol. B Microelectron. Nanom. Struct.*, vol. 17, no. 3, p. 1246, 1999.

[200] A. Ougazzaden, S. Gautier, T. Aggerstam, J. Martin, M. Bouchaour, T. Baghdadli, S. O. Saad, S. Lourdudoss, N. Maloufi, Z. Djebbour, and F. Jomard, "Progress on new wide bandgap materials BGaN, BGaAlN and their potential applications," *Quantum Sens. Nanophotonic Devices IV*, vol. 6479, no. 2007, p. 64791G, 2007.

[201] G. Orsal, N. Maloufi, S. Gautier, M. Alnot, a. a. Sirenko, M. Bouchaour, and a. Ougazzaden, "Effect of boron incorporation on growth behavior of BGaN/GaN by MOVPE," *J. Cryst. Growth*, vol. 310, no. 23, pp. 5058–5062, 2008.

[202] T. Takano, M. Kurimoto, J. Yamamoto, and H. Kawanishi, "Epitaxial growth of high quality BAlGaN quaternary lattice matched to AlN on 6H-SiC substrate by LP-MOVPE for deep-UV emission," *J. Cryst. Growth*, vol. 237–239, no. 1–4 II, pp. 972–977, 2002.

[203] M. B. McLaurin, "III-Nitride light emitting device incorporation boron," 8106403, 2012.

[204] V. Ravindran, "DESIGN AND FABRICATION OF BORON-CONTAINING III-NITRIDES BASED HIGH ELECTRON MOBILITY TRANSISTORS," Georgia Institute of Technology, 2013.

[205] Y. Cao and D. Jena, "High-mobility window for two-dimensional electron gases at ultrathin AlNGaN heterojunctions," *Appl. Phys. Lett.*, vol. 90, no. 18, pp. 21–24, 2007.

[206] H. Dumont, B. Bayle, B. Bonnetot, and J. Bouix, "Deposition and characterization of BN / Si (0 0 1) using tris (dimethylamino) borane," *Mater. Res. Bull.*, vol. 37, pp. 1565–1572, 2002.

[207] E. Lippert, “The Strengths of Chemical Bonds,” *Angew. Chemie*, vol. 72, no. 16, pp. 602–602, Aug. 1960.

[208] N. Chaaben, J. Laifi, H. Bouazizi, C. Saidi, A. Bchetnia, and B. El Jani, “Study of Al diffusion in GaN during metal organic vapor phase epitaxy of AlGaN/GaN and AlN/GaN structures,” *Mater. Sci. Semicond. Process.*, vol. 42, pp. 359–363, 2016.

[209] V. V Ilyasov, T. P. Zhdanova, and I. Y. Nikiforov, “Electronic Energy Structure and X-ray Spectra of Wide-Gap AlN and BN Crystals and B x Al 1 – x N Solid Solutions,” *Phys. Solid State*, vol. 47, no. 9, pp. 1559–1566, 2005.

[210] X. Lei, X. X. Liang, G. J. Zhao, and T. L. Song, “First-principle studies of the electronic band structure and the phonon dispersion properties of wurtzite BN,” *J. Phys. Conf. Ser.*, vol. 490, no. 1, p. 12171, 2014.

[211] Y.-N. X. and W. Y. Ching, Y.-N. Xu, and W. Y. Ching, “Calculation of ground-state and optical properties of boron nitrides in the hexagonal, cubic, and wurtzite structures,” *Phys. Rev. B*, vol. 44, no. 15, pp. 7787–7798, Oct. 1991.

[212] J. Furthmüller, J. Hafner, and G. Kresse, “Ab initio calculation of the structural and electronic properties of carbon and boron nitride using ultrasoft pseudopotentials,” *Phys. Rev. B*, vol. 50, no. 21, pp. 15606–15622, Dec. 1994.

[213] V. V Ilyasov, T. P. Zhdanova, and I. Y. Nikiforov, “Electronic Band Structure and X-ray Spectra of Boron Nitride Polytypes,” *Phys. Solid State*, vol. 45, no. 5, pp. 816–824, 2003.

[214] R. Ahmed, Fazal-e-Aleem, S. J. Hashemifar, and H. Akbarzadeh, “First principles study of structural and electronic properties of different phases of boron nitride,” *Phys. B Condens. Matter*, vol. 400, no. 1–2, pp. 297–306, 2007.

[215] S. P. Gao, “Cubic, wurtzite, and 4H-BN band structures calculated using GW methods and maximally localized Wannier functions interpolation,” *Comput. Mater. Sci.*, vol. 61, pp. 266–269, 2012.

[216] C. E. Dreyer, J. L. Lyons, A. Janotti, and C. G. Van De Walle, “Band alignments and polarization properties of BN polymorphs,” *Appl. Phys. Express*, vol. 7, no. 3, 2014.

[217] G. Martínez-Criado, A. Cros, A. Cantarero, O. Ambacher, C. R. Miskys, R. Dimitrov, M. Stutzmann, J. Smart, and J. R. Shealy, “Residual strain effects on the two-dimensional electron gas concentration of AlGaN/GaN heterostructures,” *J. Appl. Phys.*, vol. 90, no. 9, p. 4735, 2001.

[218] F. Bechstedt, U. Grossner, and J. Furthmüller, “Dynamics and polarization of group-III nitride lattices: A first-principles study,” *Phys. Rev. B - Condens. Matter Mater. Phys.*, vol. 62, no. 12, pp. 8003–8011, 2000.

[219] A. Dadgar, A. Krost, J. Christen, B. Bastek, F. Bertram, A. Krtschil, T. Hempel, J. Blasing, U. Haboeck, and A. Hoffmann, “MOVPE growth of high-quality AlN,” *J. Cryst. Growth*, vol. 297, no. 2, pp. 306–310, 2006.

[220] N. Coudurier, R. Boichot, F. Mercier, R. Reboud, S. Lay, E. Blanquet, and M. Pons, “Growth of Boron Nitride on (0001) AlN Templates by High Temperature-Hydride Vapor Phase Epitaxy (HT-HVPE),” *Phys. Procedia*, vol. 46, no. Eurocvd 19, pp. 102–106, 2013.

[221] J. S. Lewis, S. Vaidyaraman, W. J. Lackey, F. K. Agrawal, G. B. Freeman, and E. K. Barefield, “Chemical vapor deposition of boron-carbon films using organometallic reagents,” *Mater. Lett.*, vol. 27, no. August, pp. 327–332, 1996.

[222] D. R. Lamborn, D. W. Snyder, X. X. Xi, and J. M. Redwing, “Modeling studies of the chemical vapor deposition of boron films from B2H6,” *J. Cryst. Growth*, vol. 299, pp. 358–364, 2007.

[223] J.-S. Li, C.-R. Zhang, B. Li, F. Cao, and S.-Q. Wang, “Boron nitride coatings by chemical vapor deposition from borazine,” *Surf. Coatings Technol.*, vol. 205, no. 12, pp. 3736–3741, 2011.

[224] V. N. Demin, I. P. Asanov, and Z. L. Akkerman, “Chemical vapor deposition of pyrolytic boron nitride from borazine,” *J. Vac. Sci. Technol. A Vacuum, Surfaces, Film.*, vol. 18, no. 1, p. 94, 2000.

[225] M. Odawara, T. Udagawa, and G. Shimaoka, “Organometallic Chemical Vapor Deposition Growth of Heterostructure of Wide Band Gap and Transparent Boron Phosphide on Silicon,” *Jpn. J. Appl. Phys.*, vol. 44, no. 1B, pp. 681–683, 2005.

[226] Q. Wang, X. Ren, F. Wang, J. Feng, J. Lv, J. Zhou, S. Cai, H. Huang, and Y. Huang, “LP-MOCVD growth of ternary BxGa1−xAs epilayers on (001)GaAs substrates using TEB, TMGa and AsH3,” *Microelectronics J.*, vol. 39, no. 12, pp. 1678–1682, 2008.

[227] R. Dahal, J. Li, S. Majety, B. N. Pantha, X. K. Cao, J. Y. Lin, and H. X. Jiang, “Epitaxially grown semiconducting hexagonal boron nitride as a deep ultraviolet photonic material,” *Appl. Phys. Lett.*, vol. 98, no. 21, pp. 2–4, 2011.

[228] J. Li, R. Dahal, S. Majety, J. Y. Lin, and H. X. Jiang, “Hexagonal boron nitride epitaxial layers as neutron detector materials,” *Nucl. Instruments Methods Phys. Res. Sect. A Accel. Spectrometers, Detect. Assoc. Equip.*, vol. 654, pp. 417–420, 2011.

[229] W. L. Bragg, “Proceedings of the Cambridge Philosophical Society,” pp. 43–57, 1913.

[230] F. R. Corrigan and F. P. Bundy, “Direct transitions among the allotropic forms of boron nitride at high pressures and temperatures,” *J. Chem. Phys.*, vol. 63, no. 9, p. 3812, 1975.

[231] T. Sekine, “Shock-induced phase transformation of graphite-like boron nitride to denser forms,” *J. Mater. Sci. Lett.*, vol. 8, no. 8, pp. 872–874, 1989.

[232] M. M. Bindal, B. P. Singh, S. K. Singhal, R. K. Nayar, and R. Chopra, “Sintering of wurtzitic boron nitride under high pressures and temperatures,” *J. Mater. Sci. Lett.*, vol. 13, no. 1, pp. 73–75, 1994.

[233] O. Mishima and K. Era, “Science and Technology of Boron Nitride,” in *Electric Refractory Materials*, Marcel Dekker, 2004.

[234] S. Keller, H. Li, M. Laurent, Y. Hu, N. Pfaff, J. Lu, D. F. Brown, N. A. Fichtenbaum, J. S. Speck, S. P. Denbaars, and U. K. Mishra, “Recent progress in metal-organic chemical vapor deposition of (000-1) N-polar group-III nitrides,” *Semicond. Sci. Technol.*, vol. 29, p. 113001, 2014.

[235] K. Atsumi, Y. Inoue, H. Mimura, T. Aoki, and T. Nakano, “Neutron detection using boron gallium nitride semiconductor material,” *APL Mater.*, vol. 2, no. 3, pp. 1–7, 2014.